COMPLEMENTARY VASOACTIVITY AND MATRIX REMODELING IN ARTERIES: THEORETICAL FOUNDATIONS AND PREDICTED TRENDS

A Dissertation

by

ARTURO VALENTÍN III

Submitted to the Office of Graduate Studies of
Texas A&M University
in partial fulfillment of the requirements for the degree of

DOCTOR OF PHILOSOPHY

August 2009

Major Subject: Biomedical Engineering

COMPLEMENTARY VASOACTIVITY AND MATRIX REMODELING IN ARTERIES: THEORETICAL FOUNDATIONS AND PREDICTED TRENDS

A Dissertation

by

ARTURO VALENTÍN III

Submitted to the Office of Graduate Studies of
Texas A&M University
in partial fulfillment of the requirements for the degree of

DOCTOR OF PHILOSOPHY

Approved by:

Chair of Committee,	Jay D. Humphrey
Committee Members,	James E. Moore Jr.
	Christopher M. Quick
	Hsin-i Wu
Head of Department,	Gerard L. Coté

August 2009

Major Subject: Biomedical Engineering

ABSTRACT

Complementary Vasoactivity and Matrix Remodeling in Arteries: Theoretical Foundations and Predicted Trends. (August 2009)

Arturo Valentín III, B.S., University of South Carolina;

M.S., University of South Carolina

Chair of Advisory Committee: Dr. Jay D. Humphrey

Arteries possess the ability to grow and remodel in response to sustained alterations in biomechanical loading, likely via mechanisms that are similarly involved in diverse arterial pathologies and responses to treatment. In particular, myriad experminental observations suggest that cell and matrix turnover within vasoaltered states enable arteries to adapt to sustained changes in mechanical stimuli. The goal herein is to show explicitly how altered smooth muscle contractility and matrix growth and remodeling work together to adapt the geometry, structure, stiffness, and function of a representative basilar artery. This work seeks to illustrate the importance of complementary vasoactivity and matrix remodeling for basilar arteries in response to sustained alterations in mechanical stimuli. Toward this end, an extended constrained mixture model of the arterial wall is employed whereby the mass fractions, material properties, and natural configurations of individual constituents can evolve separately and thereby dictate overall growth and remodeling. This approach accounts for fundamentally important behaviors. Simulations provide important intuition and insight regarding constitutive functional forms and model parameters.

To my parents

ACKNOWLEDGMENTS

I would like to thank my advisor, Professor Jay D. Humphrey, for nearly five years of mentorship and friendship. Professor Humphrey is a true scholar and an inspirational researcher and educator. My time at Texas A&M has been more rewarding than I could have imagined, and I count myself fortunate to have had the honor to work with him.

I would also like to thank my committee members, Professors James Moore, Christopher Quick, and Hsin-i Wu, for their insightful comments and provocative questions. They have prompted me to consider several crucial nuances and exercise a higher degree of rigor with regard to communicating my work.

In addition to my advisory committee, the following co-workers have contributed substantially to my academic development and merit special mention. Doctor Seungik Baek introduced me to the challenges associated with computational growth and remodeling implementations, and much of this work builds upon his pioneering and innovative approaches. Doctor Luca Cardamone has been an influential and valuable collaborator. For nearly a year, Dr. Cardamone and I explored the intricacies and pitfalls of constrained mixture models. Much of this work is motivated by what we learned.

My parents have earned my most profound gratitude for their indefatigable support and encouragement. Their innumerable sacrifices have enabled my pursuits, and I hope to someday be as good a parent as they. Finally, I thank my wife, Carolyn, for her companionship and love. She has given me renewed purpose and strength.

TABLE OF CONTENTS

CHAPTER Page

CHAPTER Page

LIST OF TABLES

LIST OF FIGURES

FIGURE Page

FIGURE Page

FIGURE Page

FIGURE Page

FIGURE Page

FIGURE Page

FIGURE Page

CHAPTER I

INTRODUCTION: THE ROLE OF COMPUTATIONAL MODELS IN BIOMECHANICS

Human subtlety will never devise an invention more beautiful, more simple or more direct than does nature because in her inventions nothing is lacking, and nothing is superfluous.

Leonardo da Vinci (1452-1519)

The arterial systemic circulation transports oxygenated blood to all parts of the body, with the exception of the lungs. This high pressure vascular network can adjust blood flow locally in response to changing metabolic demands, complementing the heart's limited output range. Additionally, sustained changes in mechanical loads can result in dramatic compensatory changes in arteries. These remarkable capabilities stem, in part, from optimized complementary vasoactivity, passive elasticity, and growth and remodeling (G&R) mechanisms. It seems likely that a common set of cellular behaviors, in response to a myriad of local biochemomechanical stimuli during development and maturity, gives rise to the observed diverse arterial properties throughout the vascular tree. Thus, optimal arterial structure and function are ultimately consequences of a series of genetically-programmed responses to varied biochemomechanical cues.

This dissertation follows the style of the *ASME Journal of Biomechanical Engineering*.

The conjecture that cells behave consistently and work to remodel their mechanical environments towards some preferred mechanical state is the premise for a general philosophical approach: the hypothesis that synthetic vascular smooth muscle cells and fibroblasts continually produce and degrade matrix constituents in preferred modes and at altered rates in response to changing mechanical stimuli. Additionally, it is well known that smooth muscle cells exhibit vasoactive changes that contribute to overall structure, function, and mechanical behavior. Thus, in addition to complex instantaneous nonlinear mechanical responses, evolving constituent composition and organization are crucial factors affecting biomechanical behavior of soft tissues.

Scientists, of course, seek to discover the underlying mechanisms by which changes in the mechanical environment govern biological growth and remodeling. Cogent theories founded upon realistic fundamental cellular behavior and continuum mechanics promise to help in developing intuition, understanding complex biomechanical systems, and designing rational experiments and ultimately clinical interventions. Toward these ends, this dissertation employs a continuum-based mixture theory to model arterial G&R and test various competing hypotheses. The constrained mixture approach provides a useful framework in which to quantify arterial growth and remodeling, since it can account for cell-mediated changes in individually structurally significant constituents. Consequently, it is well-suited to modeling arterial adaptations and maladaptations. This work describes a model of the arterial wall wherein mass fractions, mechanical properties, and natural configurations of individual constituents can evolve separately and thereby govern overall growth and remodeling.

It is shown that the model captures many observed features of flow-, pressure- and axial stretch-induced remodeling in a representative basilar artery. It is also demonstrated that individual and variable mass density turnover of constituents, individual preferred deposition stretches and vasoactivity with evolving reference con-

figurations are indeed fundamentally important cellular behaviors, required for predicting bounded arterial G&R. A parametric study is presented to categorize different classes of parameters within the theoretical framework and assess the sensitivity of model predictions to parameter values that are not known directly from experiments. Finally, the model is extended to investigate the potentially related roles of elastin degradation, smooth muscle dysfunction, and collagen stiffening in arterial aging.

CHAPTER II

COMPLEMENTARY VASOACTIVITY AND MATRIX REMODELING IN ARTERIAL ADAPTATIONS TO ALTERED FLOW AND PRESSURE*

A. Overview

Arteries exhibit a remarkable ability to adapt to sustained alterations in biomechanical loading, likely via mechanisms that are similarly involved in many arterial pathologies and responses to treatment. Of particular note, diverse data suggest that cell and matrix turnover within vasoaltered states enables arteries to adapt to sustained changes in blood flow and pressure. The goal herein is to show explicitly how altered smooth muscle contractility and matrix growth and remodeling work together to adapt the geometry, structure, stiffness, and function of a representative basilar artery. Toward this end, we employ a continuum theory of constrained mixtures to model evolving changes in the wall that depend on both wall shear stress induced changes in vasoactive molecules (which alter smooth muscle proliferation and synthesis of matrix) and intramural stress induced changes in growth factors (which alter cell and matrix turnover). Simulations show, for example, that such considerations help explain the different rates of experimentally observed adaptations to increased versus decreased flows as well as differences in rates of change in response to increased flows or pressures.

B. Introduction

With considerable foresight, Rodbard [1] wrote:

> Let us assume that each endothelial cell is equipped with receptors which are sensitive to the magnitude of the drag force that impinges on it... Deviations of drag from this set-point initiate negative feedback mechanisms that return the magnitude of the drag to its set-point. In blood vessels, these effects appear to operate through two related mechanisms: an immediate physiological adjustment in vascular tone induced by the change in flow, and a delayed anatomical change that develops when the changed flow rate persists.

Although this scenario is most apparent in arterial adaptations to sustained alterations in blood flow, smooth muscle vasoactivity appears to play similar roles in cases of altered blood pressure and axial stretch as well as in diseases ranging from pulmonary hypertension to cerebral vasospasm. That is, diverse clinical observations and laboratory experiments over the past three decades [cf. 2] have confirmed Rodbard's general concept: many adaptations occur via matrix remodeling (i.e., delayed anatomical changes) within altered vasoactive states (i.e., adjustments in vascular tone) so as to maintain constant various mechanical factors. For a recent, lucid review of the coupling between vasoactivity and matrix remodeling, see Dajnowiec and Langille [3].

Prior computational models of the biomechanics of arterial adaptations have been based primarily on either the concept of kinematic growth [e.g. 4, 5] or a constrained mixture theory [e.g. 6, 7]. The goal of this paper is to illustrate the importance of matrix remodeling within altered vasoactive states for basilar arteries in response to sustained alterations in blood flow and blood pressure. Toward this end, we employ an

extended constrained mixture model of the arterial wall whereby the mass fractions, material properties, and natural configurations of individual constituents can evolve separately and thereby dictate overall growth and remodeling (G&R).

C. Methods

1. Wall Mechanics & Hemodynamics

We restrict our attention to elastostatics [cf. 8] and 2-D wall mechanics [cf. 6], which can capture salient features of the structural stiffness and overall geometry sufficient for many clinical and fluid-solid interaction studies [9]. Hence, note that 2-D equilibrium equations for a straight, cylindrical segment of an artery can be written, at each G&R time s, as

$$\sigma_\theta(s) = \frac{P(s)\,a(s)}{h(s)}, \tag{2.1}$$

$$\sigma_z(s) = \frac{f(s)}{\pi\,h(s)\;(2\,a(s) + h(s))}, \tag{2.2}$$

where P is the transmural pressure, a is the deformed luminal radius, h is the deformed wall thickness, and f is the applied axial force (note: although often derived for thin-walled tubes, these mean values of stress also hold for thick-walled tubes exhibiting linear or nonlinear material behavior and subjected to negligible perivascular tethering; 10). Values of a/h tend to be 7-10 in normal large arteries, thus yielding homeostatic values of circumferential stress on the order of 90-130 kPa at mean arterial pressure, which appear to be similar to computed values of axial stress [11].

Inasmuch as these two equilibrium equations are not sufficient to determine the three primary geometric variables for the wall (radius a, thickness h, and length l), even after introducing constitutive relations for the stress responses, we invoke a

constancy of total mass density [12] to close this system of equations. That is, given that the mass density of the arterial wall $\rho(s) \cong \rho(0)$, let

$$\beta(s) = \frac{\pi\, h(s)\,(2\,a(s) + h(s))\; l(s)}{\pi\, h(0)\,(2\,a(0) + h(0))\; l(0)} \;\; \forall\, s, \tag{2.3}$$

where l denotes the deformed length of the segment and $\beta(s)$ describes overall changes in mass or volume, which are potentially measurable. It is assumed, of course, that all geometric values are known at G&R time $s = 0$, where $\beta(0) \equiv 1$. Letting $l(s) \equiv l(0)$ allows us to solve for $a(s)$ or $h(s)$ at any G&R time s; marked increases in $l(s)$ can result in tortuous arteries, an important consideration in some cases [13], but this complicates the biomechanics considerably.

Among others, Rodbard [1] and Zamir [14] recognized that Murray's result of 1926 [15] could be interpreted as a "constancy of wall shear stress" if the mean wall shear stress is given by the solution of a steady, fully developed, laminar, one-dimensional, incompressible flow of a Newtonian fluid within a rigid circular tube (a rough approximation for an artery): $\tau_w = 4\,\mu\,Q/\pi\,a^3$ where μ is the viscosity of blood at high shear rates ($\sim$3.5 centiPoise), Q is the volumetric flowrate, and a is again the deformed luminal radius. That is, if a^3 remains proportional to Q for a fixed viscosity, as suggested by Murray's simple analysis, then τ_w must remain constant.

2. Growth & Remodeling Framework

We employ an extension [16] of a constrained mixture theory of isothermal G&R for soft tissues [12]. The Cauchy stress response by the arterial wall $\boldsymbol{\sigma}$ results from passive elasticity and smooth muscle activation, and thus can be approximated as

$$\boldsymbol{\sigma} = \frac{1}{\det \mathbf{F}} \mathbf{F} \frac{\partial W}{\partial \mathbf{F}^T} + \sigma_\theta^{act}(Ca^{++})\, \mathbf{e}_\theta \otimes \mathbf{e}_\theta, \tag{2.4}$$

where $\mathbf{F}$ is the deformation gradient, W is a stored energy function for the elastic

response, and σ_θ^{act} denotes the smooth muscle contractility that exists primarily in the circumferential direction and ultimately depends on intracellular calcium. Herein we restrict our attention to $\mathbf{F} = \text{diag}[\lambda_z, \lambda_\theta]$. By the rule of mixtures, the stored energy can be thought of conceptually as $W = \sum \phi^k W^k$, where $\phi^k = \rho^k/\rho$ are constituent mass fractions. Assuming that G&R commences at $s = 0$, Baek *et al.* [16] proposed the following relations for the evolving constituent mass densities and strain energy functions[1]:

$$M^k(s) = M^k(0)\, Q^k(s) + \int_0^s m^k(\tau)\, q^k(s,\tau)\, d\tau, \tag{2.5}$$

$$\begin{aligned} W^k(s) = {} & \frac{M^k(0)}{\rho(s)}\, Q^k(s)\, \widehat{W}^k\left(\mathbf{C}^k_{n(0)}(s)\right) \\ & + \int_0^s \frac{m^k(\tau)}{\rho(s)}\, q^k(s,\tau)\, \widehat{W}^k\left(\mathbf{C}^k_{n(\tau)}(s)\right)\, d\tau, \end{aligned} \tag{2.6}$$

where $Q^k(s) \in [0,1]$ account for fractions of material produced at or before time $s = 0$ that survive to time s, with $Q^k(0) \equiv 1$, $m^k(\tau) \geq 0$ are true mass density production rate functions, and $q^k(s,\tau) \in [0,1]$ account for the fractions of material produced at time $\tau \in [0,s]$ that survive to time s. Moreover, $M^k(s)$ is the mass per unit area of constituent k at time s, and $\widehat{W}^k$ is the energy stored elastically in constituent k, which depends on $\mathbf{C}^k_n$, the right Cauchy-Green tensor for that constituent defined relative to its individual natural configuration. In particular, $\mathbf{C}^k_{n(\tau)}(s) = \left(\mathbf{F}^k_{n(\tau)}(s)\right)^T \mathbf{F}^k_{n(\tau)}(s)$ where $\mathbf{F}^k_{n(\tau)}(s) = \partial \mathbf{x}^k(s)/\partial \mathbf{X}^k(\tau)$, with $\mathbf{x}^k(s) = \mathbf{x}(s)$ consistent with the concept of a constrained mixture and $\mathbf{X}^k(\tau)$ reflecting evolving natural configurations for constituent k when produced at time τ. Clearly, the survival functions $q^k(s-\tau)$ ensure that a constituent contributes to load bearing only until it is degraded, which because

[1]See the Appendix for evaluations of special cases for these constitutive functions. Note that the original paper denoted G&R time via t rather than s.

of the convolution integral is reminiscent of a fading memory behavior, characteristic of viscoelasticity, wherein a constituent contributes more to the stress response the more recently it was produced. Finally, note that $\sum \rho^k(s) = \sum \rho^k(0)$ is consistent with equation (2.3).

3. Specialization for 2-D Wall Mechanics

Combining the equilibrium equations and constitutive relations for the principal tensions $T_i = \sigma_i\, h$, where $i = z, \theta$, we have at any G&R time s

$$P\, a = T_\theta = \frac{1}{\lambda_z} \sum \frac{\partial W^k}{\partial \lambda_\theta} + \sigma_\theta^{act}\, h, \tag{2.7}$$

$$\frac{f}{\pi\,(2\,a + h)} = T_z = \frac{1}{\lambda_\theta} \sum \frac{\partial W^k}{\partial \lambda_z}. \tag{2.8}$$

In general, for a fibrous constituent k (e.g., collagen) we have

$$\begin{aligned} \frac{\partial \widehat{W}^k \left(\lambda^k_{n(\tau)}(s)\right)}{\partial \lambda_\theta(s)} =& \frac{\partial \widehat{W}^k(s)}{\partial \lambda^k_{n(\tau)}} \frac{\partial \lambda^k_{n(\tau)}}{\partial \lambda_\theta(s)} \\ =& \frac{\partial \widehat{W}^k(s)}{\partial \lambda^k_{n(\tau)}} \frac{G^k_h}{\lambda(\tau)} \frac{\partial \lambda(s)}{\partial \lambda_\theta(s)}, \end{aligned} \tag{2.9}$$

$$\begin{aligned} \frac{\partial \widehat{W}^k \left(\lambda^k_{n(\tau)}(s)\right)}{\partial \lambda_z(s)} =& \frac{\partial \widehat{W}^k(s)}{\partial \lambda^k_{n(\tau)}} \frac{\partial \lambda^k_{n(\tau)}}{\partial \lambda_z(s)} \\ =& \frac{\partial \widehat{W}^k(s)}{\partial \lambda^k_{n(\tau)}} \frac{G^k_h}{\lambda(\tau)} \frac{\partial \lambda(s)}{\partial \lambda_z(s)}, \end{aligned} \tag{2.10}$$

with $\lambda^k_{n(\tau)}(s) = G^k_h\,(\lambda(s)/\lambda(\tau))$ and

$$\lambda(\tau) = \sqrt{\lambda_z^2(\tau)\, \cos^2(\alpha_0^k) + \lambda_\theta^2(\tau)\, \sin^2(\alpha_0^k)}\ \ \forall\, \tau \in [0, s] \tag{2.11}$$

where α_0^k denotes the angle between a fiber and the z axis in a common reference configuration for the mixture (i.e., artery). These kinematic relations are derived in Baek *et al.* [16]. Note that G^k_h represents a basic hypothesis in the theory, that

new fibers are incorporated within extant tissue at a preferred (homeostatic) stretch. We call G_h^k the "deposition stretch." Finally, one must prescribe the direction in which the fiber is deposited. Without loss of generality, herein, we assume that fiber directions are preserved in the non-pathologic cases of adaptations to altered flow and pressure.

4. Illustrative Constitutive Relations

As revealed by the G&R framework, constitutive relations are needed for the true mass density productions, survival functions, and stress responses for the individual structurally significant constituents (elastin, fibrillar collagen, and smooth muscle) as well as for the deposition stretches and deposition alignment. Although there is need for much more research on the precise forms of each of these relations and best-fit values of the associated material parameters, the considerable data available in the literature enables one to postulate relations sufficient for illustrative purposes. Vascular elastin is typically assumed to be isotropic and to exhibit a neo-Hookean type response [17, 18], hence we assume that the elastin-dominated amorphous matrix is described by

$$\widehat{W}^e(s) = c\left(\lambda_\theta^e(s)^2 + \lambda_z^e(s)^2 + \frac{1}{\lambda_\theta^e(s)^2\,\lambda_z^e(s)^2} - 3\right), \tag{2.12}$$

where c is a material parameter. Moreover, we assume that most of the elastin is produced in the perinatal period and that it is normally very stable biologically [19, 20]. Hence, we assume that in non-pathological conditions $Q^e(s) = 1$ and $m^e(\tau) = 0\ \forall\, s, \tau \in [0, \infty)$. Collagen and vascular smooth muscle, on the other hand, appear to turnover continuously but slowly in the normal arterial wall, albeit at different basal rates m_0^k. We assume that for each family of collagen and circumferentially oriented

passive smooth muscle [16],

$$\widehat{W}^k(s) = c_1^k \left(e^{c_2^k \left(\lambda^k_{n(\tau)}(s)^2 - 1 \right)^2} - 1 \right), \tag{2.13}$$

and for active smooth muscle [21],

$$\begin{aligned} \sigma_\theta^{act}(s) = T_{max}\, \phi^m(s) \, \left(1 - e^{-C(s)^2} \right) \\ \times \lambda_\theta^{m(act)}(s) \, \left[1 - \left(\frac{\lambda_M - \lambda_\theta^{m(act)}(s)}{\lambda_M - \lambda_0} \right)^2 \right], \end{aligned} \tag{2.14}$$

where T_{max} is a scaling parameter with units of $\mathrm{N/m^2}$, λ_M is the circumferential stretch at which the active stress is maximum, and λ_0 is the circumferential stretch at which the active stress goes to zero. $C(s)$ is the net ratio of constrictors to dilators, and $\lambda_\theta^{m(act)}(s) = a(s)/a^{m(act)}(s)$ where $a^{m(act)}(s)$ can evolve via a first order rate equation [cf. 22]. For these simulations, we consider

$$C(s) = C_B - C_S \left(\frac{\tau_w(s) - \tau_w^h}{\tau_w^h} \right), \tag{2.15}$$

where C_B is the basal constrictor to dilator ratio, C_S is a scaling factor for the shear-induced change in constrictor concentration, and $\tau_w(s)$ and τ_w^h are the shear stress at G&R time s and the homeostatic state, respectively. The instantaneous change in active stress as a function of stretch and constrictor concentration is shown in figure 1. Note that this active behavior is taken with respect to individual unloaded configurations for smooth muscle [cf. figure 1 in 16], not for the entire mixture.

As in prior work [4–6, 22], we let mass density production rates depend in part on differences in intramural stress from homeostatic values. In addition, however, we know that vasoactive molecules regulated by the endothelium in response to altered wall shear stress also affect cell and matrix turnover. For example, nitric oxide (NO) is an inhibitor of smooth muscle proliferation and synthesis of collagen [23], whereas

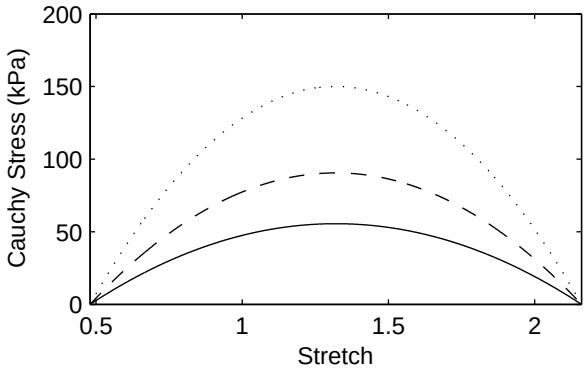

Fig. 1. Active response by smooth muscle where $C = C_B$ (solid), $2\,C_B$ (dashed), and ∞ (dotted). Stretch is expressed with respect to the muscle's natural configuration. Increases in C result in corresponding increases in active stress for a given stretch.

endothelin-1 (ET-1) is a promoter of smooth muscle proliferation and synthesis of collagen [24]; NO is upregulated in response to increased wall shear stress and ET-1 is upregulated in response to decreased shear [25, 26]. Many other endothelially derived molecules (vasoactive, growth regulatory, and proteases) are regulated similarly. In principle, then, $m^k = f^k(\sigma_\theta, \sigma_z, \tau_w)$ for $k =$ collagen and smooth muscle. Alternatively, anticipating the future use of reaction-diffusion equations to determine concentration histories for diverse soluble substances, we can let $m^k = f^k(\sigma_\theta, \sigma_z, C)$, where C is the aforementioned ratio of constrictors to dilators. Specifically, we consider the following candidate constitutive relation for true mass density productions,

$$m^k = m_0^k(1 + K_\sigma^k\,\Delta\sigma + K_C^k\,\Delta C), \tag{2.16}$$

where m_0^k is the basal production rate, K_j^k are "rate parameters" that govern stress-mediated and constrictor-mediated changes in production, and σ is a scalar metric for wall stress as in Baek *et al.* [22]. In a 3-D model, σ and C would be field quantities,

but we focus on mean values here. For example, mass density productions can be prescribed individually for fiber families based on the stress borne by that family. Moreover, $\Delta\sigma$ and ΔC represent normalized differences in stress or constrictors from their homeostatic values. Hence, in the case where these differences are zero, one recovers homeostatic production rates. Finally, although the kinetics of cell apoptosis and matrix degradation are extremely complex, it appears that gross responses follow first order type kinetics. Hence, let the survival functions

$$q^k(s,\tau) = e^{-\int_\tau^s K^k(\widetilde{\tau})d\widetilde{\tau}}, \tag{2.17}$$

where the functions $K^k(\widetilde{\tau})$ are rate-type parameters for mass removal having units of days^{-1}. Of course, rates of removal can also depend explicitly on changes in the tension within fibers, hence one specific form to consider is

$$K^k(\widetilde{\tau}) = K_h^k + K_h^k\,\Delta\zeta(\widetilde{\tau})^2, \tag{2.18}$$

where K_h^k is an initial value for the rate parameter, $\Delta\zeta(\widetilde{\tau})$ is the difference in fiber tension from its homeostatic value, and $\zeta^{k(\tau)}$ is the level of tension on constituent k that was produced at time τ and defined by

$$\zeta^{k(\tau)}(s) = \frac{\partial\widehat{W}^k/\partial\lambda_n^k\left(\lambda_{n(\tau)}^k(s)\right)}{\partial\widehat{W}^k/\partial\lambda_n^k\left(G_h^k\right)}. \tag{2.19}$$

In summary, our two primary governing equations are

$$P\,a = T_\theta^e + \frac{1}{\lambda_z}\sum\frac{\partial W^j}{\partial\lambda_\theta} + \frac{1}{\lambda_z}\frac{\partial W^m}{\partial\lambda_\theta} + \sigma_\theta^{act}\,h\ \ \forall\, s, \tag{2.20}$$

$$\frac{f}{\pi\,(2\,a+h)} = T_z^e + \frac{1}{\lambda_\theta}\sum\frac{\partial W^j}{\partial\lambda_z}\ \ \forall\, s, \tag{2.21}$$

subject to the mass density constraint (equation (2.3)), where T_i^e are tensions borne by elastin. Recall that superscripts m and e denote passive smooth muscle and

unchanging elastin. Moreover, we allow j families of collagen fibers, each defined by different parallel orientations. In particular, it appears that $j = 2$ or 4 allows one to model the complex contributions of the collagen reasonably well [18, 22]. We employ four families of collagen [cf. 27] for basilar arteries: axial, circumferential, and two helical families with $\alpha_0^k = \pm 45^\circ$.

D. Illustrative Results

1. Altered Flow

It is well accepted that sustained increases (or decreases) in blood flow result in an increased (or decreased) arterial caliber [28–32], often with increased (or decreased) thickening of the wall and possible changes in length [13, 33].

A change in blood flow will have an almost immediate effect on vessel geometry due to smooth muscle relaxation or contraction in response to endothelial production of NO or ET-1, respectively. Of course, smooth muscle can only relax or contract within a certain range. If τ_w^h can be restored by an acute dilation or constriction within the active range of the smooth muscle, no further change in caliber will be observed. In the cases herein, the basilar artery is allowed to accommodate up to a $\sim$3% active dilation and a $\sim$30% active constriction. Figure 2 illustrates the consequences of altered muscle tone as a function of altered flowrate as well as the beginning of G&R as prescribed by the above dependencies of mass density production and removal on changes in wall stress and constrictor concentration. The model captures the maximum dilation and constrictions inherent to smooth muscle due to the prescribed λ_M and λ_0 (table I).

If flow rate is altered beyond a certain threshold, however, the smooth muscle will not be able to restore τ_w^h by a single instantaneous change in diameter. Rather, a

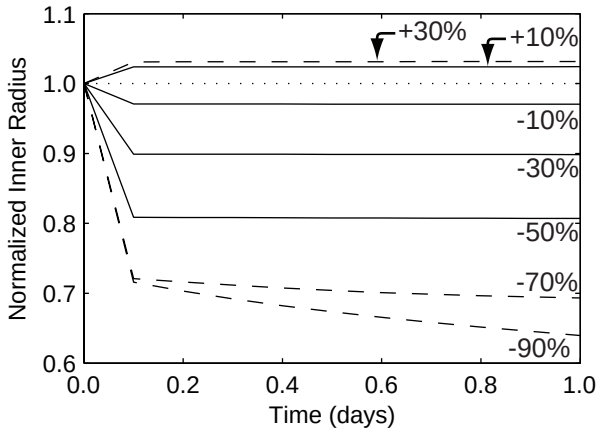

Fig. 2. Numerically instantaneous (i.e. first computational time step) constrictions and dilations for a range of flow rates (shown as ± percent changes from Q_h). Solid lines represent cases in which the instantaneous change in radius returns $\tau_w = \tau_w^h$. Dashed lines represent cases for which the vessel cannot accommodate the altered flow with a single instantaneous constriction or dilation. The dotted line represents the case for which $Q(s) = Q_h$. Note the bias toward constriction rather than dilation, which is consistent with the behavior of cerebral arteries [34]. Also note the clearly defined limit for maximal instantaneous constriction. One can see initial G&R governed changes for large reductions in flowrate (beyond what the vessel can accommodate instantaneously) as a gradual decrease in radius after the step change. A corresponding delayed increase in radius for the 30% increase in flow is not discernible at this short timescale. All parameters $K_\sigma^k = K_C^k = 1$.

Table I. Parameter values used to simulate the response of a basilar artery, which consists primarily of smooth muscle and collagen.

Prestretches and Elastic Parameters
$G_h^e = 1.4, G_h^c = 1.08, G_h^m = 1.2$
$c = 382.4$ kPa
$c_2^c = 22, c_2^m = 3.5$
$c_1^c = 280.2$ kPa, $c_1^m = 36.5$ kPa
Muscle Activation Parameters
$T_{max} = 150$ kPa
$\lambda_M = 1.1, \lambda_0 = 0.4$
$C_B = 0.68, C_S = 20\, C_B$
Initial Mass Fractions and Half-lives
$\phi_0^c = 0.22, \phi_0^e = 0.02, \phi_0^m = 0.76$
$K_h^m = 1/80$ day^{-1}, $K_h^c = 1/80$ day^{-1}

maximum instantaneous dilation or constriction will occur, to be followed by a more gradual convergence via G&R (see equations (2.15) to (2.18) and figures 3 and 4) to the caliber at which shear stress returns to normal. This 2-step change in inner radius is due to reorganization and/or turnover of smooth muscle and collagen (see below) as new constituents are deposited at their homeostatic prestretches, thus allowing further dilation or constriction as needed [6, 22, 35, 36].

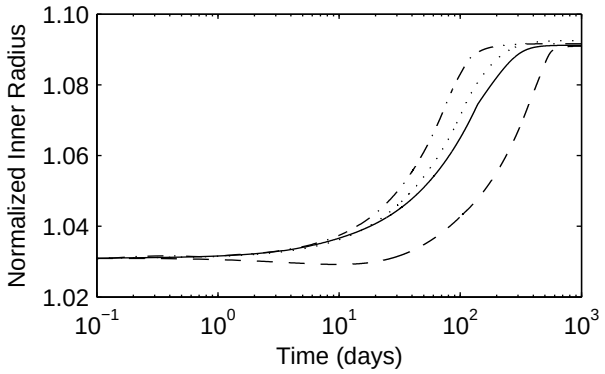

Fig. 3. Normalized inner radius over 1000 days for 30% increases in flow where $K_\sigma^k = K_C^k = 1$ (dotted), $K_\sigma^k = 1$ and $K_C^k = 10$ (dash-dotted), $K_\sigma^k = 10$ and $K_C^k = 1$ (dashed), and $K_\sigma^k = K_C^k = 10$ (solid). Note the dramatically delayed dilation for the case in which $K_\sigma^k > K_C^k$. Note, too that a 30% increase in flow should produce a 9% increase in caliber, which is predicted by the model.

For cases in which reductions in flow were beyond what the extant active muscle could accomodate, predictions suggested that inner radius could be stabilized within 2 weeks (figure 4). The model imposes no upper bound to constrictor concentrations, which in addition to changes in stress can drive substantial instantaneous constrictions and rapid subsequent G&R-driven changes. On the other hand, the lowerbound limit of $C = 0$ means that any G&R-driven dilations beyond that limit must be governed exclusively by changes in stress (see equations (2.14) and (2.16)). Thus, delayed

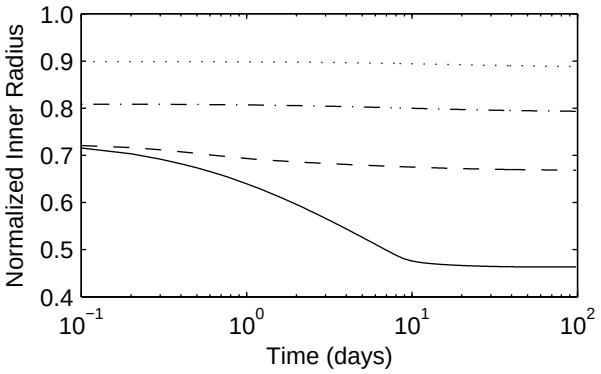

Fig. 4. Normalized inner radius over 100 days for 30% (dotted), 50% (dash-dotted), 70% (dashed), and 90% (solid) reductions in flow. Note the instantaneous constrictions and the marked delayed changes for the case of a 90% reduction in flow. Note, too, that a 90% reduction in flow should produce a 54% decrease in caliber, which is predicted by the model. All parameters $K_\sigma^k = K_C^k = 1$.

dilations occur much more slowly than delayed constrictions (figures 2 and 3) as a consequence of the inherent bias toward constrictors within our relations for mass density production and active muscle behavior, consistent with NO inhibiting and ET-1 promoting turnover. Indeed, increasing flow in adult rabbit carotids by 60% results in no enlargement within 2 months and no changes in thickness or medial cross sectional area [31]. This is consistent with our model's predictions, as inner radius restores wall shear stress only after at least 100 days following a substantial increase in flow.

As inner radius increases (or decreases) to return $\tau_w(s)$ toward its homeostatic target, the mean circumferential stress will initially increase (or decrease) due to the thinning (thickening) of the vessel wall from an isochoric motion. These changes in circumferential stress drive further, albeit perhaps more gradual, G&R and wall thickness continues to change long after the step change in flow (figure 5). Because

τ_w is nearly returned to its homeostatic value almost immediately, this manifestation of G&R occurs more slowly, being driven by changes in circumferential stress without the additive effect of changes in constrictor concentration (figures 6 to 8).

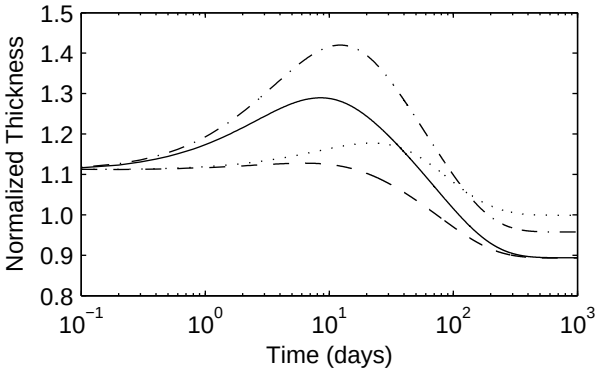

Fig. 5. Normalized wall thickness over 1000 days for a 30% reduction in flow where $K_\sigma^k = K_C^k = 1$ (dotted), $K_\sigma^k = 1$ and $K_C^k = 10$ (dash-dotted), $K_\sigma^k = 10$ and $K_C^k = 1$ (dashed), and $K_\sigma^k = K_C^k = 10$ (solid). The model predicts an initial thickening as the production rate of smooth muscle increases and causes accumulation (figures 6 and 7). After the first week, however, some collagen is degraded, and the wall begins to lose mass. In all cases, wall thickness is stable after ∼500 days, although the expected value (88% of original) is only attained for cases where $K_\sigma^k > 1$.

As the vessel constricts in response to reduced τ_w, collagen fibers are unloaded, and the stresses borne by collagen are drastically reduced. This provides a negative input to the production function (see equation (2.16)); that is, it promotes atrophy. On the other hand, the increase in constrictors (figure 8) provides a positive input to the production rate. Depending on the values of K_C^k and K_σ^k, this dynamic interplay can have drastically different consequences on the simulated morphology and overall wall composition (figure 7). For instance, when $K_\sigma^k = 10$, the negative input from the unloaded collagen serves to effectively halt its production (figure 6 panels b and c).

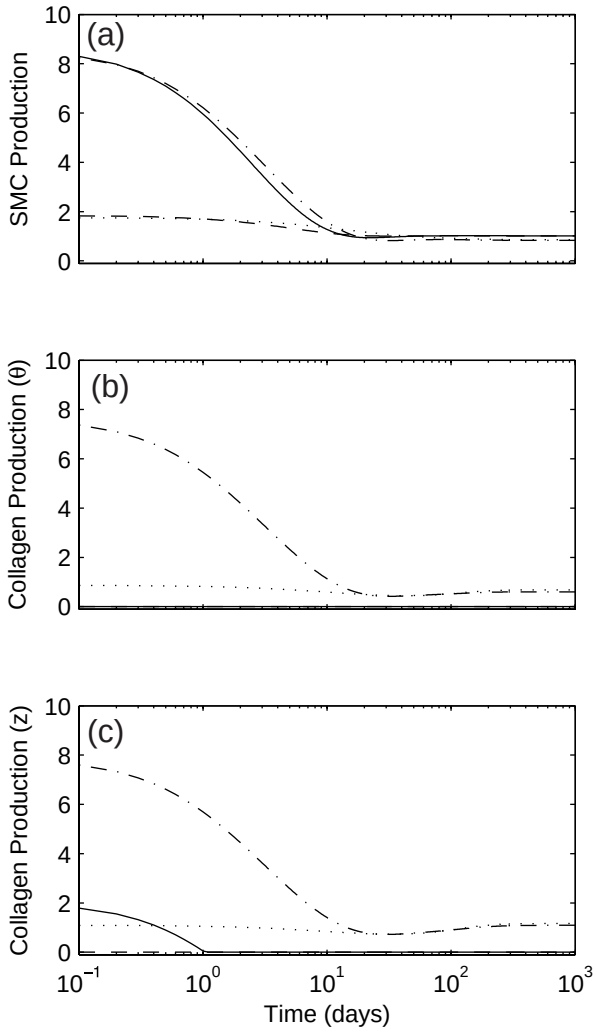

Fig. 6. Time courses of mass density production rates, normalized with respect to homeostatic rates, for smooth muscle (panel a), circumferentially oriented collagen (panel b), and axially oriented collagen (panel c) for a 30% reduction in flow where $K_\sigma^k = K_C^k = 1$ (dotted), $K_\sigma^k = 1$ and $K_C^k = 10$ (dash-dotted), $K_\sigma^k = 10$ and $K_C^k = 1$ (dashed), and $K_\sigma^k = K_C^k = 10$ (solid). Note the rapid (unrealistic) drop in the rate of collagen production for the cases where $K_\sigma^k = 10$. Time courses for helical collagen (not shown) follow the same general trends as axial collagen. Note, too, that fold changes in production rates are within expected ranges [cf. 37].

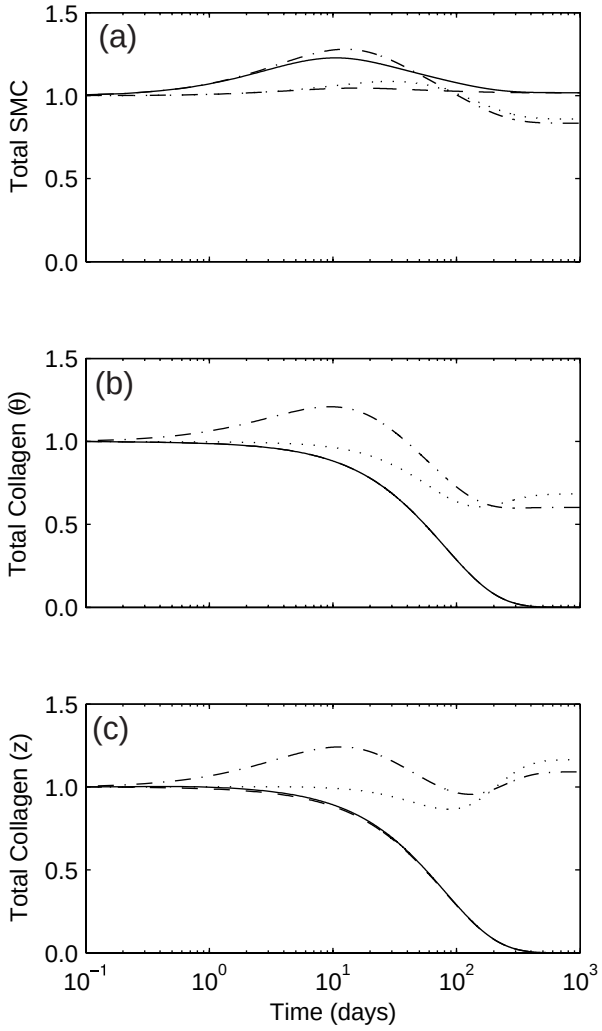

Fig. 7. Time courses of changes in total mass, normalized with respect to homeostatic values, for smooth muscle (panel a), circumferentially oriented collagen (panel b), and axially oriented collagen (panel c) for a 30% reduction in flow where $K_\sigma^k = K_C^k = 1$ (dotted), $K_\sigma^k = 1$ and $K_C^k = 10$ (dash-dotted), $K_\sigma^k = 10$ and $K_C^k = 1$ (dashed), and $K_\sigma^k = K_C^k = 10$ (solid). Note the eventual (unrealistic) complete loss of collagen for the cases where $K_\sigma^k = 10$. The time courses for helical collagen (not shown) follow the same general trends as axial collagen.

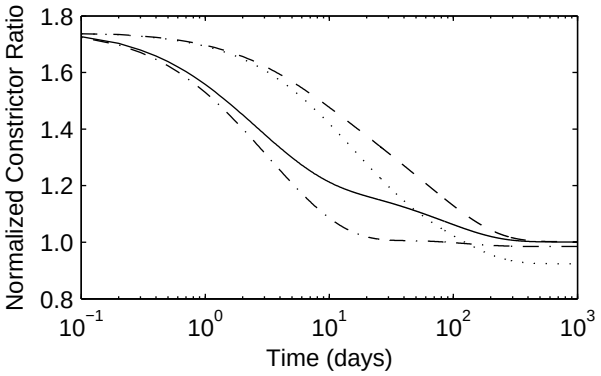

Fig. 8. Time courses of constrictor concentration ratio $C(s)$, normalized with respect to C_B, for a 30% reduction in flow where $K_\sigma^k = K_C^k = 1$ (dotted), $K_\sigma^k = 1$ and $K_C^k = 10$ (dash-dotted), $K_\sigma^k = 10$ and $K_C^k = 1$ (dashed), and $K_\sigma^k = K_C^k = 10$ (solid). Note the return to baseline, but at very different rates depending on the values for the production rate parameters. This emphasizes the complex coupling between endothelial function and wall biomechanics.

Conversely, when $K_C^k \geq K_\sigma^k$, the production rates for collagen increase substantially as the increase in $C(s)$ overwhelms reductions due to stress-mediated mass production. Since smooth muscle can actively generate force, its production rate remains positive. In fact, because muscle is always actively constricting the vessel in cases of reduced flow, its production rates are always above the homeostatic value as both the stress and constrictor levels provide positive inputs into muscle production (figure 6 panel a). Langille *et al.* [30] reported no significant change in medial mass or constituent fraction ratios after one month of reduced flow in carotids. Our results predict little medial remodeling after 30 days (figure 7), consistent with this observation. Although they reported no significant changes in mass or wall constituents, they did report a markedly undulated appearance in internal elastic laminae. This is most likely a result of the unloading of elastin due to the reduced inner radius and is consistent with our hypothesis that elastin does not remodel in adults. Brownlee and Langille

[31] reported that after one week of reduced flow and a subsequent restoration of flow, the vessel reverted to its original caliber. This implicates different and as yet unknown mechanisms for remodeling in cases of increased flow (from normal) versus cases of decreased and subsequent restoration of normal flow. This may be related to the elastin not turning over and retaining its ability to return to its original length without exceeding its homeostatic stress. Our model predicts similar behavior (figure 9).

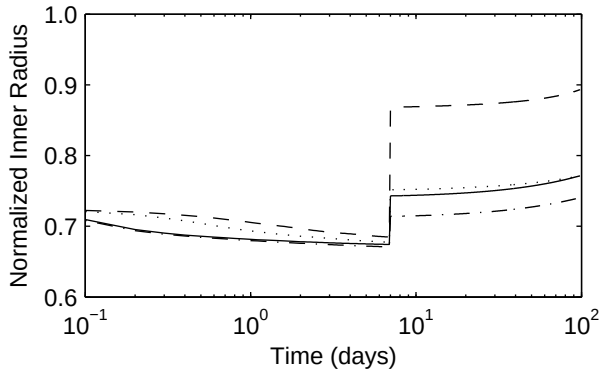

Fig. 9. Normalized inner radius over 100 days for a 70% reduction in flow at day 0 and a restoration of blood flow at day 7 where $K_\sigma^k = K_C^k = 1$ (dotted), $K_\sigma^k = 1$ and $K_C^k = 10$ (dash-dotted), $K_\sigma^k = 10$ and $K_C^k = 1$ (dashed), and $K_\sigma^k = K_C^k = 10$ (solid).

Histological changes in collagen and muscle have measurable mechanical effects on the vessel. The simulated passive response to reduced blood flow involves an initial stiffening, due to a modest increase in muscle deposition, followed by a gradual increase in compliance as the vessel loses circumferential collagen (figure 7). After 1000 days, the vessel is predicted to be slightly more compliant than at day 0 (figure 10 panel a), though this difference would be within experimental noise. In fact, this shift towards compliance is complete after 500 days (not shown) when all parameters $K_\sigma^k = K_C^k = 1$. For cases where $K_\sigma^k \geq K_C^k$, the vessel's eventual shift towards

increased compliance is complete within 300 days (not shown), due to a (unrealistic) nearly complete loss of collagen. This difference in the time to converge on a stable passive mechanical behavior highlights the importance of the parameters within equation (2.16) from the point of view of the time course of the vessel's evolution. Nonetheless, the model predicts a modest passive softening regardless of the values used therein.

Finally, figure 10 panel b shows the evolving active behavior as the vessel accommodates a 30% reduction in flow. Note the rapid leftward shifting of the curve due to smooth muscle being turned over in the new vasoconstricted state. The maximum values for stress are related to evolving constrictor levels (see equation (2.14) and figure 8) as well as the evolving loaded active muscle length $a^{m(act)}(s)$, with increasing constriction occurring in the first 7 days and gradual relaxation occurring as the constrictor levels return to normal. Langille *et al.* [30] observed an early reduction in radius associated with the vasoactive response followed by entrenchment (2 weeks), with the vessel essentially functioning as a smaller vessel after 1 month. After 3 days, papaverine (a vasodilator) was able to reverse the constriction, suggesting that little to no G&R entrenchment had taken place. After 1 week, papavarine was able to reverse only half of the constriction suggesting modest smooth muscle G&R entrenchment had taken place, and after 2 weeks, papavarine was unable to reverse the constriction, suggesting full entrenchment. Similarly, Brownlee and Langille [31] reported fully reversible dilation after 3 days of reduced flow but irreversible vasoactive entrenchment after 1 month. This progression suggests a full shift in contractile response by 2 weeks. Our model predicts comparable time courses (figure 10 panel b). This progression can be observed morphologically since a large nuclear profile in SMCs indicates that SMCs have not yet returned to their normal lengths [30].

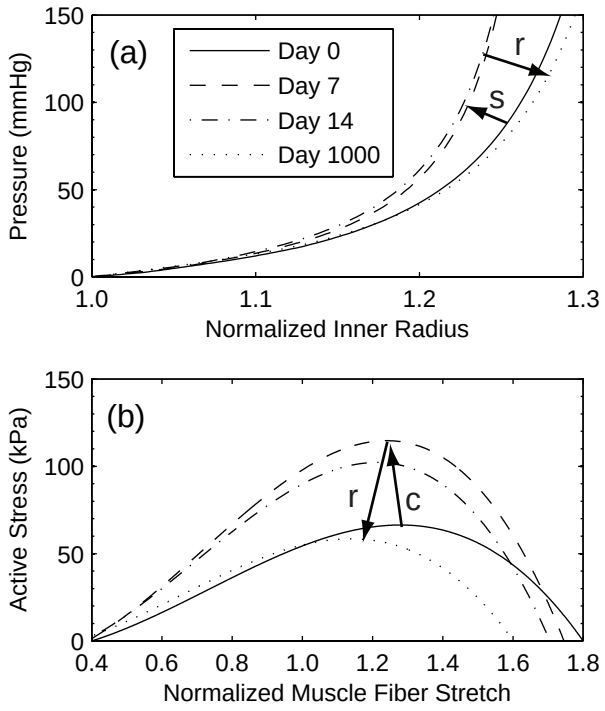

Fig. 10. Evolving passive "pressure-diameter" curves (panel a) at days 0 (solid), 7 (dashed), 14 (dash-dotted), and 1000 (dotted) for a 30% reduction in flow. All parameters $K_\sigma^k = K_C^k = 1$. The abscissa "Normalized Inner Radius" is expressed as the ratio of the current deformed inner radius to the current unloaded inner radius ($a(s)/A(s)$). The rapid initial shift to the left (s) indicates stiffening due to gradual turnover of constituents such as collagen and resultant thickening of the vessel wall in the vasoconstricted state. The gradual rightward shift (r) indicates passive relaxation while the vessel loses mass. Note that after 1000 days, the simulated vessel is slightly more compliant than at day 0, but this would be within experimental noise. Panel b shows predicted shifting of the active muscle response due to G&R at days 0 (solid), 7 (dashed), 14 (dash-dotted), and 1000 (dotted), also for a 30% decrease in flow. The abscissa "Normalized Muscle Fiber Stretch" is expressed as a range of values for $\lambda_\theta^{m(act)}(s)\, a^{m(act)}(s)/a^{m(act)}(0)$. Increasing constriction (c) occurs over the first 7 days followed by a gradual relaxation (r) as the constrictor levels return to normal.

2. Altered Pressure

The most conspicuous consequence of hypertension in arteries is a thickening of the wall that tends to restore the circumferential stress toward its normal value [38–42]. This is a more delayed manifestation of vascular adaptation compared to the instantaneous reduction in caliber observed in the case of reduced flow simply because the vessel must accumulate mass over some period. In the case of an increase of transmural pressure, the vessel instantaneously distends due to the gross passive behavior of the mixture (figure 11 panel a). All constituents thus initially support greater loads, causing $\Delta\sigma$ to increase. In addition, the increase in inner radius results in a decrease in τ_w and an associated increase in $C(t)$. These effects work synergistically to increase mass production (figure 12), resulting in mass accumulation (figure 13) and wall thickening (figure 11 panel b). Note the trend for the wall to thicken by nearly 50% for a 50% increase in pressure, which is consistent with expectations based on a simple force balance.

The predicted accumulation of collagen is qualitatively similar to observed morphological changes in basilar arteries [cf. figure 6 in 41] and causes irreversible passive stiffening (figure 14 panel a). Our model predicts stiffening within 2 weeks, with only modest subsequent stiffening to day 100. Similar behavior has also been observed within 2-4 weeks in basilar arteries in animal models [41, 42]. The model also predicts a negligible change in the active muscle length (figure 14 panel b), as the inner diameter changes only slightly, with maximum active stresses varying with $C(s)$ (figure 15). The values for K_σ^k and K_C^k again had large influences on the various predicted time courses. Clearly, production rates are directly proportional to these parameters; higher values result in accelerated changes in morphology and geometry.

Changes in unloaded length have been reported with decreasing longitudinal re-

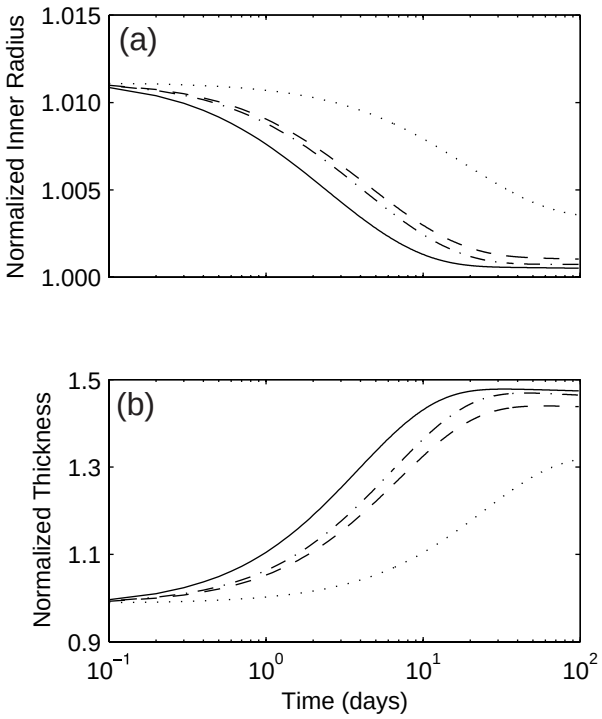

Fig. 11. Geometric changes over 100 days in normalized radius (panel a) and thickness (b) in response to a 50% increase in pressure where $K_\sigma^k = K_C^k = 1$ (dotted), $K_\sigma^k = 1$ and $K_C^k = 10$ (dash-dotted), $K_\sigma^k = 10$ and $K_C^k = 1$ (dashed), and $K_\sigma^k = K_C^k = 10$ (solid). The inner radius initially increases due to the passive response to an increase in pressure, but the vessel can largely recover its inner radius within 2 weeks in order to restore τ_w^h. Wall thickness increases as collagen and smooth muscle are deposited in response to increased circumferential stresses. The vessel can also attain a stable wall thickness within 2 weeks.

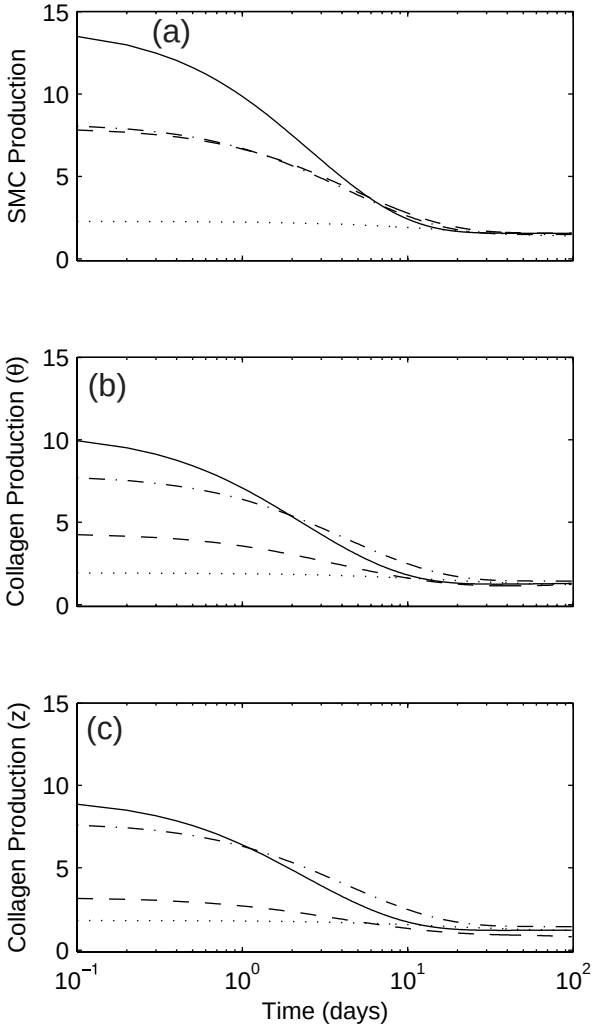

Fig. 12. Time courses of mass density production rates, normalized with respect to the homeostatic rates, for smooth muscle (panel a), circumferentially oriented collagen (panel b), and axially oriented collagen (panel c) for a 50% increase in pressure where $K_\sigma^k = K_C^k = 1$ (dotted), $K_\sigma^k = 1$ and $K_C^k = 10$ (dash-dotted), $K_\sigma^k = 10$ and $K_C^k = 1$ (dashed), and $K_\sigma^k = K_C^k = 10$ (solid). Time courses for helical collagen (not shown) follow the same general trends as axial collagen.

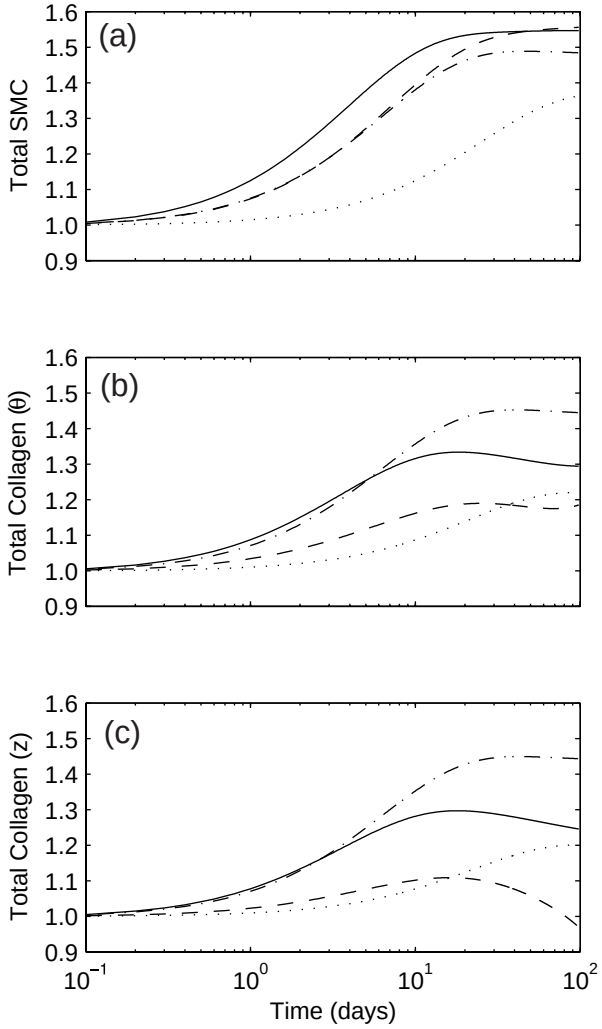

Fig. 13. Time courses of total mass, normalized with respect to the homeostatic masses, for smooth muscle (panel a), circumferentially oriented collagen (panel b) and axially oriented collagen (panel c) for a 50% increase in pressure where $K_\sigma^k = K_C^k = 1$ (dotted), $K_\sigma^k = 1$ and $K_C^k = 10$ (dash-dotted), $K_\sigma^k = 10$ and $K_C^k = 1$ (dashed), and $K_\sigma^k = K_C^k = 10$ (solid). Note the accumulation of mass for almost all fiber families. The time courses for helical collagen (not shown) follow the same general trends as axial collagen.

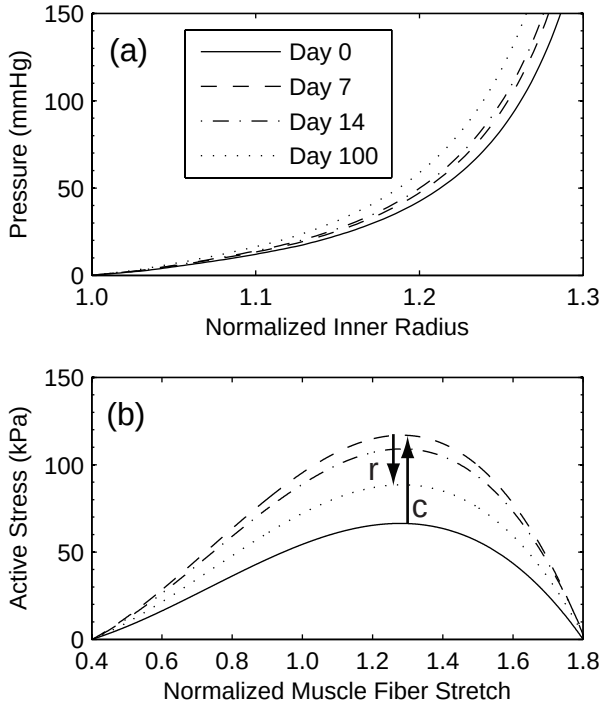

Fig. 14. Evolving passive "pressure-diameter" curves (panel a) at days 0 (solid), 7 (dashed), 14 (dash-dotted), and 100 (dotted) for a 50% increase in transmural pressure. All parameters $K_\sigma^k = K_C^k = 1$. The abscissa "Normalized Inner Radius" is expressed as the ratio of the current deformed inner radius to the current unloaded inner radius ($a(s)/A(s)$). The irreversible shift to the left indicates stiffening due to gradual accumulation of constituents as the vessel wall thickens in response to increased circumferential stress. Panel b shows predicted shifting of active muscle response due to G&R at days 0 (solid), 7 (dashed), 14 (dash-dotted), and 100 (dotted), also for a 50% increase in pressure. The abscissa "Normalized Muscle Fiber Stretch" is expressed as a range of values for $\lambda_\theta^{m(act)}(s)\, a^{m(act)}(s)/a^{m(act)}(0)$. Note the very modest shifting of the curve, due to a correspondingly modest change in vessel radius. The maximum values for stress are related to evolving constrictor levels (see equation (2.14) and figure 15). The "residual" elevation in active stress may reflect the lower NO production reported in hypertension and often referred to as "endothelial dysfunction."

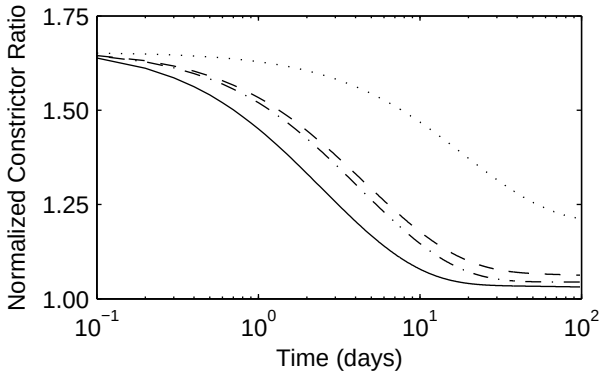

Fig. 15. Time courses of constrictor concentration ratio $C(s)$, normalized with respect to C_B, for a 50% increase in pressure where $K_\sigma^k = K_C^k = 1$ (dotted), $K_\sigma^k = 1$ and $K_C^k = 10$ (dash-dotted), $K_\sigma^k = 10$ and $K_C^k = 1$ (dashed), and $K_\sigma^k = K_C^k = 10$ (solid). The early vasoconstriction offsets the initial increased elastic distension [11].

tractions in hypertensive canine aorta [43]. Our model predicts an increased unloaded length and inner radius with time (figure 16), which is qualitatively consistent with this observation. These changes are related to the quantities in axially and circumferentially oriented collagen, as collagen's smaller prestretch serves to restrict the retractive effects of elastin.

E. Discussion

We have learned much about the biomechanics of the arterial wall over the past four decades [cf. 2, 44], yet we are just beginning to understand and quantify the remarkable ability of arteries to adapt in response to altered mechanical loading. For example, arteries increase in caliber in response to increased flow, they thicken in response to increased pressure, and they lengthen in response to increased axial loading [e.g., see 28, 30, 38, 39, 45, 46].

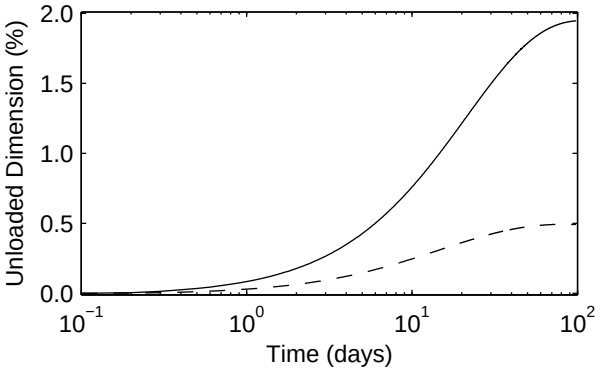

Fig. 16. Time courses of percent changes in unloaded axial length (solid) and unloaded inner radius (dashed) for a 50% increase in transmural pressure. All parameters $K_\sigma^k = K_C^k = 1$.

It is instructive to consider simple geometric implications of stress-mediated G&R in response to altered flow and pressure [47]. Let homeostatic values be given by

$$\tau_w^h = \frac{4\,\mu\,Q_h}{\pi\,a_h^3}, \quad \sigma_\theta^h = \frac{P_h\,a_h}{h_h}, \tag{2.22}$$

and consider a step-change to new values of flow and pressure via $Q = \varepsilon\,Q_h$ and $P = \gamma\,P_h$. Hence, if both wall shear and circumferential stress are returned toward homeostatic values, then

$$\tau_w = \frac{4\,\mu\,(\varepsilon\,Q_h)}{\pi\,a^3} \to \frac{4\,\mu\,Q_h}{\pi\,a_h^3}, \tag{2.23}$$

$$\sigma_\theta = \frac{\gamma\,P_h\,a}{h} \to \frac{P_h\,a_h}{h_h}, \tag{2.24}$$

or $a \to \varepsilon^{1/3}\,a_h$ and $h \to \gamma\,(a/a_h)\,h_h = \gamma\,\varepsilon^{1/3}\,h_h$. In other words, we see that changes in flow affect both wall shear stress and circumferential stress, and thus both luminal radius and wall thickness, provided the vessel attempts to restore these stresses to normal. As seen in figures 2 to 5 and 11, the present simulations predict this trend,

and, as noted in the figure captions, provide the correct degree of change (e.g. $a = (0.7)^{1/3}\, a_h = 0.88\, a_h$ for a 30% reduction in flow).

Whereas these simple results suggest what should happen, the G&R framework addresses how these changes can occur. Our model predicts changes in geometry, structure, and mechanical behavior as natural consequences of biochemomechanically mediated G&R and the need to satisfy equilibrium at each G&R time. This is in contrast to other models that prescribe changes in geometry, properties, and/or constituent mass fractions as functions of time or evolving stress differences [4–6, 48]. Thus, our approach allows for a more realistic framework in which to model vascular G&R. Also, in contrast to previous work [e.g., 6], where the focus was on modeling geometric and morphological changes as functions of nondimensional time, we have also extended the constrained mixture approach to occur continuously in actual time.

Although we focused on the basilar artery, we did not attempt to model any one experimental data set from the literature (largely because no single study provides data sufficient for detailed modeling). Nevertheless, the current predictions represent a marked improvement over prior models in capturing salient features of flow and pressure induced adaptations in diverse arteries. Predictions show the importance of combined effects of altered vasoactivity and matrix turnover [cf. 3, 40], including potential differences between the initial extents of vasodilatation and vasoconstriction; they show that adaptations can occur faster in cases of decreased compared to increased flow [cf. 31]; they show that wall shear stress can be restored to normal faster than intramural stress in cases of increased flow [cf. 49]; they show that active length-tension behaviors can evolve but be restored at a different diameter due to adaptations [cf. 30]; and they show that inner radius remains constant while wall thickness increases and thus circumferential wall stress normalizes within a few weeks in cases of increased pressure [cf. 40, 41, 50, 51]. Indeed, by yielding reasonable time

courses, in days to weeks or months, the current predictions suggest that complete adaptations may take longer than studied in some animal models. For example, Kamiya and Togawa [28] reported carotid adaptations to increased flows at 6 to 8 months and suggested "an incomplete regulatory response to this extreme stress", that is, to flows more than 4-fold higher than normal. Rather than an "inherent limitation of the adaptive capacity" it may well be that longer times would be needed to achieve a complete adaptation for such a large perturbation.

Notwithstanding the ability of the current model to capture many observed features of flow and pressure induced remodeling in an artery, it cannot do so with a single set of model parameters. Therefore, there remains a pressing need for better constitutive relations for G&R and the data upon which they must be based. In particular, there is a need for more data on the time courses of stress-mediated alterations in cell proliferation and apoptosis as well as the synthesis and degradation of extracellular matrix. That is, although we know that the expression of growth factors, cytokines, and MMPs change significantly during adaptations to altered hemodynamics [e.g. 37, 52–55], much remains unknown with regard to specific molar changes and the degree to which these affect cell activity. There is similarly a need for quantitative relationships that describe the multi-functional effects of vasoactive molecules. For example, we know that NO promotes endothelial cell proliferation while inhibiting both smooth muscle proliferation and its synthesis of matrix [23, 56], but we lack precise empirical correlations for the extent of such changes as a function of shear induced changes in the concentration of NO. Similarly, we know that ET-1 promotes smooth muscle proliferation and its synthesis of matrix [24, 57], but we lack precise relations in terms of shear induced changes in the concentrations of ET-1. There is also a need to quantify relative changes in cell and matrix turnover in response to altered shear versus intramural stress. For example, decreased flow downregulates NO

and upregulates ET-1, both of which should increase intramural production rates. Yet, the associated decrease in radius and initial isochoric increase in thickness due to vasoconstriction at a constant pressure will decrease intramural stress and thereby should decrease intramural production rates. We must understand better how specific changes in vasoactive concentrations and degrees of wall stress collectively control rates of turnover.

Once additional biochemical information is available, we could employ full mixture equations for mass balance whereby the arterial wall can consist of N distinct types of constituents, n of which are structurally significant (e.g., elastin, fibrillar collagens, smooth muscle). Separate mass balance equations for the $N-n$ soluble (e.g., nitric oxide, endothelin-1, growth factors) constituents $i = 1, 2, \ldots, N-n$ and the n insoluble (structural) constituents $k = 1, 2, \ldots, n$ can then be written as

$$\frac{\partial \rho^i}{\partial s} + \mathrm{div}(\rho^i \, \mathbf{v}^i) = \widetilde{m}^i, \quad \frac{\partial \rho^k}{\partial s} + \mathrm{div}(\rho^k \, \mathbf{v}^k) = \widetilde{m}^k. \tag{2.25}$$

Here, ρ^α ($\alpha = i$ or k) are constituent (apparent) mass densities, $\mathbf{v}^\alpha$ are velocities, and $\widetilde{m}^\alpha$ are net mass density productions. Consistent with the above, we could consider quasi-static deformations whereby the velocity of the arterial wall $\mathbf{v}$ is negligible. If we then invoke usual assumptions for dilute solutes (e.g., Fick's law of diffusion), the first of these two mass balance relations reduces to the standard reaction-diffusion equation

$$\frac{\partial C^i}{\partial s} = R^i + D^i \, \nabla^2 C^i, \tag{2.26}$$

where C^i is the molar density for constituent i [58], which is obtained from the mass density via the molecular weight, R^i are reactions related to the net productions/losses, and D^i are diffusivities. The diffusion term is important in 3-D problems, but less so for 2-D analyses of the arterial wall. Regardless, one could then use indi-

vidual values of C^i in the appropriate mass density production and removal functions (cf. equations (2.16) and (2.17)). As noted, however, this will require significantly more information on the specific biological responses.

Finally, we emphasize that constitutive relations do not describe a material (or cell activity) per se; rather, they describe responses by a tissue or cell to particular stimuli under specific conditions of interest. It is thus unreasonable to expect that a single kinetic relation for mass density production or mass removal will model all responses of a vascular cell to all stimuli. With regard to the present discussion, we note that extreme increases in flow from normal could induce endothelial damage [59] whereas extreme decreases in flow, including cessation of flow, could cause endothelial cells to upregulate adhesion molecules that capture circulating monocytes and promote local inflammatory processes or atherogenesis. Our current illustrative forms for mass density production and removal are not intended to capture such extremes. Likewise significant differences are expected during the progression from development to maturity and aging; such differences were not addressed herein. For example, adaptations to increased blood flow are faster in younger compared to older animals [e.g. 31, 60], but we did not attempt to account for such differences. Indeed, there is a need to determine if such differences are due primarily to higher basal turnover rates in younger animals [cf. 19] or if the basic functional forms of the kinetic relations change with age. Finally, there is a need to delineate differences in response by elastic versus muscular arteries, intracranial versus extracranial, and systemic versus pulmonary. Fortunately, it appears that the same fundamental hypotheses and theoretical framework hold for diverse vessels.

In summary, the present theoretical framework for arterial growth and remodeling and illustrative constitutive relations yield predictions similar to many observations reported in the literature. Nevertheless, there is a continued need for more

data and better constitutive relations so that models can not only capture the consequences of growth and remodeling, but also the mechanisms by which such changes occur. For purposes of illustration, we employed simple descriptions of wall mechanics and hemodynamics. Such simplicity can represent the situation in a straight cylindrical region such as the basilar artery, but more importantly it is a prudent way to test basic concepts and to build intuition. One obvious advantage of this type of model is the ease with which various hypotheses can be proposed and tested. For example, results for a 30% reduction in flow suggest that this model is very sensitive to values of K_σ^k and K_C^k (figures 6 and 7). This calls into question the relative roles of smooth muscle and collagen in cases of large reductions in flow. These results may motivate experiments to determine actual morphological changes, thus narrowing the range of values for the parameters used in this model. Nevertheless, given our growing understanding of modeling arterial mechanobiology and the associated growth and remodeling mechanics, there is a need to begin to move toward more complex situations wherein actual hemodynamics and wall mechanics can be solved together. See Humphrey and Taylor [9] for a description of one such approach.

CHAPTER III

MODELING EFFECTS OF AXIAL EXTENSION ON ARTERIAL GROWTH AND REMODELING

A. Overview

Diverse mechanical perturbations elicit arterial growth and remodeling responses that appear to optimize structure and function so as to achieve mechanical homeostasis. For example, it is well known that functional adaptations to sustained changes in transmural pressure and blood flow primarily affect wall thickness and caliber to restore circumferential and wall shear stresses toward normal. More recently, however, it has been shown that changes in axial extension similarly prompt dramatic cell and matrix reorganization and turnover, resulting in marked changes in unloaded geometry and mechanical behavior that presumably restore axial stress toward normal. Because of the inability to infer axial stress from *in vivo* measurements, simulations are needed to examine this hypothesis and to guide the design of future experiments. In this paper, we show that a constrained mixture model predicts salient features of observed responses to step increases in axial extension, including marked increases in fibrous constituent production, leading to a compensatory lengthening that restores original mechanical behavior. Because axial extension can be modified via diverse surgical procedures, including bypass operations and exploited in tissue regeneration research, there is a need for increased attention to this important aspect of arterial biomechanics and mechanobiology.

B. Introduction

Considerable evidence now suggests a fundamental role for axial wall stress in

compensatory arterial adaptations to genetic defects and diverse perturbations in mechanical loading. It has been suggested, for example, that an artery may have more control over its local axial force than it does over local blood flow and pressure, which are dictated largely by proximal cardiac output and distal resistance vessels, and that it may exploit this local capability to regulate stress-mediated changes in geometry or structure that tend to achieve or restore mechanical homeostasis [61]. Much of the renewed interest in axial behaviors was motivated by the provocative finding reported by Jackson *et al.* [45]†. Briefly, they showed, in a rabbit model, that extending common carotid arteries well beyond their *in vivo* length causes them to grow lengthwise and remodel rapidly because "arterial tissue, especially extracellular matrix, accumulated at a nearly unprecedented rate after axial strain was imposed." Moreover, they suggested that this remodeling appeared to be stimulated primarily by the imposed change in axial stress or stretch, not related changes in pressure-induced circumferential stress or flow-induced wall shear stress. In other words, changes in axial stress or stretch appear to be strong stimuli for significant arterial growth and remodeling (G&R); they even appear to affect the orientation of the mitotic axis of the smooth muscle cells, which in turn likely affects the orientation at which newly produced collagen is incorporated within extant matrix [3].

Gleason and Humphrey [36] used both a standard stress analysis and a simple model of arterial G&R to study numerically the experiment reported by Jackson and colleagues. Briefly, using a 3-D analysis that included complexities related to residual stresses and nonlinearly anisotropic material behaviors, they confirmed that imposed axial extensions at physiologic pressures affect primarily the axial, not circumferential, stress and that the transmural distributions of stress remain nearly uniform. This

†We are saddened to acknowledge the untimely passing of Prof. B. L. Langille (October 29$^{\text{th}}$, 2008), a true pioneer in studies of arterial adaptation.

finding motivated the use of a 2-D constrained mixture model that accounted for different material properties, natural (stress-free) configurations, and constant rates of turnover of structurally significant passive constituents at constant rates. It appears, however, that rates of turnover - both for constituent production and removal - can change throughout stress-mediated adaptations [e.g., 37, 55, 62] and vasoactivity plays an important complementary role in many cases [3, 47, 63].

In this paper, therefore, we revisit the class of experiments reported by Jackson and colleagues and employ an extended constrained mixture model that includes potentially complementary effects of vasoactivity and matrix turnover as well as functions for mass production and removal that depend on changing differences in biaxial intramural and wall shear stresses from homeostatic targets [64]. Moreover, rather than study the carotid artery, we consider a model intracranial (basilar) artery, which has a much lower percentage of elastin than central arteries such as the carotids and aorta and consequently a lower value of homeostatic axial prestretch. Although structurally significant elastin does not turnover in maturity, it nonetheless appears to play a key role in governing axial mechanical properties, including axial prestretch [65]. Flow-induced changes in axial stretch have also been reported in the basilar artery [13], again emphasizing the potentially fundamental role of axial behaviors in many different cases of arterial adaptation.

C. Methods

Following Baek *et al.* [22] and Valentín *et al.* [63], we model the basilar artery as a thin walled axisymmetric cylindrical pressure vessel. Hence, mean circumferential and axial Cauchy stresses are

$$\sigma_\theta(s) = \frac{P(s)\, a(s)}{h(s)}, \tag{3.1}$$

$$\sigma_z(s) = \frac{f(s)}{\pi\, h(s)\,(2\,a(s) + h(s))}, \tag{3.2}$$

where P is the transmural pressure, a is the current inner radius, h is the current thickness, and f is the applied axial force at G&R time s. These equilibrium equations can be combined with constitutive relations for the principal Cauchy stress resultants $T_i = \sigma_i\, h$, where $i = z, \theta$ and, by the rule of mixtures, the stored energy function for the artery $W = \sum W^k$ for $k = 1, 2, \ldots n$ families of structurally significant constituents. Hence, we have at any G&R time s [2, 66]

$$P(s)\, a(s) = T_\theta(s) = \frac{1}{\lambda_z(s)} \sum \frac{\partial W^k(s)}{\partial \lambda_\theta(s)} + \sigma_\theta^{act}(s)\, h(s), \tag{3.3}$$

$$\frac{f(s)}{\pi\,(2\,a(s) + h(s))} = T_z(s) = \frac{1}{\lambda_\theta(s)} \sum \frac{\partial W^k(s)}{\partial \lambda_z(s)}, \tag{3.4}$$

where λ_θ and λ_z are stretches for the artery and σ_θ^{act} is the stress actively generated by smooth muscle, which is prescribed as a function of vasoactive molecule concentration C and muscle fiber stretch [22, 63, 64, 67], namely

$$\begin{aligned} \sigma_\theta^{act}(s) = T_{max}\, \phi^m(s)\, \left(1 - e^{-C(s)^2}\right) \\ \times\, \lambda_\theta^{m(act)}(s)\, \left[1 - \left(\frac{\lambda_M - \lambda_\theta^{m(act)}(s)}{\lambda_M - \lambda_0}\right)^2\right], \end{aligned} \tag{3.5}$$

where T_{max} is a scaling parameter with units kPa, ϕ^m is the evolving mass fraction of active smooth muscle, λ_M is the stretch at which the active force generating capability is maximum, λ_0 is the stretch at which muscle cannot generate any force, and $\lambda_\theta^{m(act)}(s)$ is the current active muscle fiber stretch.

With regard to passive properties, structurally significant collagen and smooth muscle turnover continuously, that is, they are continuously produced (via synthesis or proliferation) and removed (via degradation or apoptosis). Noting that constitutuents only carry load as long as they exist, we let the evolving strain energy function for

constituent k be written as [63]

$$W^k(s) = \frac{M^k(0)}{\rho(s)}\, Q^k(s)\, \widehat{W}^k\left(\mathbf{F}^k_{n(0)}(s)\right) + \int_0^s \frac{m^k(\tau)}{\rho(s)}\, q^k(s,\tau)\, \widehat{W}^k\left(\mathbf{F}^k_{n(\tau)}(s)\right)\, d\tau, \tag{3.6}$$

where $M^k(0)$ are initial mass densities, $Q^k(s) \in [0,1]$ are fractions of material produced at or before time $s = 0$ that survive to current time s, $m^k(\tau)$ are mass density production rate functions, and $q^k(s,\tau) \in [0,1]$ are fractions of material produced at any past time $\tau \in [0,s]$ that survive to current time s. Note, therefore, that prior to G&R (i.e., at $s = 0$), the standard mass-averaged rule of mixtures is recovered as it should be. Note, too, that the individual stored energy functions depend on individual, constituent dependent deformations, namely $\mathbf{F}^k_{n(\tau)}(s) = \partial \mathbf{x}^k(s)/\partial \mathbf{X}^k(\tau)$, the 2-D deformation gradient tensor for constituent k, subject to the kinematic constraint $\mathbf{x}^k(s) = \mathbf{x}(s)$ that all constituents deform together despite individual natural (stress-free) configurations $\mathbf{X}^k(\tau)$ being allowed to evolve separately.

The membrane assumption and assumed loading allows us to write all deformations in terms of stretches. The total stretch experienced at G&R time s by a fibrillar constituent k deposited at time τ is

$$\lambda^k_{n(\tau)}(s) = G^k_h\, \frac{\lambda(s)}{\lambda(\tau)}, \tag{3.7}$$

with

$$\lambda(\tau) = \sqrt{\lambda^2_z(\tau)\, \cos^2(\alpha^k_0) + \lambda^2_\theta(\tau)\, \sin^2(\alpha^k_0)} \quad \forall\, \tau \in [0,s], \tag{3.8}$$

where α^k_0 denotes the angle between a fiber and the the artery's axial (z) direction. These kinematic relations represent a series of multiplicative deformations and are discussed in detail by Baek *et al.* [16]. Note, too, that G^k_h is the deposition stretch

for the k^{th}; it represents the fundamental hypothesis that synthetic cells produce and deposit new constituents within the existing extracellular matrix at preferred mechanical states [64].

As in previous constrained mixture implementations [22, 63], we modeled the passive mechanical response of elastin using a neo-Hookean strain energy function [17, 18]

$$\widehat{W}^e(s) = c\left(\lambda_\theta^e(s)^2 + \lambda_z^e(s)^2 + \frac{1}{\lambda_\theta^e(s)^2\,\lambda_z^e(s)^2} - 3\right), \tag{3.9}$$

where $\lambda_\theta^e(s) = \tilde{G}_h^e\,\lambda_\theta(s)$ and $\lambda_z^e(s) = \tilde{G}_h^e\,\lambda_z(s)$ are the stretches experienced by elastin, which can be determined from arterial stretches $(\lambda_\theta(s), \lambda_z(s))$ and "growth-induced" prestretches $\tilde{G}_h^e$ [68]. Note that the total stretches experienced by elastin do not depend on deposition time τ. This assumption reflects the observation that elastin is not continually produced in maturity as are collagen and smooth muscle. In contrast, functional elastin is produced and cross-linked exclusively during the perinatal period, and subsequently stretched elastically throughout normal development and maturation [65]. Finally, we employed Fung exponential strain energy functions for both collagen [18, 69]

$$\widehat{W}^c(s) = c_1^c\left(e^{c_2^c\left(\lambda^c_{n(\tau)}(s)^2-1\right)^2} - 1\right), \tag{3.10}$$

and passive smooth muscle [6]

$$\widehat{W}^m(s) = c_1^m\left(e^{c_2^m\left(\lambda^m_{n(\tau)}(s)^2-1\right)^2} - 1\right). \tag{3.11}$$

The stretch $\lambda^k_{n(\tau)}(s)$ experienced by each of these constituents depends on its deposition stretch, and the stretch experienced by the arterial wall from deposition time τ to current G&R time s, as described by equation (3.7). We allow four fiber families of collagen, oriented axially, circumferentially, and helically [18, 22, 63]. Table II lists

values of the associated material parameters.

Table II. Important parameter values used to model a representative mature basilar artery, before any perturbation.

Role	*Value*
Geometry/Loads	$a_h = 1.42$ mm, $h_h = 0.176$ mm
	$P = 93$ mmHg, $Q = 3.075$ ml/s, $\tau_w^h = 5.06$ Pa
	$\sigma_\theta^h = \sigma_z^h = 100$ kPa
Mass Kinetics	$\phi_0^c = 0.22, \phi_0^e = 0.02, \phi_0^m = 0.76$
	$K_{qh}^m = 1/80$ day^{-1}, $K_{qh}^c = 1/80$ day^{-1}
Vasoactivity	$T_{max} = 150$ kPa
	$\lambda_M = 1.1$, $\lambda_0 = 0.4$
	$C_B = 0.68, C_S = 20\, C_B$
Passive Elasticity	$c = 588.3$ kPa, $c_1^c = 560.4$ kPa, $c_1^m = 36.5$ kPa
	$c_2^c = 22$, $c_2^m = 3.5$
	$\tilde{G}_h^e = 1.4, G_h^c = 1.08, G_h^m = 1.2$

It is well known that vascular smooth muscle cells and fibroblasts actively produce and organize new extracellular matrix proteins and glycoproteins in response to altered stretch and/or stress [70]. Moreover, endothelial cells change their production of vasoactive molecules in response to changes in wall shear stress [71], which in turn affects rates of matrix production [23, 24]. Hence, we prescribe the following constitutive relation for mass density productions [63]

$$m^k = m_0^k(1 + K_\sigma^k\, \Delta\sigma + K_C^k\, \Delta C), \tag{3.12}$$

where $\Delta\sigma$ and ΔC are normalized changes in constituent fiber stresses and the net

ratio of constrictors to dilators from their homeostatic values, respectively. The former vary with changes in transmural pressure and vasoactivity whereas the latter are functions of wall shear stress [cf. 4], namely

$$C(s) = C_B - C_S \left(\frac{\tau_w(s) - \tau_w^h}{\tau_w^h} \right), \tag{3.13}$$

where $\tau_w(s)$ and τ_w^h are current and homeostatic wall shear stresses, respectively, with $\tau_w(s) = 4\,\mu\,Q/\pi\,a^3(s)$, where μ is viscosity and Q is blood flow, and C_B is the basal concentration and C_S is a shear stress sensitivity factor. equation (3.12) recovers basal rates of mass production m_0^k under homeostatic conditions ($\Delta\sigma = \Delta C = 0$) as it should.

It is generally accepted that degradation of extracellular matrix follows a first order type kinetics [72]. Hence, removal rates are prescribed herein as [cf. 22, 63]

$$q^k(s,\tau) = e^{-\int_\tau^s K_q^k(\widetilde{\tau})\,d\widetilde{\tau}}, \tag{3.14}$$

where $K_q^k(\widetilde{\tau})$ are rate-type parameters for mass removal having units of days^{-1}. Among others, Willett *et al.* [73] show that degradation rates depend on stress level. Hence, these rate parameters, in turn, are prescribed as $K_q^k(\widetilde{\tau}) = K_{qh}^k + K_{qh}^k\,|\Delta\zeta(\widetilde{\tau})|$, where K_{qh}^k is a basal value, $\Delta\zeta(\widetilde{\tau})$ is the difference in fiber tension from its homeostatic value, and $\zeta^{k(\tau)}$ is the level of tension on constituent k that was produced at time τ [63]. This formulation results in accelerated constituent removal (degradation) for altered levels of tension. Table II lists values for these and many other parameters, including constituent prestretches and homeostatic mass fractions and half-lives.

By prescribing *in vivo* axial length l, transmural pressure P, and volumetric flowrate Q at all G&R times s, we can calculate the evolving inner radius via equation (3.3); we can also calculate evolving wall thickness given the assumption that overall mass density $\rho(s) \equiv \rho(0)\ \forall s$. Additional details of the implementation and

associated fundamental assumptions are discussed elsewhere [22, 63, 64, 67]. Herein, we prescribe step increases in *in vivo* axial length $l = \delta\, l_h$, where l_h is the homeostatic length, and investigate subsequent G&R-governed evolution of the wall.

D. Illustrative Results

Consistent with values reported by Wicker *et al.* [27], the model basilar artery (at $s = 0$) exhibited an *in vivo* axial stretch $l_h/L(0) = 1.24$ and an associated axial force of 3.68 mN at homeostatic conditions. While maintaining constant (homeostatic) transmural pressure ($P = 93$mmHg) and flow ($Q = 3.075$ml/s), we prescribed 1 to 5 percent step increases in *in vivo* axial extension at G&R time $s = 0$ (with $K_i^k = 0.1$, see equation (3.12)) to initiate the evolution of arterial geometry and properties. Instantaneous reductions in caliber and thickness due to isochoric motion were small, and thereafter the artery maintained its inner radius to within 1% of its preferred value despite non-monotonic changes that peaked near day 40 (figure 17, panel a). This negligible (i.e., not measurable clinically) change in inner radius and thus wall shear stress suggests that axial stretch-induced G&R is primarily an intramural stress-dominated process consistent with the original interpretation of Jackson *et al.* [45]. Changes in wall thickness (figure 17, panel b) were more pronounced, however. The wall instantaneously thinned isochorically and continued to thin as original material, deposited before time $s = 0$, degraded under the higher axial fiber tensions (see equation (3.14)). This atrophy resulted in a slight distending trend (due to decreased structural stiffness at constant pressure) until approximately day 40 (figure 17, panel a). After day 40, the model predicted increasing thicknesses, indicating that mass production outpaced mass removal. Indeed, despite sustained elevated rates of collagen production (figure 18, panel a), total axial and helical collagen masses decreased

until approximately day 40 (figure 18, panel b). The evolving collagen to elastin ratio (figure 18, panel c) further revealed a biphasic evolution process, that is, competition between altered production and removal.

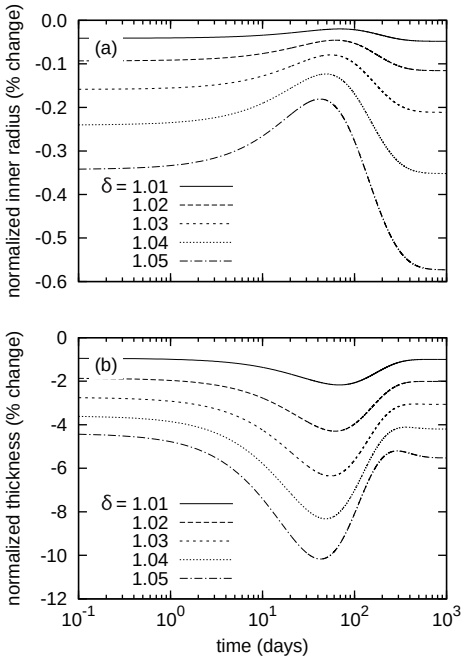

Fig. 17. Time courses of evolving inner radii (panel a) and thicknesses (panel b), each normalized with respect to values for the unperturbed artery, for indicated step changes in *in vivo* axial length $l(s) = \delta\, l_h$. Note the decreased inner radii and wall thicknesses at the instant of elongation due to isochoric motion. The evolution is characterized by a two-phased G&R process in which the first phase ($s \in [0, \sim 40]$ days) is dominated by stretch-induced mass removal and atrophy, followed by a second phase characterized by a gradual thickening that causes slight luminal encroachment($s \in [\sim 40, 1000]$ days).

Evolving changes in unloaded geometry also revealed salient G&R trends and illustrated the important biaxial effects of comparatively highly prestretched and biologically stable elastin. Predicted unloaded axial lengths (figure 19, panel a) followed the evolving collagen to elastin ratios. The predicted initial losses of collagen, par-

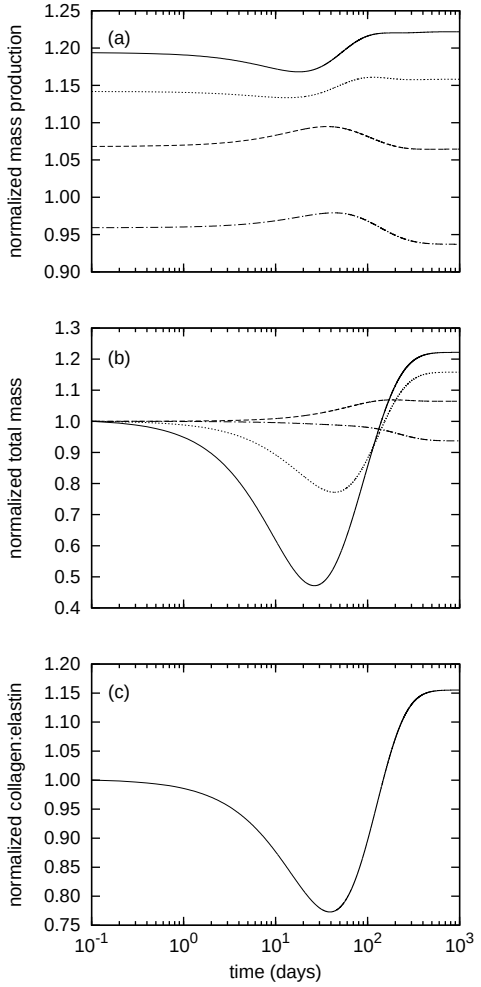

Fig. 18. Time courses of mass production rates per unit area (panel a) and total masses per unit area (panel b) for axially- (solid), helically- (dashed), and circumferentially- (dotted) aligned collagen and smooth muscle (dash-dotted) for a 5% step increase in *in vivo* axial length. Panel (c) shows the evolving total collagen to elastin ratio. All quantities are normalized with respect to homeostatic values. Note the elevated and sustained increases in axial and helical collagen production. Circumferential collagen saw more modest increases in production, while smooth muscle production diminished. Although mass production rates remained relatively stable, the effects of stretch-induced degradation (see equation (3.14)) can be appreciated by the substantial reductions in total axial and helical collagen (panel b). This considerable atrophy was chiefly responsible for the predicted reductions of thickness up to day 40 (figure 17, panel b) and the associated reduction of the collagen to elastin ratio (panel c). After approximately 40 days, total axial and helical collagen masses began to increase, suggesting that mass production outpaced mass removal.

ticularly with axial orientation, allowed the elastin to retract the artery further upon unloading; that is, reduced axial and helical collagen mass provided reduced compressive resistance to the elastin. The opposite was true after the collagen to elastin ratio rose above the baseline value ($M^c(0)/M^e(s) = 11.0$). The additional collagen, much of it oriented axially and helically, provided higher compressive resistance to elastin, resulting in larger unloaded lengths. Also, this new collagen was deposited in the new (elongated) configuration, thereby entrenching the artery in the elongated state, again consistent qualitatively with the interpretation of Jackson *et al.* [45]. In contrast, unloaded inner radii experienced slight monotonic decreases (figure 19, panel b) as circumferential collagen production increased only modestly and (circumferentially aligned) smooth muscle production decreased. This slight net reduction of stiff circumferential constituents resulted in a reduced compressive resistance to elastin.

Passive "pressure-diameter" behaviors (figure 20) revealed small evolving G&R-governed changes in overall mechanical properties. Nevertheless, these responses suggested superficially different trends depending on the normalizing value for inner radius. For example, by normalizing the current pressurized inner radius $a(s)$ by the original unpressurized inner radius before extension $A(0^-)$ (figure 20, panel a), the response curve shifted to the left at the instant of extension at time $s = 0^+$. As the artery remodeled around the new (elongated) configuration, the response curves eventually shifted to the right. Notwithstanding some "overshoot," the artery's passive response at 1000 days approached the original (day 0^-) response. This suggested an instantaneous slight circumferential stiffening resulting from a coupled biaxial behavior and isochoric motion following the step axial extension, with a subsequent gradual return to the homeostatic response.

On the other hand, by normalizing the current pressurized inner radius $a(s)$ by the the current unpressurized inner radius after extension $A(s)$ (figure 20, panel b),

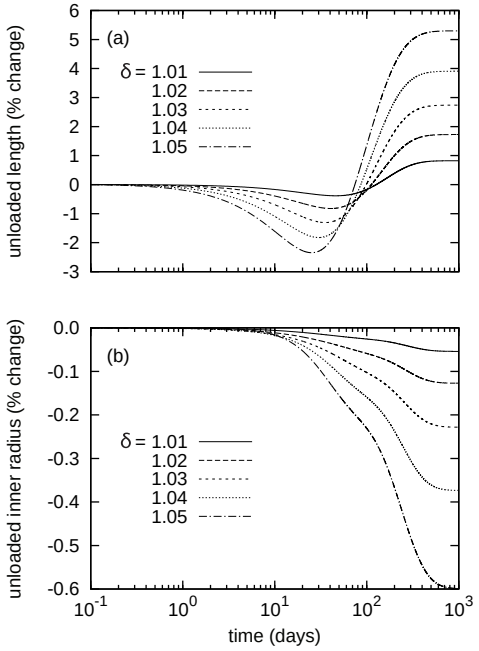

Fig. 19. Time courses of evolving unloaded lengths (panel a) and inner radii (panel b), normalized with respect to those of the unperturbed artery, for indicated step changes in *in vivo* axial length $l = \delta\, l_h$. The model predicted decreasing unloaded lengths up to day 40, followed by an increase and asymptotic stabilization. Note that this behavior follows the evolving collagen to elastin ratio (figure 18, panel c). The decreased unloaded inner radii resulted from a loss of smooth muscle.

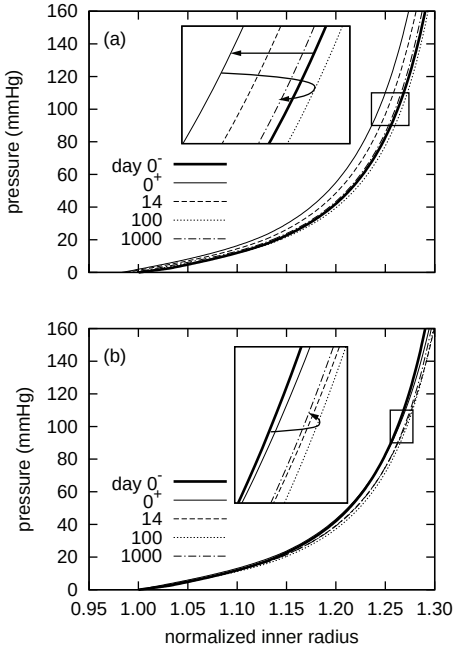

Fig. 20. Evolving passive "pressure-diameter" responses due to G&R for a 5% step increase in *in vivo* axial length, where the abscissa 'normalized inner radius' is expressed as the ratio of the current deformed inner radii to the original unpressurized inner radius before elongation $a(s)/A(0^-)$ (panel a) or the current unpressurized inner radius $a(s)/A(s)$ (panel b). Results are for the current *in vivo* axial length $l = \delta\, l_h$. The solid bold curve represents the response before the extension at time $s = 0^-$. The light solid curve represents the response at the instant of the step increase in length at time $s = 0^+$. Note the instantaneous leftward shift indicating a stiffer response as a consequence of coupled biaxial behavior and isochoric motion, followed by a gradual rightward shift as the artery remodeled towards its original compliance (inset, panel a). The model predicted some "overshoot" at day 100 followed by a slight reversal. Normalizing with respect to the current unpressurized configuration obscures the instantaneous effect of elongation and suggests that the artery became more compliant (inset, panel b). This result highlights the importance of choosing appropriate and consistent reference configurations, which affect substantially data interpretation.

the response curve exhibited no leftward shift at the instant of extension. Rather, the response curves shifted to the right, suggesting a progressive increase in compliance with time. Eventually, and after some "overshoot", the response curve settled on a slightly more compliant behavior, one that would likely not be discernible experimentally. This interpretation is consistent with the prediction that the artery loses (stiff) circumferential smooth muscle (figure 18, panels a and b and figure 19, panel b), thereby reducing effective circumferential stiffness. These two interpretations of the same results emphasize the importance of choosing appropriate and consistent measures of stretch, particularly when comparing experimental findings and numerical predictions.

Gleason *et al.* [46] observed evolving passive axial "force-pressure" behavior in arteries following sustained increases in axial extension. Our model predicted similar trends (figure 21) in response to a sustained 5% increase in axial stretch; applied axial forces gradually decreased for any given pressure. By day 1000, the axial force-pressure response at $l = \delta\, l_h$ was nearly equal to that at day 0 and $l = l_h$, further suggesting that the artery remodeled around its new increased length so as to recover its original behavior. The evolving axial "force-pressure" behavior depends primarily on the natural configurations of axial and helical collagen. The gradual shift by nearly 5% corresponds closely to the change in natural configurations for axially and helically oriented collagen. Note, too, that the artery was able to closely match its original axial "force-pressure" behavior despite elastin not turning over. This suggests that the passive effects of axial and helical collagen dominate axial tensile behavior in basilar arteries.

Predicted passive axial "force-length" behavior also evolved as a result of a sustained 5% increase in axial extension. By measuring overall axial stretch with respect to the current *in vivo* axial length $l = \delta\, l_h$ (figure 22, panel a), the model suggested

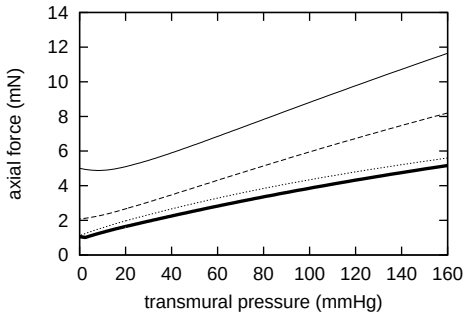

Fig. 21. Evolving passive axial "force-pressure" responses due to G&R for a 5% step increase in *in vivo* axial extension at days 0 (solid), 14 (dashed), and 1000 (dotted). The original "force-pressure" response is indicated by the solid bold curve. Response curves shifted down as the artery remodeled around its new axial length [cf. 46]. Note that by 1000 days, the passive response nearly equaled the original response, indicating a near complete recovery of the artery's original axial "force-pressure" behavior at the new *in vivo* axial length.

an instantaneous axial stiffening as a result of biaxial behavior at the new *in vivo* axial length with a gradual return to its original behavior. The instantaneous stiffening is an artifact of shifting the normalizing axial stretch by $1 - 1/\delta$. As the artery remodeled around its new axial extension, it almost completely recovered its original axial "force-length" behavior. By measuring stretch with respect to the original *in vivo* axial length l_h (figure 22, panel b), the model revealed a gradual rightward shift as the artery remodeled. After 1000 days, the axial "force-length" behavior shifted to the right by approximately 5%, indicating gradual G&R driven compliance. As in the case of evolving "pressure-diameter" behavior, the two different axial "force-length" interpretations depend upon the normalizing measure of stretch used.

E. Discussion

It has long been known that sustained alterations in blood pressure and flow induce significant arterial adaptations that appear to restore circumferential and wall shear stress to homeostatic values [e.g., 2–4, 6, 20, 28, 37, 38, 47, 55, 74, 75]. More recently, however, it has become apparent that arteries similarly adapt to sustained changes in axial stretch or stress [36, 45, 46, 61]. The goal of this paper was to explore, via computational modeling, possible means by which such adaptations occur.

1. Ubiquitous G&R Mechanisms

Because of the highly nonlinear axial stress-stretch behavior exhibited by most arteries, even modest step changes in axial extension can cause dramatic increases in intramural stress as compared to those induced by typical *in vivo* changes in transmural pressure or volumetric flow. That is, a restricted vasoactive range can limit initial changes in caliber in response to abrupt changes in flow and the passive circumferen-

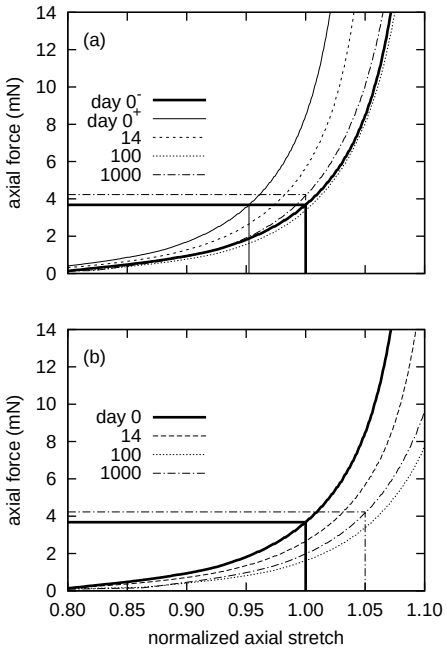

Fig. 22. Evolving passive axial "force-length" responses due to G&R for a 5% step increase in *in vivo* axial length, where the abscissæ 'normalized axial length' are expressed as the ratios of the current axial length to the current *in vivo* axial length $l(s)/\delta\, l_h$ (panel a) and the original *in vivo* axial length $l(s)/l_h$ (panel b). Results shown are for constant transmural pressure $P = P_h$. Panel (a) reveals an instantaneous initial leftward shift of $1 - 1/\delta$ in response to the axial extension, followed by a gradual rightward shift as the artery remodeled around the new (extended) *in vivo* axial length. The axial force-length response at day 1000 approached that of day 0^-. The same results, when normalized with respect to l_h (panel b), revealed a gradual rightward shift. By day 1000, the axial force at $l(s)/l_h = 1.05$ was nearly equal to that at day 0 and $l(s)/l_h = 1$. Note the slight "overshoot" at day 100. This behavior at time $s = 0^+$, when normalized with respect to l_h, is identical to that at time $s = 0^-$.

tial stiffness of the artery can limit the severity of its distension in response to abrupt changes in transmural pressure. In contrast, an imposed increase in axial extension represents a different type of perturbation since dimensions are changed directly, thus resulting in marked changes in stress. Nevertheless, despite differences in perturbations (changing flow, pressure, or axial extension), we posit that the associated G&R responses occur via similar fundamental mechanisms: mechanically-mediated rates of constituent turnover, changes in vasoactivity, and deposition of new matrix that is prestretched to preferred values. Hence, the time-dependent nature of G&R results primarily from the type and severity of the perturbation.

2. Predicted Mechanisms

The most obvious consequence of axial extension-induced arterial G&R is an increase in unloaded length, which is consistent with Jackson *et al.* [45] noting that "the stretched artery grew into its new length." The present simulations suggest that this response results primarily from an increased deposition of axially and helically-oriented collagen at its preferred value of deposition stretch within the new stretched configuration, which provides greater compressive resistance to the highly prestretched elastin. The model arteries were predicted to almost completely recover their original *in vivo* axial force-length and force-pressure responses by essentially shifting the response curves. This remarkable ability is due to the predicted sustained changes in mass fractions and production rates in response to the dramatically altered state of intramural axial stress, not changes in circumferential or wall shear stress. Predicted changes in pressure-diameter behavior were less pronounced, but were consistent with expected behavior.

The model also predicted competing effects of mass removal and production, resulting in biphasic evolutions in geometry and properties. As the collagen to elastin

ratio decreased during the first phase, unloaded lengths decreased; then, as collagen deposition outpaced removal and the collagen to elastin ratio increased, the unloaded length increased. Changes in unloaded length manifest *in vivo* as changes in axial stretch, which in turn affect the biaxial state of stress since $\sigma_\theta = \widehat{\sigma}_\theta(\lambda_\theta, \lambda_z)$ and $\sigma_z = \widehat{\sigma}_z(\lambda_\theta, \lambda_z)$. This association between *in vivo* axial stretch and collagen to elastin ratio was recently seen to explain, in part, normal species-to-species differences in the former [74], thus it should not be surprising that changing axial stretches manifest in normal adaptations to altered loading. Indeed, for this reason, axial mechanics likely plays a strong role in all aspects of arterial health and disease progression, including hypertension, development of aneurysms, Marfan syndrome, and aging to name a few.

3. Clinical Relevance

Jackson *et al.* [45] observed that significant axial unloading can result in tortuosity, which was not resolved experimentally over periods usually sufficient for arterial G&R. Although the case of a sustained decrease in axial stretch was not investigated numerically herein, we can consider some possible reasons based on intuition gleaned from our simulations. Irreversible tortuosity may result, in part, from a much lower rate of degradation and particularly synthesis of collagen fibers when they experience a dramatic decrease in tension as compared to when they experience an increase in tension. Also, because functional elastin is not produced in mature arteries, an artery subjected to a stretch less than its original *in vivo* stretch would continue to have much less stressed elastin, noting that stressed elastin appears to be fundamental in mechanical homeostasis; its loss results in aneurysmal dilatation and/or tortuousity [cf., 76].

Recognition of the importance of axial stress in arterial homeostasis and adap-

tations is clearly much more recent (ca. 2002) than the longstanding knowledge of the importance of pressure-induced circumferential stress and flow-induced wall shear stress. Consequently, there is a pressing need for increased attention to its clinical importance. Given that axial stress appears to be such a strong regulator of arterial G&R, there is a need to study effects of bypass procedures, using either native or synthetic grafts, on the host vessel response. Similarly, there is a need to consider potential effects of axial extension on construct development in tissue engineering of blood vessels.

4. Conclusion

The present constrained mixture model appears to capture salient features of arterial G&R in response to increased axial extension similar to prior results for altered pressure and flow [63]. Nevertheless, it is important to note that the present simulations were found to be much more sensitive to prescribed values of the rate parameters in the relations for matrix production. It is possible that this increased numerical sensitivity reflects, in part, the increased biological sensitivity in responses observed experimentally by Jackson *et al.* [45]. Alternatively, this observation may also serve as an important reminder that there is a pressing need for more biological data to formulate improved constitutive relations for the stress mediated production and removal, including their dependence on perturbations in all stresses from homeostatic values. That is, we currently do not know the best functional forms for $m^k(\tau)$ and $q^k(s,\tau)$ - recall equations (3.12) and (3.14) - and we do not know the best metric of stress on which they depend. Nevertheless, the present results are encouraging and suggest that a single theory of arterial growth and remodeling, containing a single set of material parameters, should be able to describe and predict responses to diverse perturbations in the chemomechanical environment once we have refined the requisite

constitutive relations and material parameters based on improved data, particularly on stress-mediated constituent turnover rates. Together, therefore, continued parallel advances in vascular mechanobiology, medical imaging, biomechanical modeling, and computational methods promise to increase significantly our understanding of vascular physiology, pathophysiology, injury, and clinical intervention, and thus to improve clinical care via more personalized and pre-emptive treatments [9, 77].

CHAPTER IV

EVALUATION OF FUNDAMENTAL HYPOTHESES UNDERLYING CONSTRAINED MIXTURE MODELS OF ARTERIAL GROWTH AND REMODELING

A. Overview

Evolving constituent composition and organization are important determinants of the biomechanical behavior of soft tissues. In arteries, vascular smooth muscle cells and fibroblasts continually produce and degrade matrix constituents in preferred modes and at altered rates in response to changing mechanical stimuli. Smooth muscle cells similarly exhibit vasoactive changes that contribute to the control of overall structure, function, and mechanical behavior. Constrained mixture models provide a useful framework in which to quantify arterial growth and remodeling for they can account for cell-mediated changes in individual structurally significant constituents. Our simulations show that the combined effects of changing mass density turnover and vasoactivity, as well as the prestretch at which constituents are incorporated within extant matrix, are essential to capturing salient features of bounded arterial growth and remodeling. These findings emphasize the importance of formulating biologically-motivated constitutive relations in any theory of growth and remodeling and distinct advantages of the constrained mixture approach in particular.

B. Introduction

It is well accepted that arteries grow and remodel via cell and matrix turnover, and different constituents, possessing different natural configurations and mechanical properties, exhibit different (although likely intricately linked) rates of turnover

that can change with mechanical stimuli. Thus, in addition to complex instantaneous nonlinear mechanical behaviors, time varying changes in composition resulting from mass turnover are important determinants of arterial biomechanics. Rodbard [1] introduced the concept of coupled vasoactivity and matrix remodeling via a two-phase process of acute changes in vasoactive tone followed by long term entrenchment. This hypothesis has since been substantiated by numerous observations and is summarized well by Dajnowiec and Langille [3]. Experimental observations [78–80] reveal further that cells achieve such growth and remodeling (G&R) by actively manipulating structural proteins during and following deposition. That is, mechanical forces exerted by synthetic cells during deposition or reorganization contribute to the unique mechanical properties exhibited by the extracellular matrix, which in general can lead to residual stresses in unloaded tissues and thus optimal states of stress *in vivo* [cf. 65]. Indeed, it appears that new constituents are deposited at preferred (homeostatic) stretches, which need not be equal for all constituents. In short, myriad studies, observed over diverse conditions in as many contexts [cf. 2, 12], strongly suggest that mechano-controlled variable mass turnover, vasoactivity, and preferred constituent deposition stretches are important fundamental mechanisms in arterial G&R. The goal of this paper is to explore numerically the individual and coupled roles of these different adaptive mechanisms via null hypothesis testing.

C. Background

Arterial homeostasis is a stable dynamic process that varies mass production and removal to optimize structure and function. Considering normal situations allows a heuristic investigation of some key concepts. Consider a healthy artery, with no loss of vasoactivity or elastin, that must maintain a constant geometry (radius, thickness,

and unloaded length) in response to an unchanging steady state transmural pressure and flow despite continual turnover of collagen and smooth muscle; we call this tissue maintenance. The normal half-life of arterial collagen is ∼70 days, for example, and smooth muscle turns over at $< 0.06\%$ per day [19, 81]. If load bearing "old" collagen is degraded and replaced with new fibers that are stress-free, that is, having a 0% deposition stretch, then because of the nonlinear properties, it is intuitive that smooth muscle would need to contract more to maintain the original inner radius in response to unchanging pressure and flow. This accommodation would be energetically unfavorable, however, and could reduce the vessel's vasoactive range. Mechanistically, this suggests that cells should be capable of depositing or arranging new extracellular matrix fibers within extant matrix to have a stretch greater than unity. In this way, synthetic cells could effectively solve the problem of tissue maintenance without the need for an elevated and sustained exertion of active force by smooth muscle cells and the associated energy expenditure required to maintain circumferential equilibrium and an optimal luminal radius. It shall prove useful below to consider this situation numerically, however.

Our group has employed continuum based constrained mixture models to investigate arterial G&R [6, 7, 22, 36, 63]. These studies represent progressively more detailed implementations of the same general theoretical framework; they have captured salient trends by qualitatively (and in some cases quantitatively) predicting important experimental observations. A unique strength of the constrained mixture approach stems from its ability to include effects of fundamental cellular behaviors that contribute to mechanically driven G&R. Although the innovative concept of kinematic growth [4, 82–84] approximates the consequences of underlying mechanisms, it assumes that growth occurs in fictitious stress free configurations, which it does not, and it does not account for basic cellular production (synthesis) and removal

(degradation) of matrix. In this work, we aim to provide a more robust level of model verification [cf. 85] by scrutinizing the basic hypotheses upon which constrained mixture models are built and by showing that the currently implemented framework faithfully captures theoretical expectations and exhibits many observed consequences of arterial G&R.

D. Methods

1. General Continuum Framework

Employing 2-D wall mechanics for a cylindrical segment of an artery, two equilibrium equations can be written in terms of the mean circumferential and axial stresses, namely

$$\sigma_\theta(s) = \frac{P(s)\, a(s)}{h(s)}, \tag{4.1}$$

$$\sigma_z(s) = \frac{f(s)}{\pi\, h(s)\, (2\, a(s) + h(s))}, \tag{4.2}$$

where P is the transmural pressure, a is the deformed inner radius, h is the deformed wall thickness, and f is the applied axial force, each defined at G&R time s. Note that these two equations are not sufficient to solve for the three primary geometric variables, a, h, and axial length l. Together with a constancy of mass density $\rho(s) \equiv \rho(0)$, however, prescribing $l(s)$ allows us to solve for $a(s)$ and $h(s)$, two variables of particular importance in flow- and pressure-induced adaptations.

The total Cauchy stress, including contributions from multiple passive constituents and active smooth muscle, can be computed as

$$\boldsymbol{\sigma} = \frac{1}{\det \mathbf{F}} \mathbf{F} \frac{\partial W}{\partial \mathbf{F}^T} + \sigma^{act}([\mathrm{Ca}^{2+}], \lambda^{m(act)})\, \mathbf{e}_\theta \otimes \mathbf{e}_\theta, \tag{4.3}$$

where $\mathbf{F}$ is the deformation gradient tensor, W is the homogenized strain energy

function for the mixture, and σ^{act} is the active muscle contribution (ultimately a function of intracellular calcium ion concentration [Ca^{2+}] and muscle fiber stretch $\lambda^{m(act)}$) in the direction $\mathbf{e}_\theta$. Employing a rule of mixtures approach, this strain energy function can be conceptualized as the sum of constituent contributions $W = \sum \phi^k W^k$, where ϕ^k are constituent mass fractions and W^k are the strain energy functions for each structurally significant constituent (e.g., collagen, elastin, smooth muscle). More generally, however, one can account for changing mass fractions by following changing mass densities. Evolving constituent mass densities M^k, defined per unit area, can be computed as [cf. 16]

$$M^k(s) = M^k(0)\, Q^k(s) + \int_0^s m^k(\tau)\, q^k(s,\tau)\, d\tau, \tag{4.4}$$

where $Q^k(s) \in [0,1]$ are survival fractions for constituents deposited before time $s = 0$, $m^k(\tau)$ are variable mass density production rates, and $q^k(s,\tau) \in [0,1]$ are survival fractions for constituents deposited at time $\tau \in [0,s]$ that survive to current G&R time s. The possibly evolving constituent strain energy functions, also defined per reference area, can thus be written as [cf. 16]

$$\begin{aligned} W^k(s) = {} & \frac{M^k(0)}{\rho(s)}\, Q^k(s)\, \widehat{W}^k\left(\mathbf{F}^k_{n(0)}(s)\right) \\ & + \int_0^s \frac{m^k(\tau)}{\rho(s)}\, q^k(s,\tau)\, \widehat{W}^k\left(\mathbf{F}^k_{n(\tau)}(s)\right)\, d\tau, \end{aligned} \tag{4.5}$$

where $\rho(s)$ is the mass density of the mixture, which is assumed to be constant [12, 83], and $\mathbf{F}^k_{n(\tau)}(s) = \partial \mathbf{x}^k(s)/\partial \mathbf{X}^k(\tau)$, with $\mathbf{x}^k(s) = \mathbf{x}(s)$ constraining all constituents to deform together and $\mathbf{X}^k(\tau)$ reflecting different evolving natural configurations for constituents k when produced at time τ. In other words, subscripts $n(0)$ and $n(\tau)$ denote individual natural configurations associated with times of deposition (at $s = 0$

or before, versus $\tau \in [0, s]$). These configurations facilitate the tracking of evolving constituent properties from the time of deposition. Additional details of the basic framework can be found in Baek *et al.* [16] and Valentín *et al.* [63].

2. Fundamental Hypotheses

a. Deposition Stretch

The stretches at which constituents are deposited within extant extracellular matrix and the target homeostatic mechanical states for cells and matrix represent central assumptions within constrained mixture models of G&R [cf. 74]. The basic hypothesis that synthetic cells deposit new fibrillar proteins (such as collagens types I and III) at a preferred (homeostatic) stretch and that SMCs remodel to maintain a target state of stretch is married to the constrained mixture approach through a sequence of multiplicative deformations. For example, the total stretch experienced at G&R time s by a fiber deposited at time τ is [16]

$$\lambda^k_{n(\tau)}(s) = G^k_h \frac{\lambda(s)}{\lambda(\tau)}, \tag{4.6}$$

where G^k_h is the homeostatic deposition stretch for the k^{th} constituent and $\lambda(s)$ and $\lambda(\tau)$ are potentially measurable stretches experienced by the mixture at times s and τ, respectively. This result follows directly from the assumption that constituent motions follow those of the artery, despite having individual natural (stress-free) configurations, which is fundamental to the idea of a constrained mixture as proposed by Humphrey and Rajagopal [12]. Letting $G^k_h = 1$ thus allows us to simulate consequences of disallowing fibroblasts and synthetic SMCs to endow fibrillar collagens [79, 80] or cytoskeletal proteins [86] with a homeostatic stretch at deposition time τ.

b. Smooth Muscle Contractility

Arteries possess the ability to constrict or dilate rapidly in response to a range of decreasing or increasing volumetric blood flow (i.e., wall shear stress). This vasoactivity is achieved via a $[Ca^{2+}]$ mediated actin-myosin contractile mechanism, which can be abstracted as a product of two functions: a chemical dose response function, modulating the maximum force developed, and a length dependent force generation envelope, which relates to the degree of actin and myosin filament overlap [87, 88]. Briefly, diverse substances such as nitric oxide (NO), endothelin-1 (ET-1), norepinephrine (NE), and acetylcholine (ACh) control vasoactivity. For example, subjecting endothelial cells to increased shear stress upregulates the production of NO, a potent vasodilator. For a given level of $[Ca^{2+}]$, smooth muscle develops peak force at an optimal length L_{max} and diminished forces as $|L_{max} - L|$ increases.

These two separate mechanisms were elucidated experimentally in Price *et al.* [89] for canine anterior tibial arteries, with dose response curves exhibiting roughly sigmoidal behavior and force length curves exhibiting the familiar inverse parabolic behavior characteristic of skeletal muscle [cf. 21]. Force-length behavior was only reported for one constrictor dose (corresponding to 50% maximum contraction), but one can imagine a family of force-length curves for varying constrictor dosages. The combined effect of these two mechanisms can be generalized conceptually as

$$\sigma^{act}(s) = T_{max}\, \widetilde{g}(C, \lambda^{m(act)}), \tag{4.7}$$

where T_{max} is a scaling factor with units kPa, C is a net ratio of constrictors to dilators, and $\lambda^{m(act)}$ is a measure of active smooth muscle fiber stretch, which can be related to L_{max}. Letting $T_{max} = 0$ kPa eliminates the active response.

c. Variable Mass Turnover

Tissue maintenance requires balanced basal rates of mass production and removal to preserve normal structure and function. The vasculature must also accommodate changing physiological demands through functional adaptations, which may require deviations from basal turnover rates [55, 90]. Numerous studies have investigated relationships between mechanical stimuli and changing synthetic and degradative behavior [74]. Consistent with this idea, mass density production rates can be conceptualized as [cf. equation 1 in 91]

$$m^k(s) = m_0^k \, \widehat{g}(\Delta\sigma, \Delta\tau_w), \tag{4.8}$$

where m_0^k is a basal production rate, $\Delta\sigma$ is the difference between the current and target value of an appropriate scalar measure of intramural stress, $\Delta\tau_w$ is difference between the current and target value of the magnitude of the luminal wall shear stress, and $\widehat{g}(0,0) = 1$, which recovers the basal rate. Note that this basal production rate corresponds to normal conditions in maturity (homeostatic constituent deposition stretches and full vasoactive capability) and yields a constant geometry and mechanical properties (i.e., tissue maintenance provided balanced removal via q^k) as long as there are no mechanical perturbations. Allowing m^k to vary with changing mechanical stimuli enables the vessel's geometry and properties to adapt so as to maintain τ_w, σ_θ, and σ_z near homeostatic values while maintaining a preferred mechanical state. Forcing $m^k(s) = m_0^k$ effectively renders the vessel incapable of modulating its G&R response to changes in mechanical environment.

3. Illustrative Functional Forms

In contrast to the general functional forms introduced above, specific forms are

needed to illustrate numerically the consequences of fundamental characteristics of wall maintenance and adaptation. Many different functional forms have been or could be postulated based on the available data and there is a pressing need for more research in this area. Nevertheless, we utilize the same specific functional forms and parameter values for the basilar artery as in Valentín *et al.* [63], which were found to give rise to well-behaved G&R. That is, we use a neo-Hookean stored energy function for elastin and Fung exponentials for fibrillar collagen and passive smooth muscle. Moreover, a specific form of equation (4.7) can be written as [cf. 21, 89]

$$\sigma_\theta^{act}(s) = \phi^m(s)\,\left(1 - e^{-C(s)^2}\right) \times \lambda_\theta^{m(act)}(s)\,\left[1 - \left(\frac{\lambda_M - \lambda_\theta^{m(act)}(s)}{\lambda_M - \lambda_0}\right)^2\right], \tag{4.9}$$

where ϕ^m is the mass fraction of active smooth muscle, λ_M and λ_0 are the stretches at which the force generating capacity is maximum and zero, respectively, and $\lambda_\theta^{m(act)}(s) = a(s)/a^{m(act)}(s)$ where $a^{m(act)}(s)$ evolves via a first order rate equation. Toward this end, note that Murray [15] led others [1, 14] to the conclusion that blood vessels change caliber to maintain a target wall shear stress. For fully developed laminar flow of a Newtonian fluid in a rigid tube, the mean wall shear stress can be approximated as $\tau_w = 4\,\mu\,Q/\pi\,a^3$, where μ is the viscosity of blood, Q is the volumetric flow rate, and a is the luminal radius. The ratio of constrictors to dilators $C(s)$ is thus ultimately a function of wall shear stress

$$C(s) = C_B - C_S\left(\frac{\tau_w(s) - \tau_w^h}{\tau_w^h}\right), \tag{4.10}$$

where C_B is the basal ratio, C_S is a scaling factor for shear stress induced changes, and τ_w^h is the homeostatic (target) wall shear stress. Note that increases in τ_w above homeostatic tend to increase the production of NO (a vasodilator) by the endothe-

lium, whereas decreases in τ_w below homeostatic give rise to ET-1 (a vasoconstrictor) production.

Mass density production of collagen (synthesis) and smooth muscle (proliferation) is known to vary with changes in smooth muscle cell stretch/stress [92–94] as well as with changes in endothelial release of NO and ET-1 [23, 24, 56]. For illustrative purposes, let production be prescribed as a linear function of mechanical stimuli [cf. 4, 95]

$$m^k(s) = m_0^k(1 + K_\sigma^k \, \Delta\sigma - K_{\tau_w}^k \, \Delta\tau_w), \tag{4.11}$$

where k denotes individual families of fibrillar collagen or contractile smooth muscle, σ is a scalar measure of intramural stress, and K_j^k are rate parameters that govern the stress-mediated production rates. Degradation of structural proteins and cell apoptosis appear to be well described by first order type kinetics, with appropriate half-lives [72, 96]. Hence, let the survival functions be [cf. 22, 63]

$$q^k(s,\tau) = e^{-\int_\tau^s K^k(\widetilde{\tau})d\widetilde{\tau}}, \tag{4.12}$$

where $K^k(\widetilde{\tau})$ are rate-type parameters for mass removal having units of days^{-1}. These rate parameters, in turn, are prescribed as $K^k(\widetilde{\tau}) = K_h^k + K_h^k \, |\Delta\zeta(\widetilde{\tau})|$, where K_h^k is a basal value (inverse the half-life), $\Delta\zeta(\widetilde{\tau})$ is the difference in fiber tension from its homeostatic value, and $\zeta^{k(\tau)}$ is the level of tension on fiber family k that was produced at time τ. Note that elastin is assumed to be highly stable under non-pathological conditions [20] and produced exclusively during early development, thus $Q^e(s) \equiv 1$ and $m^e(s) \equiv 0 \; \forall s \in [0, \infty)$ in maturity.

4. Solution Procedure

Assumptions of quasi-static 2-D wall mechanics reduce the equilibrium equations

to nonlinear algebraic equations (cf. equations (4.1) and (4.2)), which are solved easily for the proposed G&R framework (cf. equation (4.5)) by equating them with Cauchy membrane stress resultants T_i for the principal directions $i = z, \theta$ [63], namely

$$P\,a = T_\theta = \frac{1}{\lambda_z}\sum \frac{\partial W^k}{\partial \lambda_\theta} + \sigma_\theta^{act}\,h, \tag{4.13}$$

$$\frac{f}{\pi\,(2\,a + h)} = T_z = \frac{1}{\lambda_\theta}\sum \frac{\partial W^k}{\partial \lambda_z}, \tag{4.14}$$

where λ_θ and λ_z are stretches experienced by the mixture in the circumferential and axial directions, respectively. Note also that σ_θ^{act} is a function of inner radius via equations (4.9) and (4.10) and $h = \sum \left(M^k(s)\right)/(\rho\,\lambda_z\,\lambda_\theta)$. Prescribing *in vivo* axial length l, transmural pressure P, and luminal flow Q at all G&R times s permits one to solve for the inner radius via equation (4.13). At each computational time step δ, we can solve for a_δ such that

$$F\,(a_\delta) = \frac{1}{\lambda_z}\sum \frac{\partial W^k}{\partial \lambda_\theta\,(a_\delta)} + \sigma_\theta^{act}\,(a_\delta)\;h\,(a_\delta) - P\,a_\delta = 0, \tag{4.15}$$

via the Newton-Raphson method. The resulting intramural stresses and stretches and wall shear stresses control mass production (equation (4.11)), mass removal (equation (4.12)), and vasoactivity (equations (4.9) and (4.10)). Finally, consistent with Valentín *et al.* [63], illustrative values of the material parameters represent a normal basilar artery (table III).

Although 2-D equations to not allow one to consider transmural differences in G&R, including associated experimental findings from histology, immunohistochemistry, or opening angle tests [cf. 65], they enable one to examine clinically relevant changes in caliber and structural stiffness, including reasons for the latter. Moreover, we emphasize that the constrained mixture model enables one to incorporate significant biological information, including mechano-stimulated rates of matrix production

Table III. Material parameters and their values for a representative mature basilar artery under homeostatic conditions.

Role	*Value*
vessel geometry	$a_h = 1.42$ mm, $h_h = 0.176$ mm
initial loads	$P = 93$ mmHg, $Q = 3.075$ ml/s
constituent mass fractions	$\phi_0^c = 0.22, \phi_0^e = 0.02, \phi_0^m = 0.76$
homeostatic kinetics	$K_h^m = 1/80$ day^{-1}, $K_h^c = 1/80$ day^{-1}
vasoactive parameters	$T_{max} = 150$ kPa, $\lambda_M = 1.1, \lambda_0 = 0.4$ $C_B = 0.68, C_S = 20\,C_B$
target stresses	$\sigma^h = 100$ kPa, $\tau_w^h = 5.06$ Pa
deposition stretches	$G_h^e = 1.4, G_h^c = 1.08, G_h^m = 1.2$

or cell proliferation [92–94], known degradation kinetics and half-lives [19, 72, 90], the possibility of different deposition stretches for different constituents [79, 80], and different mechanical properties for different constituents [17, 18, 69]. There are, of course, many other types of models possible for arterial G&R [e.g., 4, 5, 48, 84, 95, 97–102], but our focus herein is on constrained mixture models.

E. Illustrative Results

1. Deposition Stretch

We have conjectured that constituents are deposited at preferred (homeostatic) values of stretch in maturity that render them optimally stressed when first incorporated within the extant matrix; these stretches are necessarily greater than unity, but differ considerably in basilar arteries for elastin (e.g., $G_h^e = 1.4$), collagen (e.g., $G_h^c = 1.08$), and smooth muscle (e.g., $G_h^m = 1.2$). Note that elastin is likely deposited

at a smaller value during development, but due to its long half-life, it is stretched further by normal maturation; we consider here the net effect of these two processes, thus it can be thought of more as a net prestretch rather than a deposition stretch [cf. 65]. One way to test the consequences of such an assumption numerically is to let $G_h^k = 1$ for $k = c$ and m for all G&R times $s \in [0, \infty)$. Simulations show that this results in suboptimal tissue maintenance or remodeling (figure 23). To appreciate this, recall that mean values of the homeostatic (target) wall shear stress and circumferential stress are

$$\tau_w^h = \frac{4\,\mu\,Q_h}{\pi\,a_h^3}, \quad \sigma_\theta^h = \frac{P_h\,a_h}{h_h}, \tag{4.16}$$

thus with sustained step-changes in flow and pressure given by $Q = \varepsilon\,Q_h$ and $P = \gamma\,P_h$, respectively, the idealized expected radius and wall thickness are $a = \varepsilon^{1/3}\,a_h$ and $h = \gamma\,\varepsilon^{1/3}\,h_h$ [47]. In all cases considered ($\varepsilon, \gamma = 0.9, 1.0, 1.1$), the artery with $G_h^k = 1$ exhibited modest increases from the expected inner radius ($< 1\%$), but wall thicknesses that were far greater ($\sim 720\%$) than expected based on a simple force balance. Figure 24 shows that increased production of smooth muscle accounted for this hypertrophy. Increased smooth muscle contractility was required to generate greater circumferential stresses (figures 25 and 26) in an attempt to offset the trend of enlargement due to increased collagen and smooth muscle deposition at $G_h^k = 1$; this compensatory mechanism is perhaps best appreciated in the case of increased pressure wherein increased contractility is needed to maintain wall shear stress despite the distending action of pressure. Nevertheless, this overall finding is consistent with the idea that if collagen is replaced with initially stress-free fibers, the only way that the artery can maintain its caliber is to increase active force generation by increasing the total mass of smooth muscle, increasing the contraction of extant active muscle, or some combination of both. Coupled with the decreased wall shear stress due to

passive distension (which would likely induce ET-1 production and thus increase C), an increase in smooth muscle stress worked to increase the mass density production rate of smooth muscle (see equations (4.10) and (4.11)). Indeed, this already muscular basilar artery numerically gained much more smooth muscle than expected as it remodeled to maintain equilibrium.

Increases in transmural pressure resulted in passive distension and thus increased fiber tensions and decreased τ_w. These effects worked to temporarily increase rates of collagen production. As extant collagen was subjected to increased tension, however, its removal rate accelerated (see equation (4.12) and Willett *et al.* [73]). Because new fibers were deposited at $G_h^k = 1$, the stresses borne by newly deposited collagen fibers were much lower than the homeostatic value, which initially prevented new collagen from attaining the high levels of stress experienced by original collagen (which was offset closer to the stiffer portion of the Fung exponential response curve) and provided a negative input for the rate of collagen production. Eventually, collagen production fell while smooth muscle production increased. An exception occurred when transmural pressure and fluid flow remained unperturbed (figure 24 panels a & b, solid curves). In this case, the decrease in τ_w as the vessel passively distended was able to outweigh the changes in fiber stress, thus resulting in a sustained increase in collagen production. Figure 27 shows that, in addition to the increasing active contribution by smooth muscle cells, increased collagen and smooth muscle deposition rates resulted in irreversible passive stiffening. Similar stiffening trends were predicted for cases of changed pressure and flow (not shown).

2. Vasoactivity

Whereas letting $G_h^k = 1$ prevented the artery from maintaining, or when perturbed attaining, an expected geometry, removing vasoactivity (i.e., $T_{max} = 0$ kPa)

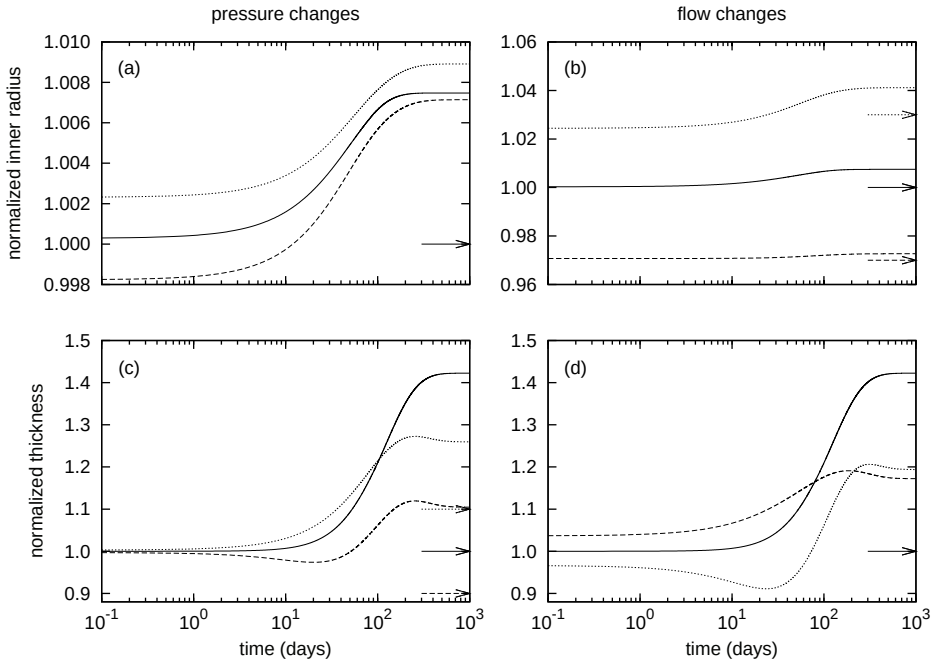

Fig. 23. Time courses of changing inner radius (panels a and b) and wall thickness (panels c and d) for changes in pressure (left) and flow (right) of -10% (dashed) and +10% (dotted) from the homeostatic value (solid) with $G_h^k = 1$ $\forall s \in [0, 1000]$ days. Expected values (cf. equation (4.16)) are indicated by corresponding arrows on the right ordinate. Although the vessel could neither maintain nor attain expected geometries, these changes stabilized asymptotically after long periods. Note the predicted large increase in wall thickness for all cases, suggesting the need for excessive deposition of sub-optimal material to compensate for the loss of the originally optimally deposited material. All quantities normalized with respect to homeostatic values at time $s = 0$. These results can be compared to those in Valentín *et al.* [63] which shows "normal" evolution toward expected values.

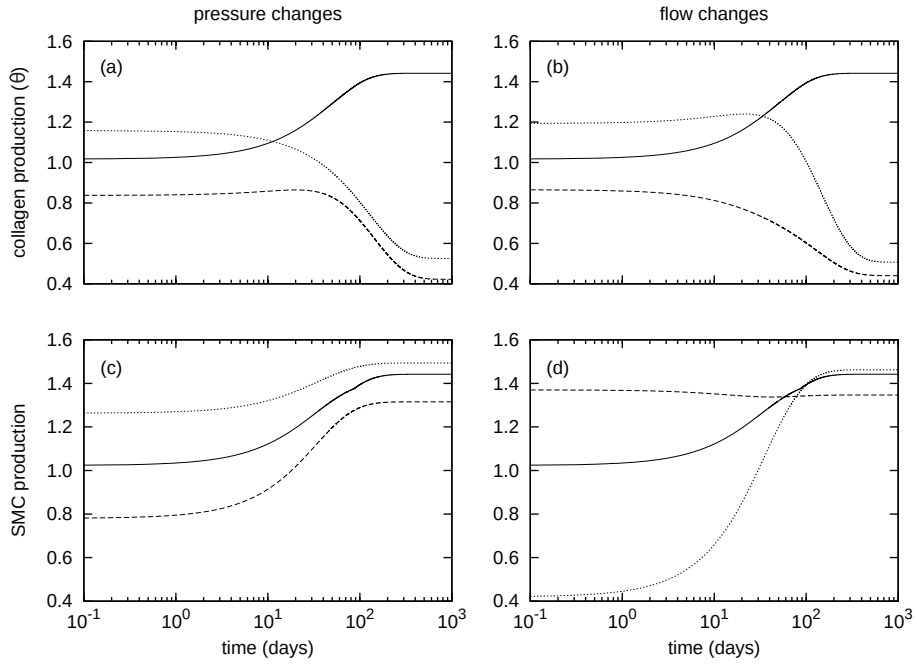

Fig. 24. Time courses of rates of mass density production for circumferential collagen (panels a and b) and smooth muscle (panels c and d), normalized with respect to homeostatic rates at $s = 0$, for changes in pressure (left) and flow (right) of -10% (dashed) and +10% (dotted) from the homeostatic (solid) value where $G_h^k = 1 \ \forall s \in [0, 1000]$ days. Note the predicted large and sustained increases in smooth muscle production.

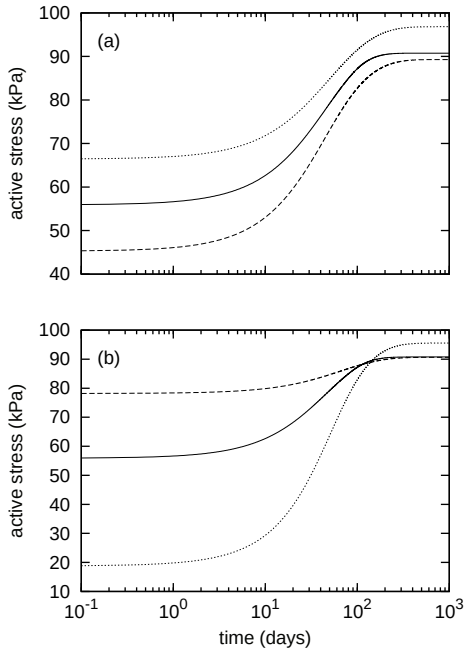

Fig. 25. Time courses of actively generated stress for changes in pressure (panel a) and flow (panel b) of -10% (dashed) and +10% (dotted) from the homeostatic (solid) value where $G_h^k = 1 \ \forall s \in [0, 1000]$ days. Initial decreases in active stress in the cases of decreased pressure and increased flow resulted from decreasing C as the vessel compensated for an increase in τ_w. Subsequent increases in active stress resulted from the enhanced need for active muscle to compensate for the diminished ability of the original prestretched constituents to contribute to circumferential equilibrium as they degraded and were replaced by constituents without a preferred deposition stretch.

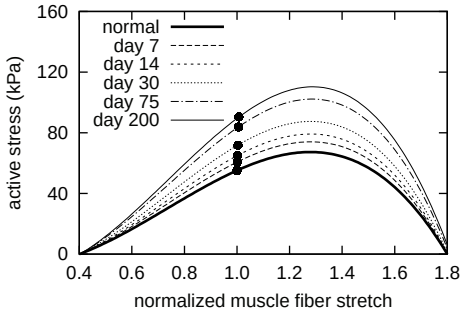

Fig. 26. Evolving active muscle response due to G&R for the case of $G_h^k = 1$ $\forall s \in [0, 200]$ days, $P = P_h$ and $Q = Q_h$. The bold curve represents the active response before any perturbation. Solid points represent the state of activity for the vessel at the corresponding time. The abscissa 'normalized muscle fiber stretch' is expressed as a range of values for $\lambda_\theta^{m(act)}(s)\, a^{m(act)}(s)/a^{m(act)}(0^-)$. Note the gradual increase in active stress from the time of perturbation (day 0) as the vessel becomes more muscular. While active muscle stress increased irreversibly, which would be energetically unfavorable, the vessel was able to maintain vasoactive function.

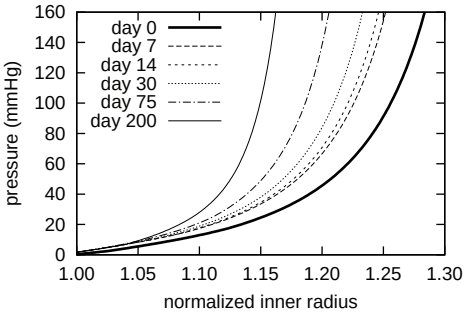

Fig. 27. Evolving passive response due to G&R for the case of $G_h^k = 1$ $\forall s \in [0, 200]$ days, $P = P_h$ and $Q = Q_h$. The abscissa 'normalized inner radius' is expressed as the ratio of the current deformed inner radius to the current unloaded inner radius. The bold curve represents the passive response before any perturbation. Note the marked leftward shift, indicating increasing passive structural stiffening.

primarily delayed the artery from approaching optimal inner radii for cases of increased pressure or reduced flow (figure 28, panel b; cf. figure 23, panel b wherein changes in radius are not delayed). Increased transmural pressure initiated a G&R sequence independent of Rodbard's phase 1 (i.e., vasoactivity). Because the artery experienced only modest passive distension, there was comparatively little stimulus to return to the expected inner radius (figure 28, panel a). Passive distension and the associated increase in fiber stresses and decrease in wall shear stress stimulated increased mass productions as the wall approached its expected thicknesses (figure 28, panel c). The most obvious limitation, however, was the inability to respond instantaneously to changes in flow (figure 28, panel b). Although the artery could not constrict instantaneously in response to decreased flow, increases in flow-induced wall shear stress resulted in positive inputs to the mass production rate (figure 29, panels b and d). That is, while vasoactivity no longer influenced vessel geometry, wall shear stress still influenced G&R via equation (4.11).

The degree to which changes in flow and pressure affected G&R depended upon their respective rate parameters K_j^k. For example, the artery could only attain expected thicknesses for changes in flow where $K_\sigma^k > 1$ [figure 5 in 63]. Reducing Q while maintaining transmural pressure constant effectively renders inner radius as the primary geometric variable; the artery will rapidly remodel a towards its new expected value, possibly at the expense of not reaching an optimal thickness (figure 28, panel d). That is, such G&R is driven primarily by τ_w, which depends only on $a(s)$ and $Q(s)$. Conversely, increased transmural pressure renders wall thickness as the primary geometric variable; the artery will rapidly remodel h towards its new expected value while not attaining the expected inner radius.

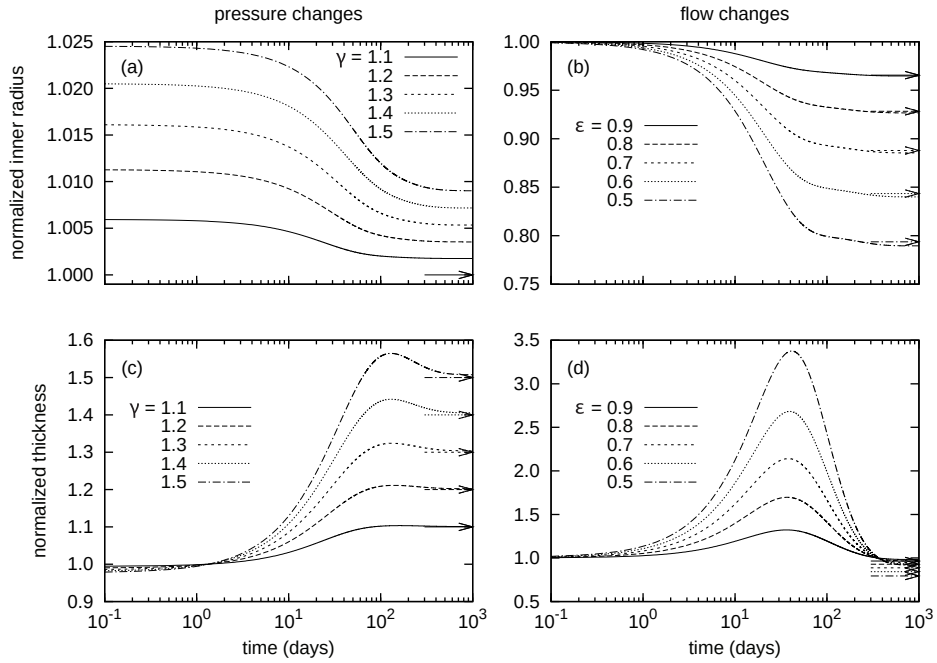

Fig. 28. Time courses of evolving inner radius (panels a and b) and wall thickness (panels c and d) for indicated changes in pressure $P = \gamma\, P_h$ (left) and flow $Q = \varepsilon\, Q_h$ (right) where $T_{max} = 0$ kPa $\forall s \in [0, 1000]$ days. Expected values are indicated by corresponding arrows on the right ordinate. Note the delayed change in inner radius for cases of reduced flow (panel b), due to the vessel's inability to instantaneously vasoregulate after the perturbation. This is consistent with the observation that arteries are insensitive to changes in flow when denuded of endothelium [81].

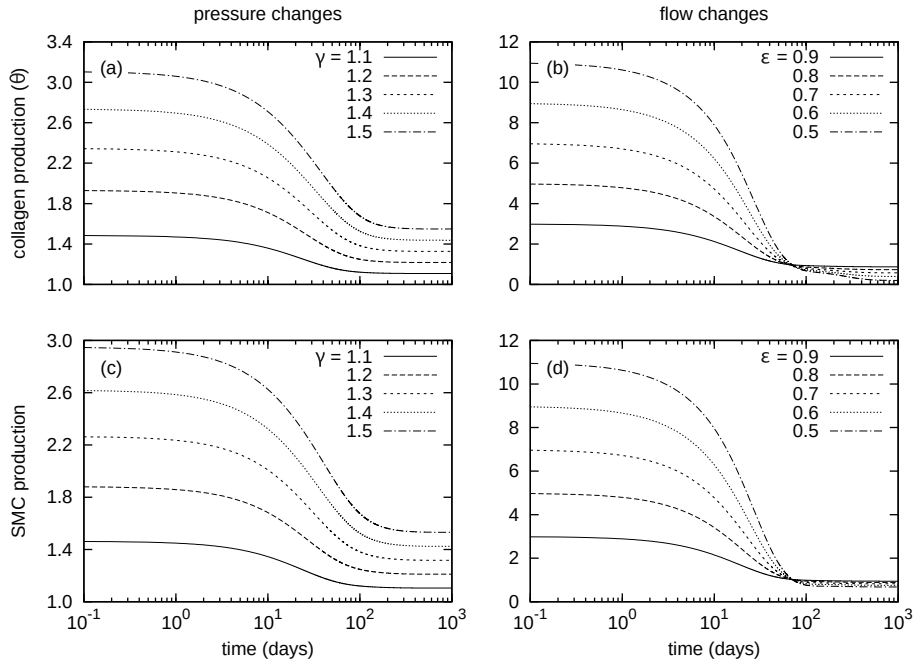

Fig. 29. Time courses of rates of mass density production for circumferential collagen (panels a and b) and smooth muscle (panels c and d), normalized with respect to homeostatic rates for indicated changes in pressure $P = \gamma\, P_h$ (left) and flow $Q = \varepsilon\, Q_h$ (right) where $T_{max} = 0$ kPa $\forall s \in [0, 1000]$ days. Note the high levels of production, especially for cases of reduced flow.

3. Basal Turnover

Restricting $m^k(s) = m^k_{basal}$ and $q^k(s,\tau) = \exp\left(-K^k_h(s-\tau)\right)$ is, in many ways, opposite the case of $T_{max} = 0$ kPa. Because turnover was constant, with $K^k_h = m^k_{basal}/M^k(0)$, the artery had a constant mass $\forall s \in [0,\infty)$, and all motions were isochoric. The simulated artery was thus capable of vasoactively adjusting its inner radius instantaneously in response to changes in pressure and flow (figure 30), but its long-term G&R capabilities were limited seriously. Simulations predicted that the artery could not achieve expected values for inner radius (figure 30, panel a) or thickness (not shown) for cases of increased pressure. Whereas an artery would normally maintain the homeostatic inner radius and accumulate additional mass to reach a new (greater) optimal thickness, this vessel could not accumulate any additional mass. As inner radius increased, the simulated artery only reached G&R stability because of increased vasoactivity (not shown) and elevated passive stiffness provided by extant (non-degrading) elastin at higher stretches.

The artery could only achieve the expected inner radius for cases of reduced flow, and even then, only within a limited range (figure 30, panel b). Thicknesses (not shown) were far greater than the expected values. Initially, vasoactivity increased in response to increased C, thus reducing the inner radius and returning τ_w to its homeostatic value. If the expected inner radius was within the normal vasoactive range, then the vessel could maintain a stable configuration. As the vessel remodeled in this state, however, the active stresses eventually decreased to some new steady state due largely to an excess accummulation of mass at the reduced caliber. In contrast, if the optimal inner radius was below the instantaneous vasoactive range, the active muscle stress eventually fell to zero (figure 31). At this time, the geometry changed in an unbounded manner; that is, the growth was unstable. The unrelenting

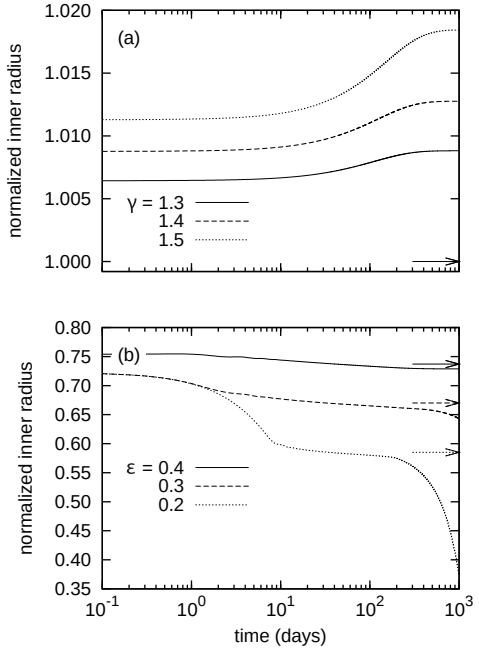

Fig. 30. Time courses of evolving inner radius for indicated changes in pressure $P = \gamma\, P_h$ (panel a) and flow $Q = \varepsilon\, Q_h$ (panel b) where $m^k(s) = m^k_{basal}$ and $q^k(s,\tau) = \exp(-K^k_h(s-\tau))\ \forall s \in [0, 1000]$ days. Expected values (cf. equation (4.16)) are indicated by corresponding arrows on the right ordinate. Note that for the cases of decreasing flow, the stable evolution range lies within the vessel's instantaneous vasoactive range; note, too, the strongly diverging behavior near day 200 for the case of $\varepsilon = 0.2$, which suggests a sudden inability to regulate inner radius.

deposition of collagen and passive muscle (with deposition stretches > 1) tended to narrow the artery further. Once C reached 0, there was no longer a mechanism to stop this trend; muscle could only generate tensile stresses, and elastin was not stiff enough to resist compression.

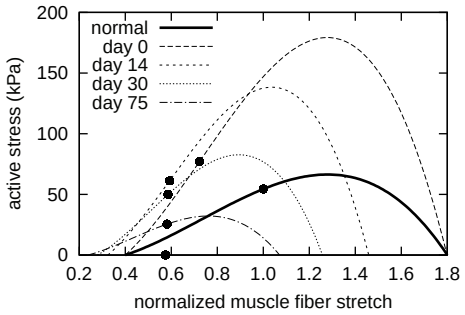

Fig. 31. Evolving active muscle response due to G&R for a change in flow where $\varepsilon = 0.2$ and $m^k(s) = m^k_{basal}$ and $q^k(s,\tau) = \exp(-K^k_h(s-\tau))\ \forall s \in [0, 200]$ days. The bold curve represents the active response before any perturbation. Solid points represent the state of activity for the vessel at the corresponding time. The abscissa 'normalized muscle fiber stretch' is expressed as a range of values for $\lambda_\theta^{m(act)}(s)\, a^{m(act)}(s)/a^{m(act)}(0^-)$. Note the dramatic increase in active stress at the time of perturbation (day 0) and the gradual leftward shift as the active muscle remodels around a reduced inner radius. Also note the gradual reduction in vasoactivity after day 0 and eventual cessation by day 200, as denoted by the solid point on the abscissa. This loss of vasoactivity, coupled with constant collagen and smooth muscle deposition rates, resulted in the unbounded reduction of lumen caliber beginning near day 200 (figure 30, panel b).

4. Combined/Synergistic Effects

Figure 32 shows results of forcing both constant turnover $\left(m^k \equiv m^k_{basal}\right)$ and no vasoactivity ($T_{max} = 0$kPa). Although changing flowrate could then never affect

vessel geometry (not shown), even small changes in transmural pressure resulted in unbounded changes in geometry. This suggests that although the artery exhibited stable G&R behavior at $P = P_h$, this was actually a meta-stable G&R equilibrium condition. Following an increase in transmural pressure, the artery distended and was unable to maintain its inner radius. Subsequently, new material was unrelentingly deposited in newly distended states. Although this new material was deposited with a deposition stretch > 1, the artery could not accumulate mass and achieve the expected thickness. Coupled with the inability to increase actively generated stress, this thinning resulted in unbounded distension.

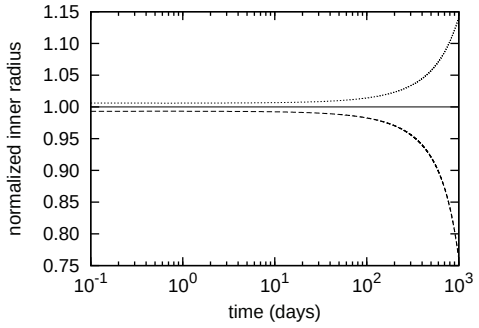

Fig. 32. Time courses of evolving inner radius for changes in pressure of -10% (dashed) and +10% (dotted) from the homeostatic (solid) value for $T_{max} = 0$ kPa, $m^k(s) = m^k_{basal}$, and $q^k(s,\tau) = \exp(-K^k_h(s-\tau))\ \forall s \in [0, 1000]$ days. Note the diverging behavior, suggesting a departure from a state of meta-stable G&R equilibrium.

Reduced transmural pressure initially resulted in a modest decrease in caliber. This perturbation initiated a subsequent uncontrolled decrease in inner radius, however. As in the case of large decreases in flow for constant turnover, the artery experienced an unbounded decrease in caliber as newly deposited material compressed extant constituents. Without an initial level of vasoactivity and the associated ability

to vasodilate, the artery could not recover the expected inner radius, thus resulting in uncontrolled G&R.

Figure 33 shows effects of restricting both $G_h^k = 1$ and $T_{max} = 0$ kPa $\forall s \in [0, \infty)$. Even for $P = P_h$ and $Q = Q_h$, the vessel exhibited unbounded distension; the artery could not maintain any inner radius, suboptimal or otherwise. As constituents were replaced at $G_h^k = 1$, the vessel tended to distend and without the ability to vasoconstrict, the artery could not reverse this trend. Although the wall could increase mass production in response to decreasing τ_w (not shown), the lack of a preferred deposition stretch and the relatively small amounts of compliant elastin prevented the artery from halting this distension. The model predicted substantial accumulation of new mass and thickening, but as the artery continued to distend, wall thickness decreased and eventually stabilized. Continued distension and increasing mass deposition eventually achieved a balance by which wall thickness stabilized.

F. Discussion

We submit that deposition of constituents at preferred prestretches, vasoactivity, and mechano-stimulated variable mass production and removal rates represent three fundamental ways by which vascular cells control overall geometry and biomechanical behavior. Contractile smooth muscle can actively change the caliber in response to various constrictors and dilators, many of which are produced by endothelial cells in response to hemodynamic loads [103], whereas synthetic smooth muscle cells and fibroblasts can change apparent mass densities of smooth muscle and collagen fibers, also as a function of mechanical and chemical stimuli. Moreover, for a pressurized vessel to maintain constant geometry, apparent mass densities, and muscle activity under even homeostatic conditions, new collagen fibers and smooth muscle must be

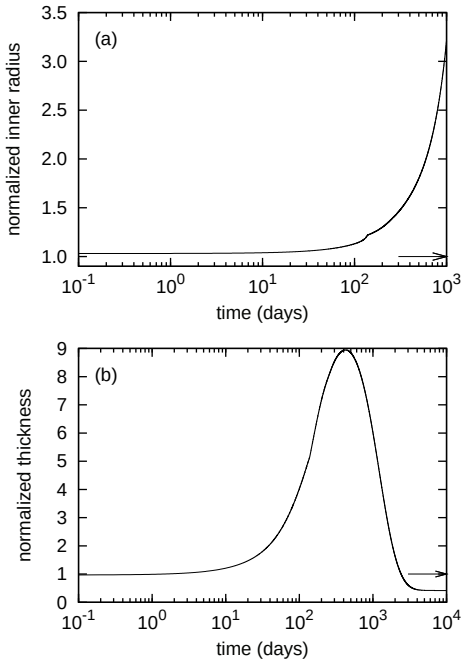

Fig. 33. Time courses of changing inner radius (panel a) and wall thickness (panel b) for the case of $G_h^k = 1$ and $T_{max} = 0$ kPa $\forall s \in [0, 10000]$ days. Transmural pressure and flow are unchanged from homeostatic. Expected values (cf. equation (4.16)) are indicated by corresponding arrows on the right ordinate. The model predicts an unbounded monotonic increase in inner radius (shown only to 1000 days) and an initial increase, followed by a gradual decrease and eventual stabilization of wall thickness.

deposited having stretches greater than unity. Accounting for these three mechanisms is essential to capturing salient G&R trends and approximating diverse observed behaviors, including (biologically stable) tissue maintenance.

Vasoactivity is a well understood and widely appreciated vascular characteristic, and many models have incorporated this behavior in diverse implementations [11, 21, 104, 105]. The concept of "deposition stretch" has seen more limited attention despite increasing biological evidence for its existence [79, 80, 106]. This study suggests, however, that preferred deposition stretches are at least as important as active muscle in maintaining a stable and optimal geometry under normal conditions as well as enabling effective adaptations to altered loads. Indeed, we have shown that, whereas $T_{max} = 0$ kPa does not preclude the vessel from approaching its expected geometry, an artery endowed with $G_h^k = 1$ cannot achieve the expected geometry. Furthermore, this study suggests that while both vasoactivity and deposition stretches are important individually, these two characteristics complement each other and endow arteries with the ability both to maintain stable geometric configurations and to adapt to diverse situations.

Variable mass density turnover is another fundamental cellular behavior, clearly operative from development to maturity [19], without which the model artery could not appropriately compensate for large changes in transmural pressure or flow. For example, forcing constant mass production and removal rates resulted in unstable G&R for large reductions in flow. Our findings that effective arterial adaptations require mechanically-mediated changes in the rates of production and removal of structural constituents are consistent with many recent findings [e.g., 45, 107–109] and confirm the longstanding speculation of Wolinsky [38] that "[t]he high degree of correlation between the amounts of medial elastin and collagen and calculated levels of tension found in these studies is the first such relation described and is compatible

with the possibility that tension, either directly or indirectly, provides the stimulus for elaboration of these fibrous proteins." Moreover, Wolinsky suggested that "it would appear that the rates of accumulation of elastin and collagen... are linearly related to the degree of tension elevation," which appears to be a reasonable first approximation of the likely nonlinear relation.

An artery may achieve a stable, albeit suboptimal, geometry for cases of either no deposition stretch ($G_h^k = 1$) or no vasoactivity ($T_{max} = 0$ kPa). Similarly, an artery may be able to achieve a stable but suboptimal geometry for limited ranges of pressures and flows if mass density turnover ($m^k = m_{basal}^k$) is constant. This degree of fault tolerance is typical of biological systems, which employ what amounts to multiple redundant or complementary systems to promote homeostasis. Combining constant mass density turnover and $T_{max} = 0$ kPa resulted in a vessel that was, in effect, in a state of unstable G&R equilibrium even under normal conditions. That is, any small perturbation in transmural pressure resulted in diverging, unbounded enlargement. Also, for cases in which $G_h^k = 1$ and $T_{max} = 0$ kPa, the vessel exhibited an unbounded change in geometry, even for the case of homeostatic transmural pressure and volumetric flowrate. In other words, although preferred deposition stretch, vasoactivity, and variable constituent turnover rates are individually important to maintaining optimal or near optimal geometry and function, they work together. Hence, arteries cannot maintain G&R stability or function without any two of these mechanisms.

In summary, continuum based constrained mixture models are well suited for simulating arterial G&R, for they allow one to account for biological characteristics that are fundamental to both tissue maintenance and adaptation: individual and variable mass density production/removal of constituents, individual preferred deposition stretches, vasoactivity with evolving reference configurations, and so forth. Moreover,

it is seen that such models are well suited to basic hypothesis generation and testing, not just parameter estimation or standard solutions to initial-boundary problems. Herein we effectively simulated, via what may be described as "numerical knockout models," the consequences of possible biological phenotypes that were found to be problematic individually but likely catastrophic when co-existing, not unlike many mouse knockouts and double knockouts. We submit that it is not necessarily a large number of values of material parameters that is most important to enabling continuum biomechanical models to describe and predict *in vivo* behaviors; rather, it is the biological appropriateness of the fundamental hypotheses that enables a model to capture and predict salient features of the biomechanics and mechanobiology. Hence, because of their inherent complexity, future fluid-solid-growth (FSG) models of the vasculature [9] should be based on physically reasonable and biologically appropriate constitutive relations that reflect underlying cell-mediated mechanisms.

CHAPTER V

PARAMETER SENSITIVITY STUDY OF A CONSTRAINED MIXTURE MODEL OF ARTERIAL GROWTH AND REMODELING

A. Overview

Computational models of arterial growth and remodeling promise to increase our understanding of basic biological processes such as development, tissue maintenance, and aging, the biomechanics of functional adaptation, the progression and treatment of disease, responses to injuries, and even the design of improved replacement vessels and implanted medical devices. Ensuring reliability of and confidence in such models requires appropriate attention to verification and validation, including parameter sensitivity studies. In this paper, we classify different types of parameters within a constrained mixture model of arterial growth and remodeling; we then evaluate the sensitivity of model predictions to parameter values that are not known directly from experiments for cases of modest sustained alterations in blood flow and pressure as well as increased axial extension. Particular attention is directed toward complementary roles of smooth muscle vasoactivity and matrix turnover, with an emphasis on mechanosensitive changes in the rates of turnover of intramural fibrillar collagen and smooth muscle in maturity. It is shown that vasoactive changes influence the rapid change in caliber that is needed to maintain wall shear stress near its homeostatic level and the longer term changes in wall thickness that are needed to maintain circumferential wall stress near its homeostatic target. Moreover, it is shown that competing effects of intramural and wall shear stress regulated rates of turnover can develop complex coupled responses. Finally, results demonstrate that the sensitivity to parameter values depends upon the type of perturbation from normalcy, with

changes in axial stretch being most sensitive consistent with empirical reports.

B. Introduction

Ubiquitous mechanosensitive growth and remodeling (G&R) processes are fundamental to many aspects of vascular biology and pathobiology as well as diverse arterial responses to injury and clinical intervention. Because of the complexity of such processes at molecular, cellular, and tissue levels, there is a pressing need for integrative multiscale computational models having both descriptive and predictive capability. Toward this end, there is first a need for reliable models at each of the individual scales. We have proposed a constrained mixture model for tissue-level G&R of arteries that accounts for individual material properties, natural configurations, and rates and extents of turnover of different structurally significant constituents that constitute the wall. This basic framework and illustrative constitutive relations have represented well the salient features of both normal arterial adaptations to altered pressure and flow [63] and different types of disease progression [16, 22, 68, 110]. Moreover, by numerically testing multiple null hypotheses [64], we have shown the reasonableness of many of the fundamental hypotheses upon which the constrained mixture model is based. The goal of this paper, therefore, is to extend our previous investigations by classifying the types of material parameters that exist in constrained mixture models of arterial G&R and then assesing the sensitivity of model predictions to realistic ranges of these material parameters, particularly those that are not well known or easily determined from experiments.

Parameter sensitivity studies based on numerical simulations can play fundamental roles within the overall verification and validation process in modeling [85]. By allowing values of parameters to approach particular limits, one can generate and

test basic hypotheses in a cost- and time-efficient manner; by comparing predictions over reasonable ranges of parameter values, one can estimate the resolution needed in an experimental measurement or restrict the search space for a best-fit regression based on data; and by comparing predictions based on different sets of parameter values, one can elucidate possible complex mechanisms of coupling and thereby provide important guidance for the design and interpretation of an experiment. Indeed, given the advances in computational methods, numerical simulation has become an important addition to the traditional method of scientific inquiry based solely on theory and experiment (figure 34). In this paper, we confirm via numerical simulation that effective cell and matrix turnover require mechano-control in arterial G&R. We also confirm that vasoactivity and matrix remodeling represent complex, complementary, coupled mechanisms of arterial adaptation to altered flows, pressures, and axial extension, including those characterized by competing effects due to wall shear and intramural stress mediated turnover. Finally, sensitivity of model predictions to parameter values in particular classes of G&R suggest that vascular cells are more sensitive to perturbations in axial loading than to those in flow or pressure. Overall, the present parameter sensitivity study of a constrained mixture model of the growth and remodeling of a basilar artery suggests that current constitutive relations provide reasonable descriptions of the behavior even though there is strong motivation to identify better, more comprehensive constitutive relations for cell and matrix turnover as a function of altered mechanical stimuli.

C. Methods

1. General Framework

The mean Cauchy stress response for an artery, accounting for a constrained

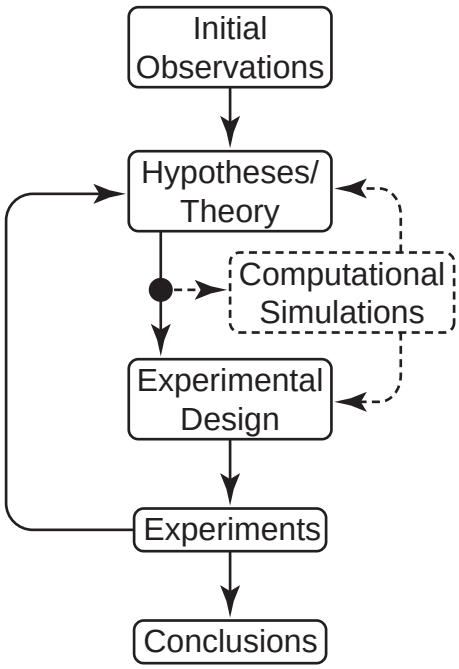

Fig. 34. Schematic representation of the iterative process of the modern scientific method, as applied to G&R biomechanics. Computational models enable time- and cost-efficient simulations that can both serve an important role in the refinement of hypotheses/theories and motivation of experiments and their design. For example, simulations enable one to evaluate competing hypotheses, thereby focusing the experimental need.

mixture of structurally significant passive constituents and active smooth muscle, was approximated using a rule of mixtures as

$$\boldsymbol{\sigma} = \frac{1}{\det \mathbf{F}} \mathbf{F} \frac{\partial W}{\partial \mathbf{F}^T} + \sigma^{act}([\mathrm{Ca}^{2+}], \lambda^{m(act)})\, \mathbf{e}_m \otimes \mathbf{e}_m, \tag{5.1}$$

where $\mathbf{F}$ is the 2-D deformation gradient tensor, $W = \sum_k W^k$ is the strain energy function for the mixture, with W^k representing energy stored in each structurally significant constituent k, and σ^{act} is the vasoactive contribution in the smooth muscle fiber direction $\mathbf{e}_m$. This active contribution depends on intracellular calcium ion concentration and muscle fiber stretch $\lambda^{m(act)}$. Extending the rule of mixtures approach to account for continuous cell and matrix turnover, this strain energy function was written as the sum of constituent contributions [16, 63]

$$\begin{aligned} W^k(s) = {} & \frac{M^k(0)}{\rho(s)}\, Q^k(s)\, \widehat{W}^k \left(\mathbf{F}^k_{n(0)}(s)\right) \\ & + \int_0^s \frac{m^k(\tau)}{\rho(s)}\, q^k(s,\tau)\, \widehat{W}^k \left(\mathbf{F}^k_{n(\tau)}(s)\right)\, d\tau, \end{aligned} \tag{5.2}$$

where $M^k(0)$ is the apparent mass density of constituent k, per reference area, at G&R time $s = 0$, $Q^k(s)$ are fractions for constituents deposited before time $s = 0$ that survive to current time s, $m^k(\tau)$ are mass density production rates, $q^k(s,\tau)$ are fractions for constituents deposited at time $\tau \in [0, s]$ that survive to current G&R time s, and $\rho(s) \equiv \rho(0)$ is the assumed constant mass density of the mixture. $\mathbf{F}^k_{n(\tau)}(s) = \partial \mathbf{x}^k(s)/\partial \mathbf{X}^k(\tau)$, where $\mathbf{x}^k(s) = \mathbf{x}(s)$ constrains all structurally significant constituents to deform together, but $\mathbf{X}^k(\tau)$ allows individual evolving natural configurations for each constituent k produced at time τ. See Baek *et al.* [16, 22] and Valentín *et al.* [63] for additional details of this basic framework and implementation.

2. Parameter Classification

Previous implementations of constrained mixture models for arterial G&R involved several classes of parameters for the requisite geometry, constitutive relations, and applied loads [cf. 22, 63]. The chosen functional forms and parameter values were motivated both by reported observations and hypothesized behaviors; they were merely required to yield biologically and physically realistic predictions. Herein, however, we classify these constitutive relations and parameters by level of consensus and function (see tables IV and V) and study parametrically those for which only bounds are known. Quantities such as arterial geometry, volumetric flowrates, and local blood pressures are easily measured *in vivo* [cf. 111] and thus are well-known. Bulk mechanical behaviors are also easily quantified *in vitro* [27] and similarly for constituent mass fractions, given appropriate histological preparations [112, 113]. In contrast, values for quantities such as the stretch at which constituents are incorporated within extant matrix, values of shear stress-regulated vasoactive molecule production, and the changing rates of of cell and matrix turnover as a function of changes in mechanical stimuli are less well known and thus amenable to parametric study.

a. Passive and Active Mechanical Behavior

Consistent with prior studies [22, 63], we used a neo-Hookean strain energy function for elastin [17, 18]

$$\widehat{W}^e(s) = c\left(\lambda_\theta^e(s)^2 + \lambda_z^e(s)^2 + \frac{1}{\lambda_\theta^e(s)^2\,\lambda_z^e(s)^2} - 3\right), \tag{5.3}$$

where $\lambda_\theta^e(s) = \tilde{G}_h^e\,\lambda_\theta(s)$ and $\lambda_z^e(s) = \tilde{G}_h^e\,\lambda_z(s)$ are constituent-specific stretches, which can be determined from arterial stretches $(\lambda_\theta(s), \lambda_z(s))$ and "growth-induced" prestretches $\tilde{G}_h^e$ [68]. Note that the latter assumes that elastin is not produced in matu-

Table IV. Classification of specific functional forms of constitutive relations employed in a constrained mixture model of the basilar artery. 'Well Accepted' relations represent those for which experimental data have established some level of consensus; references are listed as examples, not necessarily as proof of consensus. Postulated forms represent those for which experimental data are wanting; linear functions allow us to begin to explore salient behaviors and trends.

Class	*Relationship*	*Form*	*Ref.*
Well Accepted	active stress-constrictor	sigmoidal	[89]
	active force-length	inversely parabolic	[21]
	mass density removal-time	exponential decay	[72]
	energy density-strain (collagen/muscle)	Fung exponential	[114]
	energy density-strain (elastin)	neo-Hookean	[17]
Postulated	constrictor-shear stress	linear	
	mass density production-stress	linear	
	mass density production-constrictor	linear	
	mass density removal-tension	piecewise linear	

Table V. Classification of the requisite material parameters and their values for a representative mature basilar artery under homeostatic conditions. 'Observed' parameters include those reported in literature; these are readily obtained via direct measurements or fits to experimental data. 'Bounded' parameters are less well known, but can be chosen such that the model yields expected biomechanical behaviors. 'Calculated' parameters herein satisfy equilibrium for homeostatic conditions.

Class	*Role*	*Value*	*Ref.*
Observed	vessel geometry	$a_h = 1.42$ mm	[111]
	initial loads	$P = 93$ mmHg, $Q = 3.075$ ml/s	[111]
	constituent mass fractions	$\phi_0^c = 0.22, \phi_0^e = 0.02, \phi_0^m = 0.76$	[113]
	physical constants	$\rho = 1050$ kg/m^3, $\mu = 0.037$ g/cm s	[2]
	homeostatic kinetics	$K_h^m = 1/80$ day^{-1}, $K_h^c = 1/80$ day^{-1}	[19, 81]
	muscle activation parameters	$T_{max} = 150$ kPa, $\lambda_M = 1.1, \lambda_0 = 0.4$	[21]
Bounded	target stresses	$\sigma^h = 100$ kPa, $\tau_w^h = 5.06$ Pa	
	deposition stretches	$G_h^e = 1.4, G_h^c = 1.08, G_h^m = 1.2$	
	production kinetics	$K_\sigma^k, K_{\tau_w}^k \in [0, 10]$	
	shear-constrictor	$C_B = 0.68, C_S = 20\, C_B$	
	elastic parameters	$c_2^c = 22$, $c_2^m = 3.5$	
Calculated	vessel geometry	$h_h = 0.176$ mm	
	elastic parameters	$c = 588.3$ kPa, $c_1^c = 560.4$ kPa, $c_1^m = 36.5$ kPa	

rity, rather it is produced during development, cross-linked, and stretched elastically during normal development/maturation [65]. We also utilized Fung exponential strain energy functions for both collagen [18, 69]

$$\widehat{W}^c(s) = c_1^c \left(e^{c_2^c \left(\lambda^c_{n(\tau)}(s)^2 - 1\right)^2} - 1 \right), \tag{5.4}$$

and passive smooth muscle [6]

$$\widehat{W}^m(s) = c_1^m \left(e^{c_2^m \left(\lambda^m_{n(\tau)}(s)^2 - 1\right)^2} - 1 \right). \tag{5.5}$$

The stretch $\lambda^k_{n(\tau)}(s)$ experienced by each of these constituents depends on its deposition stretch, original orientation, and the stretch experienced by the arterial wall; as in Valentín *et al.* [63], we assumed four families of collagen (axial, circumferential, and symmetric diagonal). In the G&R formalism, values for the parameters c_2^c and c_2^m (table V) were specified such that the artery exhibits reasonable passive behavior while the remaining parameters c, c_1^c, and c_1^m were computed rather than prescribed so as not to overprescribe the basal behavior given the prescription of both "deposition stretches" and "homeostatic target stresses," which are discussed below.

Vasoactive function is a fundamental determinant of arterial mechanical behavior and thus G&R. Among others, Price *et al.* [89] reported constrictor dose-response curves exhibiting sigmoidal behavior and active force-length curves exhibiting inversely parabolic behavior [cf. 21]. The combined effect of these two observations was expressed as

$$\begin{aligned} \sigma_\theta^{act}(s) = T_{max}\, \phi^m(s) \, \left(1 - e^{-C(s)^2}\right) \\ \times \lambda_\theta^{m(act)}(s) \, \left[1 - \left(\frac{\lambda_M - \lambda_\theta^{m(act)}(s)}{\lambda_M - \lambda_0} \right)^2 \right], \end{aligned} \tag{5.6}$$

where T_{max} is a scaling factor with units kPa, ϕ^m is the mass fraction of active smooth

muscle, λ_M and λ_0 are the stretches at which the force generating capacity is maximum and zero, respectively, and $\lambda_\theta^{m(act)}(s)$ is the current active muscle fiber stretch. $C(s)$ is a lumped parameter ratio of constrictors to dilators, which we prescribed as a function of wall shear stress, namely

$$C(s) = C_B - C_S \left(\frac{\tau_w(s) - \tau_w^h}{\tau_w^h} \right), \tag{5.7}$$

where $\tau_w(s)$ is the current shear stress acting on the endothelium and τ_w^h is a homeostatic target value. C_B effectively defines the basal level of active stress generation and C_S models the artery's sensitivity to changing wall shear stress.

Note that equation (5.7) was motivated by interpretations by Rodbard [1] and Zamir [14] of Murray's observation [15] of an optimal (target) condition: arteries constrict or dilate to maintain a target wall shear stress. For fully developed laminar flow of a Newtonian fluid through a rigid cylindrical tube, mean wall shear stress can be approximated as $\tau_w = 4\,\mu\,Q/\pi\,a^3$, where μ is the viscosity of blood, Q is the volumetric flow rate, and a is the luminal radius, each measurable parameters. The target value for shear stress was thus derived from empirical observations [111].

b. G&R Kinetics

It is well known that arteries can functionally adapt to changing physiological demands or hemodynamic loads, in part, by changing rates of constituent turnover [19]. Mass density production rates of collagen and smooth muscle are known to vary with changing mechanical stimuli [92–94, 108]. Altered flow [52, 55, 115], pressure [37, 54, 90, 116], axial extension [45, 61], and responses to clinical interventions such as balloon angioplasty [62, 117–122] can each induce substantial changes from basal rates of turnover. For example, coarctation-induced hypertension has been observed to elicit a 15-fold increase in smooth muscle production [54] and an ∼3 fold increase in

collagen production [37]. Matrix metalloproteinase (MMP) levels increased by 4-5 fold in cases of hypoxia-induced hypertension [123]. Such changes are complicated by the multifunctional effects of other molecules such as nitric oxide (NO) and endothelin-1 (ET-1), which vary with imposed wall shear stress and affect cell and matrix turnover rates [23–26, 52, 53, 56].

For illustrative purposes, we let the production rate of constituent k be a linear function of the two primary mechanical stimuli, intramural and wall shear stresses [cf. 4, 95], namely

$$m^k(s) = m_0^k(1 + K_\sigma^k\,\Delta\sigma^k - K_{\tau_w}^k\,\Delta\tau_w), \tag{5.8}$$

where $\Delta\sigma^k$ is the difference between the current $\sigma^k(s)$ and target $\sigma_h^k(s)$ value of a scalar measure of intramural stress for constituent k, as described by Baek *et al.* [22], and $\Delta\tau_w$ is the difference between the current $\tau_w(s)$ and target τ_w^h value of the magnitude of the wall shear stress. The relationship between wall shear stress and constrictor concentration was prescribed via equation (5.7), with the assumption that constrictors such as ET-1 increase smooth muscle and matrix production and dilators such as NO decrease production [57]. Rate (gain) parameters K_σ^k and $K_{\tau_w}^k$ govern stress-mediated production rates, and m_0^k are basal production rates (assumed constant during maturity, but they likely change from development to maturity to aging) that maintain the artery under homeostatic conditions.

Despite the complex kinetics of smooth muscle and matrix turnover, half-lives for these structurally significant constituents appear to be well described by first order type kinetics [72, 96, 124–126]. We thus prescribed survival functions

$$q^k(s,\tau) = e^{-\int_\tau^s K^k(\widetilde{\tau})d\widetilde{\tau}}, \tag{5.9}$$

where $K^k(\widetilde{\tau})$ are rate-type parameters for mass removal having units of days^{-1}. These

rate parameters were prescribed to be piecewise linear functions of changing fiber tension

$$K^k(\widetilde{\tau}) = \begin{cases} K_h^k & \Delta\zeta(\widetilde{\tau}) \leq 0 \\ K_h^k + K_h^k\,\Delta\zeta(\widetilde{\tau}) & \Delta\zeta(\widetilde{\tau}) > 0 \end{cases}, \tag{5.10}$$

with higher tensions accelerating removal via MMP activity [45, 127–129]. K_h^k are basal arterial constituent rate-type parameters with values of approximately 1/80 day^{-1} [19, 81]. Finally, $\Delta\zeta(\widetilde{\tau})$ is the difference between the current and homeostatic tensions for a fiber deposited at time τ [63]. Note that $\Delta\zeta = 0$ in normalcy and that $K^k(\widetilde{\tau}) = K_h^k$ recovers a simple first order decay. Moreover, elastin is stable biologically under normal conditions in maturity, during which $Q^e(s) = 1$ and $m^e(\tau) = 0$; that is, we assumed that functional elastin does not turn over in mature, healthy arteries [20]. In the case where differences in mechanical perturbations are zero, equations (5.8) to (5.10) recover homeostatic turnover rates.

c. Deposition Stretches

The hypothesis that newly produced constituents are incorporated within extant matrix at preferred mechanical states is fundamental to the basic constrained mixture model [12]. The stretch at G&R time s experienced by a fibrous constituent deposited at time τ is [16]

$$\lambda_{n(\tau)}^k(s) = G_h^k\,\frac{\lambda(s)}{\lambda(\tau)}, \tag{5.11}$$

where G_h^k is the homeostatic deposition stretch for the k^{th} constituent and $\lambda(s)$ and $\lambda(\tau)$ are arterial level stretches in the fiber direction relative to a computationally convenient (original) unloaded reference configuration. Note that if $\lambda(s) = \lambda(\tau)$, then the newly deposited fiber is stretched only at the level at which it was deposited. Whereas deposition stretches were conjectured based on heuristic arguments [12], increasing

cell biological evidence supports this concept. Alberts *et al.* [106] summarized early observations on fibroblasts stating that they "work on the collagen they have secreted, crawling over it and tugging on it–helping to compact it into sheets and draw it out into cables." More recent works [78–80] suggest that synthetic cells exert mechanical forces during deposition and/or matrix reorganization.

It thus appears that cells can and do incorporate new constituents within extant matrix at a preferred stress or stretch. Although we do not know the precise values of these deposition stretches, they must be less than maximum values of stretch in normal tissues. Clearly, this requires deposition stretches greater than 1 and typically less than 2. Functional elastin is deposited almost exclusively during development. As such, it is likely to experience a relatively high prestretch ($\tilde{G}_h^e \in (1.4, 1.8)$) in most arteries. Stiff collagen constantly turns over and is assumed to have a relatively low deposition stretch ($G_h^c \in (1.05, 1.1)$) consistent with observations from purely collagenous tissues such as tendons and intracranial saccular aneurysms [2]. Smooth muscle is less stiff, and is likely deposited as some intermediate stretch ($G_h^m \in (1.2, 1.7)$), which would place it within its normal vasoactive range at basal tone. It is important to note that these are not experimentally derived quantities. Rather, these are estimates that fall within reasonable bounds and yield expected behavior, as, for example, results consistent with the good agreement on mean homeostatic intramural biaxial stresses σ^h of approximately 100 kPa [42, 113].

D. Illustrative Results

1. Vasoactivity

Figure 35 shows the simulated vasoactive stress response as a function of muscle fiber stretch $\lambda_\theta^{m(act)}(0)$ for a range of basal constrictor to dilator ratios C_B (cf.

equation (5.6)). The homeostatic inner radius a_h corresponds to a normalized muscle fiber stretch $\lambda_\theta^{m(act)}(0) = 1$, and C_B effectively defines the basal level of active stress. Simulations revealed that a lower value for C_B results in a lower value for σ^{act}, thus requiring passive muscle to bear higher stresses, and necessitating a larger value of the Fung parameter c_1^m to maintain a constant geometry. Thus, each curve effectively represents a different artery. The complex, coupled relationship between active muscle function and passive behavior also causes the vasoactive parameter C_B to influence the vasoactive responsiveness to changes in wall shear stress τ_w (figure 36). This effect occurs, in part, because of the stiffer passive smooth muscle behavior for low C_B; a more compliant passive muscle allows the artery to adjust its caliber more easily to achieve the target inner radius.

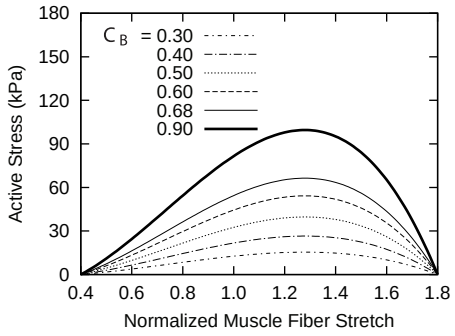

Fig. 35. Active stress-stretch muscle responses for indicated basal values of constrictor to dilator ratio C_B at time $s = 0$ (cf. equations (5.6) and (5.7)). All other parameters are as listed in table V. Each curve represents a functionally different artery. The abscissa 'normalized muscle fiber stretch' is expressed as a range of values for $\lambda_\theta^{m(act)}(0)$, because no G&R is taking place. Note the inverse parabolic behavior [cf. 89].

The shear stress scaling parameter C_S (cf. equation (5.7)) plays a similarly important role in vasoactivity. Figure 37 shows effects of changing the constrictor to

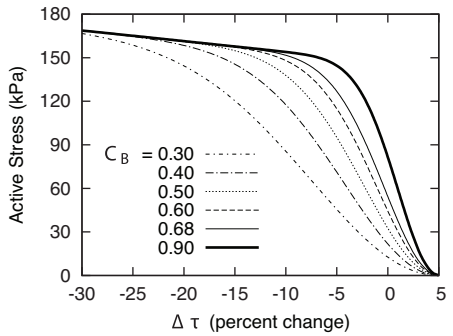

Fig. 36. Active muscle responses for indicated basal values of constrictor to dilator ratio C_B. All other parameters are as listed in table V. Increasing values for C_B result in increasing vasoactive responsiveness to changes in τ_w. Note the near sigmoidal behavior.

dilator ratio C on inner radius (panel a) and active stress (panel b) at a prescribed constant (homeostatic) flow. Higher values of C_S allow the artery to maintain inner radius over a wider range of C and yield a sigmoidal behavior similar to that reported by Price *et al.* [89]. As the inner radius increases, ΔC increases due to shear stress regulation. For a given inner radius a, lower C_S results in lower values of C. Coupled with the inversely parabolic active force-length behavior (figure 35), lower C_S also results in peak active stress generation occurring at lower C. Thus, by choosing C_B and C_S appropriately, we can endow the simulated artery with vasoactive biases to certain ranges of C and τ_w. The parameters listed in table V yield vasoactive behavior comparable to that of basilar arteries [27].

2. Mass Production

In addition to instantaneous passive and active behavior, the constrained mixture G&R framework relates mechanical stimuli to constituent mass density production rates. For example, an increase in blood pressure at a constant flow results initially in

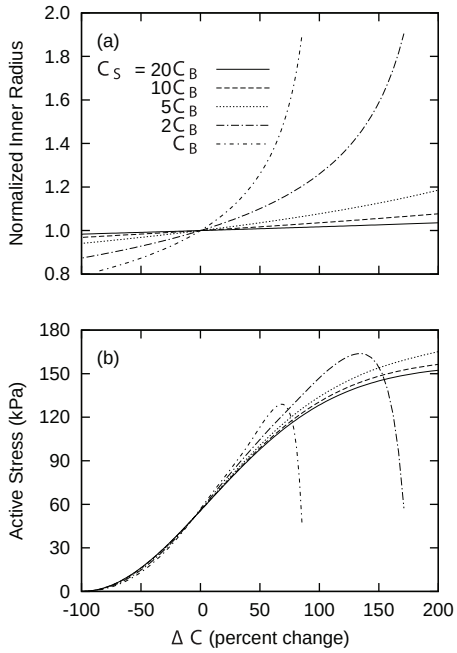

Fig. 37. Normalized target inner radius (panel a) and active muscle responses (panel b) as functions of changing constrictor to dilator ratio C (shown here as the percentage of $\Delta C = C - C_B$) for indicated values of C_S. Flowrate Q is constant at the homeostatic value. Higher values of C_S allow the artery to better maintain the target inner radius over a wider range of C. Lower values of C_S cause the artery to generate peak active stresses for smaller changes in C. By increasing C_S, the artery is able to accommodate larger changes in constrictor concentration (see equation (5.6)). Note the generally sigmoidal behavior [cf. 89].

passive dilation due to wall distensibility. This dilation, along with isochoric thinning, elevates stresses in circumferentially aligned constituents while decreasing τ_w, which in turn leads to increases in C. Thus a sustained increase in pressure increases "circumferential" mass production for two reasons (cf. equation (5.8)), increased intramural stress and increased shear mediated constrictor concentration. Hence, the mechanical stimuli work in unison in this case; there are no competing effects. It proves useful, however, to consider cases in which changing mechanical stimuli induce competing effects. Consider, therefore, the case of a step decrease in flow while pressure remains constant. Following the reduction in flow, the artery constricts to restore τ_w to τ_w^h. This initial vasoactivity unloads circumferential collagen, and the lower intramural stress serves as a negative input for mass production, while the increased constrictor to dilator ratio C, which is a function of τ_w, serves as a positive input for mass production.

Figure 38 illustrates relationships between changing mechanical and mechanically induced stimuli ($\Delta\sigma$ and ΔC) and the mass density production rate of circumferential collagen for a sustained 30% decrease in flow. Recalling equation (5.8), consider cases in which $K_\sigma^k = 1$ and $K_{\tau_w}^k = 0$ (panels a and b), $K_\sigma^k = 0$ and $K_{\tau_w}^k = 1$ (panels c and d), and $K_\sigma^k = K_{\tau_w}^k = 1$ (panels e and f). As prescribed, setting $K_\sigma^k = 1$ and $K_{\tau_w}^k = 0$ yields a direct relationship between $\Delta\sigma$ and m^k (figure 38, panel a). Similarly, setting $K_\sigma^k = 0$ and $K_{\tau_w}^k = 1$ yields a direct relationship between ΔC and m^k (figure 38, panel d). In contrast, results for the case in which $K_\sigma^k = K_{\tau_w}^k = 1$ suggest a biphasic G&R response (figure 38, panels e and f). From days 0 to 30, mass production is related inversely to σ while related directly to C; after day 30, mass production is related directly to σ while related inversely to C. An inverse correlation of one stimulus plus a direct correlation with the other stimulus reveals strong competing effects. Specifically, the relationship between mass production and ΔC from days 0 to 30

suggests that early flow induced G&R is dominated by shear induced stimulation of vasoactive molecule production whereas that between mass production and $\Delta\sigma$ from days 30 to 1000 suggest a second phase dominated by changes in wall stress. This finding is consistent with flow-induced changes in caliber preceding changes in thickness as reported in the literature and extends the earlier speculation of Rodbard [1] with regard to a "two-phase" response by to a sustrained alteration in flow.

Changing axial length elicits similar competing effects. Figure 39 illustrates relationships between changing $\Delta\sigma$ and ΔC and the mass density production rate of axially aligned collagen for a 2% increase in *in vivo* axial length at a constant pressure and flow. This increase in axial length reduces slightly the inner radius and the wall thickness, due to an initial isochoric response. As the inner radius decreases, τ_w increases and causes the vessel to dilate, thus restoring τ_w to τ_w^h. These factors serve to decrease C and increase stresses in the axially aligned constituents. As in the case of a step decrease in flow, setting $K_\sigma^k = 1$ and $K_{\tau_w}^k = 0$ results in a direct relationship between $\Delta\sigma$ and m^k (figure 39, panel a) whereas $K_\sigma^k = 0$ and $K_{\tau_w}^k = 1$ results in a direct relationship between ΔC and m^k (figure 39, panel d). Setting $K_\sigma^k = K_{\tau_w}^k = 1$ again reveals a biphasic behavior: ΔC has a weak influence from days 0 to 40 whereas $\Delta\sigma$ dominates m^k from approximately day 20 to 1000. Comparatively large changes in σ override the competing effects of ΔC, indicated by the nearly direct relationship with respect to $\Delta\sigma$ and inverse relationship with respect to ΔC.

3. Evolving Geometry

Time courses of evolving radius, thickness, unloaded inner radius, and unloaded axial length depend greatly on mechanical stimuli and the associated mass density production parameters [63]. To appreciate better the complex coupled roles of changing wall shear stress and intramural constituent stresses, we analyzed the observable

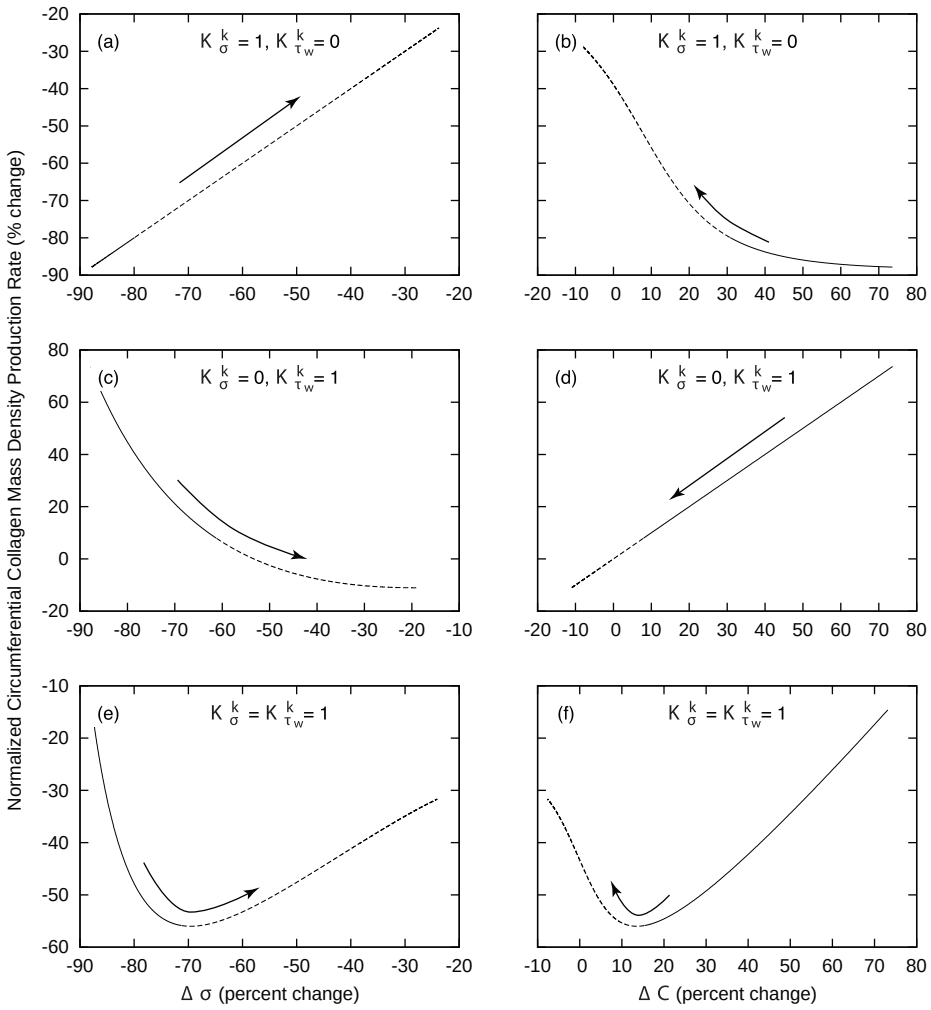

Fig. 38. Comparison of intramural and wall shear stress regulation of circumferential collagen production rates. Values given as functions of changes in the scalar measure of stress borne by circumferential collagen (panels a, c, and e) and changes in constrictor to dilator ratio C (panels b, d, and f) for G&R in response to a sustained 30% decrease in flow from days 0 to 30 (solid) and from days 30 to 1000 (dashed). Arrows indicate advancing time. Note the direct relationship between changes in σ and mass production when $K_\sigma^k = 1$ and $K_{\tau_w}^k = 0$ (panel a) and the direct relationship between changes in C and mass production when $K_\sigma^k = 0$ and $K_{\tau_w}^k = 1$ (panel d), each linear as postulated separately (table IV). In contrast, note the biphasic progression of G&R when $K_\sigma^k = K_{\tau_w}^k = 1$ (panels e and f), that is, when production rates depend on changes in both intramural and wall shear stresses, which reveals potentially competing effects.

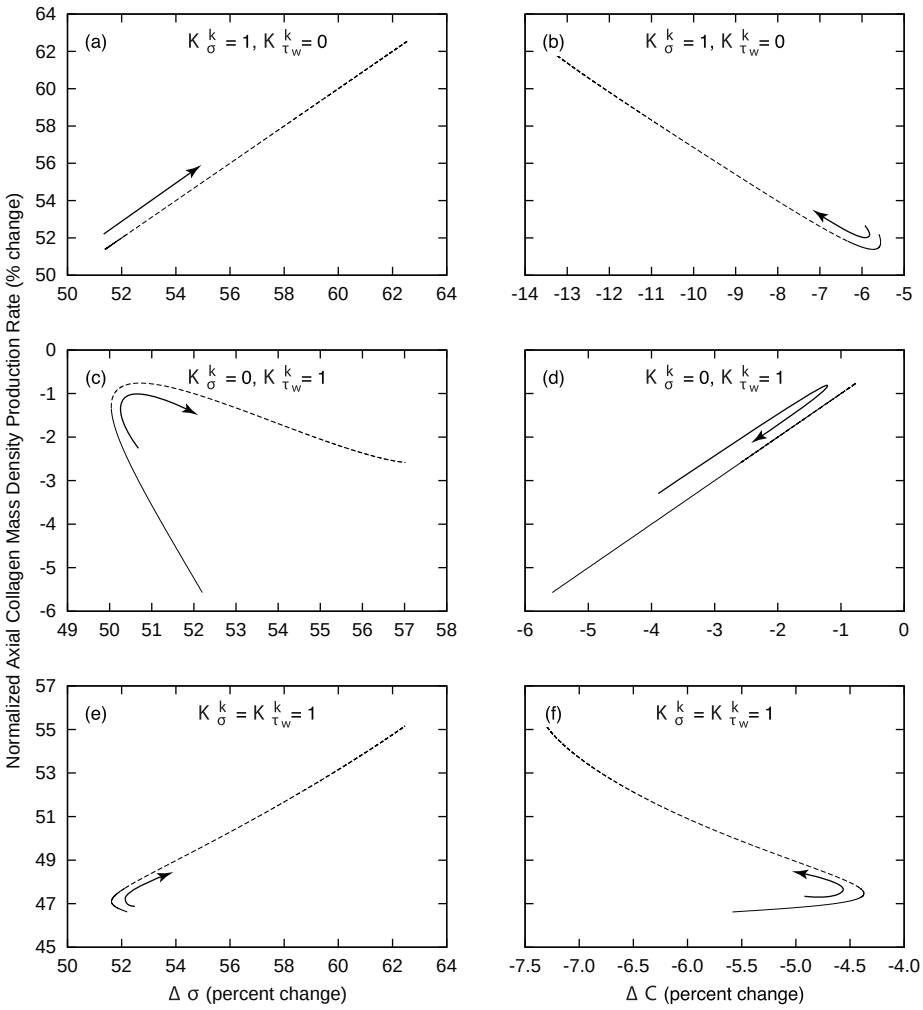

Fig. 39. Comparison of intramural and wall shear stress regulation of axial collagen production rates. Values given as functions of changes in the scalar measure of stress borne by circumferential collagen (panels a, c, and e) and changes in constrictor to dilator ratio C (panels b, d, and f) for G&R in response to a sustained 2% increase in axial length from days 0 to 40 (solid) and from days 40 to 1000 (dashed). Arrows indicate advancing time. Note the biphasic progression when $K^k_\sigma = K^k_{\tau_w} = 1$ (panels e and f). From days 0 to 40, mass production is inversely related to σ while directly related to C. After day 40, mass production is directly related to σ while inversely related to C.

evolving geometric quantities as functions of the kinetic parameters K_σ^k and $K_{\tau_w}^k$ for cases of increased transmural pressure, decreased luminal flow, and increased axial length. These parameter sensitivity studies over multiple orders of magnitude (from 0.1 to 10) provide important insight and intuition regarding the differing modes of interaction among similarly involved mechanisms.

Figure 40 illustrates time varying consequences of a sustained 50% increase in pressure, at a constant flow and length, as functions of K_σ^k and $K_{\tau_w}^k$. *In vivo* geometries generally approached their targets more rapidly with larger values of both K_σ^k and $K_{\tau_w}^k$, but important differences surfaced. Note that the "singular" behavior at $K_\sigma^k = K_{\tau_w}^k = 0$, which models constant mass density production, is not biologically relevant [64]. Inner radius (figure 40, panel a) shifts toward its target rapidly and is least sensitive to K_σ^k and $K_{\tau_w}^k$. This finding suggests that inner radius is mostly regulated by an early vasoactive behavior as expected. In contrast, K_σ^k and $K_{\tau_w}^k$ exert a greater influence on the evolution of wall thickness (figure 40, panel b); larger values of K_σ^k and $K_{\tau_w}^k$ accelerate evolution. In the limiting case of $K_\sigma^k = K_{\tau_w}^k = 0$, mass density production rates are constant while mass removal remains a function of fiber tension (see equation (5.9)). After 100 days, the artery atrophies appreciably as degradation outpaces production, resulting in a dilation of 3% and a reduction in thickness of ∼40%. Such a loss of stiff collagen and muscle requires a higher level of muscle activation to maintain inner radius constant, which would seem to be energetically unfavorable. Figure 40 (panel c) shows that after 100 days, the artery's unloaded inner radius (without vasoactivity) increases when $K_\sigma^k = K_{\tau_w}^k = 0$. For $K_\sigma^k > 0$ or $K_{\tau_w}^k > 0$, unloaded inner radius remains nearly constant as it should in response to constant flow.

Evolution of the unloaded axial length is more complex (figure 40, panel d). For the limiting case of $K_\sigma^k = K_{\tau_w}^k = 0$, the unloaded axial length decreases (which

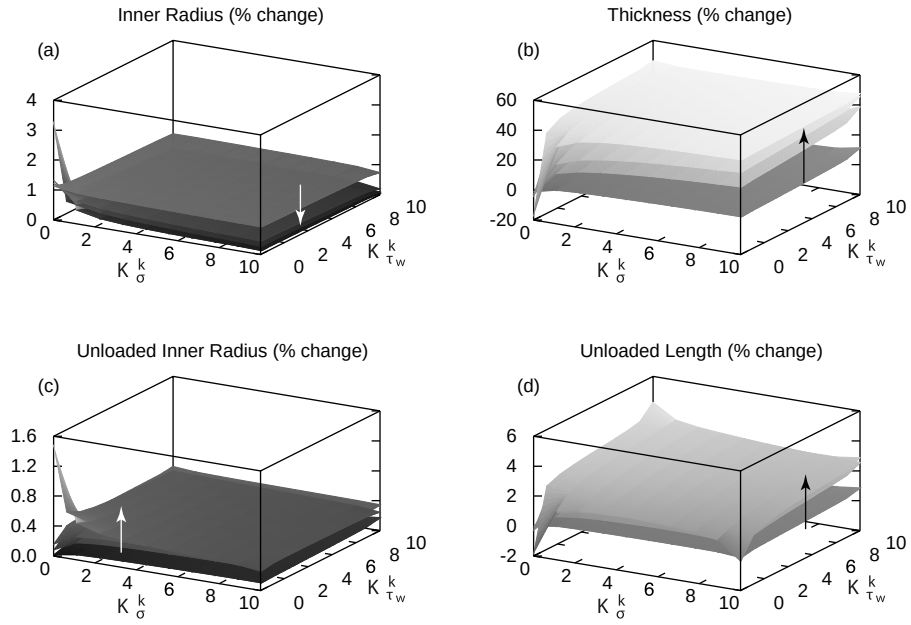

Fig. 40. Percent changes in inner radius (panel a), thickness (panel b), unloaded inner radius (panel c), and unloaded length (panel d) for a sustained 50% increase in pressure; results shown at days 1, 7, 14, and 100 of G&R with the arrows denoting advancing time. The model predicts small changes in inner radius as the vessel restores τ_w toward τ_w^h. Wall thickness increased by 50% as it should, with higher values of K_i^k accelerating the process. Unloaded length increases with increased collagen deposition, thus resisting the recoiling effects of elastin. Note the near singular behavior at $(K_\sigma^k, K_{\tau_w}^k) = (0, 0)$, consistent with prior findings that such values are unrealistic biologically [64].

implies a larger *in vivo* axial stretch), as decreased axial and helical collagen allow highly prestretched (unchanging) elastin to recoil the artery further. Focus, however, on values of $K_{\sigma}^{k} > 0$ and $K_{\tau_w}^{k} > 0$ and recall that each fiber family's mass production rate was defined individually as a function of its unique scalar measure of stress but a common τ_w (equation (5.8)). Moreover, note that helically and axially oriented collagen fiber families greatly influence the unloaded axial length. As pressure increases, C and σ^k increase for all constituents. Due to the prescribed constant *in vivo* axial length, however, circumferentially oriented constituents experience greater increases in σ than do those aligned helically and axially. Hence, as time progresses and the wall thickens, σ^k can decrease for helical and axial collagen, thereby resulting in a competition of influences between K_{σ}^{k} and $K_{\tau_w}^{k}$, but an overall increase in unloaded length and consequently a lower *in vivo* axial stretch similar to experimental observations.

Evolving inner radius in response to a 30% reduction in luminal flow (figure 41, panel a) is nearly insensitive to changing K_{σ}^{k} and $K_{\tau_w}^{k}$. Similarly, evolution of the unloaded inner radius (figure 41, panel c) is remarkably insensitive to these kinetic parameters. The unloaded inner radius follows *in vivo* inner radius as the artery remodels around its new vasoconstricted state. Evolving thickness (figure 41, panel b) is a function of isochoric motion and mass kinetics, with the initial vasoconstriction resulting in an $\sim$10% isochoric increase in wall thickness. Note that in the limiting case when $K_{\sigma}^{k} = K_{\tau_w}^{k} = 0$, wall thickness does not change because mass production rates remain constant. Setting $K_{\sigma}^{k} > 0$ or $K_{\tau_w}^{k} > 0$ results in gradual thinning in response to reduced intramural constituent stresses, with diminishing rates of evolution beyond $K_{\sigma}^{k} > 2$ or $K_{\tau_w}^{k} > 2$. Long-term evolution of wall thickness is largely insensitive to $K_{\tau_w}^{k}$ because the initial vasoconstriction nearly restores τ_w to τ_w^h. Also, a decrease in intramural constituent stress results in reduced mass density production

below m_0^k, with a minimum production rate of zero. Any $\Delta\sigma$ such that mass production is zero will yield the same wall thickness evolution, regardless of K_σ^k. For these same reasons, evolving unloaded axial length is less sensitive to $K_{\tau_w}^k$, with diminishing sensitivity beyond $K_\sigma^k = 2$ (figure 41, panel d).

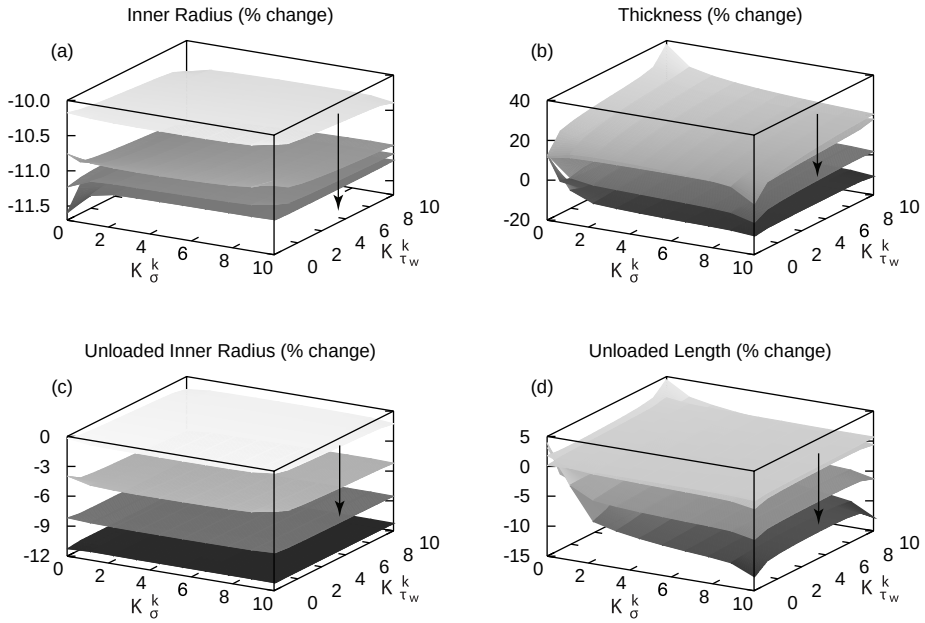

Fig. 41. Percent changes in inner radius (panel a), thickness (panel b), unloaded inner radius (panel c), and unloaded length (panel d) for a sustained 30% decrease in flow; results shown at days 1, 30, 100, and 1000 of G&R with the arrows denoting advancing time. The inner radius ultimately decreases by the predicted amount ($0.7^{1/3} = 0.88$ [74]) as it should. Note the large changes in unloaded inner radius as the artery remodels around its new constricted state. Unloaded axial length decreases as the artery's collagen to elastin ratio decreases and the thickness decreases, thereby allowing the elastin to retract the artery further when unloaded.

Increased axial stretching, at constant pressure and flow, results in a decreased inner radius and decreased thickness due to an initial isochoric motion. Yet, a 2% increase in axial length (figure 42) causes negligible changes in inner radius (panel a),

and thus unloaded inner radius (panel c), as the artery vasodilates to restore τ_w^h. For low values of K_σ^k and $K_{\tau_w}^k$, the unloaded inner radius decreases more appreciably as the wall atrophies. Evolution of wall thickness (figure 42, panel b) clearly reveals a competition between the effects of shear- and stress-mediated mass production: because luminal flow is constant, the reduced inner radius elevates τ_w, which works to diminish mass production, while a decreased wall thickness increases intramural constituent stresses, which heightens mass production. For these reasons, the wall thickens the most when $K_\sigma^k = 1$ and $K_{\tau_w}^k = 0$ at any given G&R time s. Similarly, deposition rates for axial and helical fiber increase with increasing K_σ^k, thereby increasing the unloaded axial length. This change in unloaded length is largely independent of $K_{\tau_w}^k$ (figure 42, panel d).

E. Discussion

Truesdell and Noll [130] articulated well the complementary roles of theory and experiment:

> The task of the theorist is to bring order into the chaos of the phenomena of nature, to invent a language by which a class of these phenomena can be described efficiently and simply. Here is the place for "intuition," and here the old preconception, common among natural philosophers, that nature is simple and elegant, has led to many great successes. Of course, physical theory must be based on experience, but experiment comes after, not before, theory. Without theoretical concepts one would neither know what experiments to perform nor be able to interpret their outcome.

As theories and experiments have become more detailed and complex, numerical simulations have emerged as a third pillar of scientific research. Numerical simulations

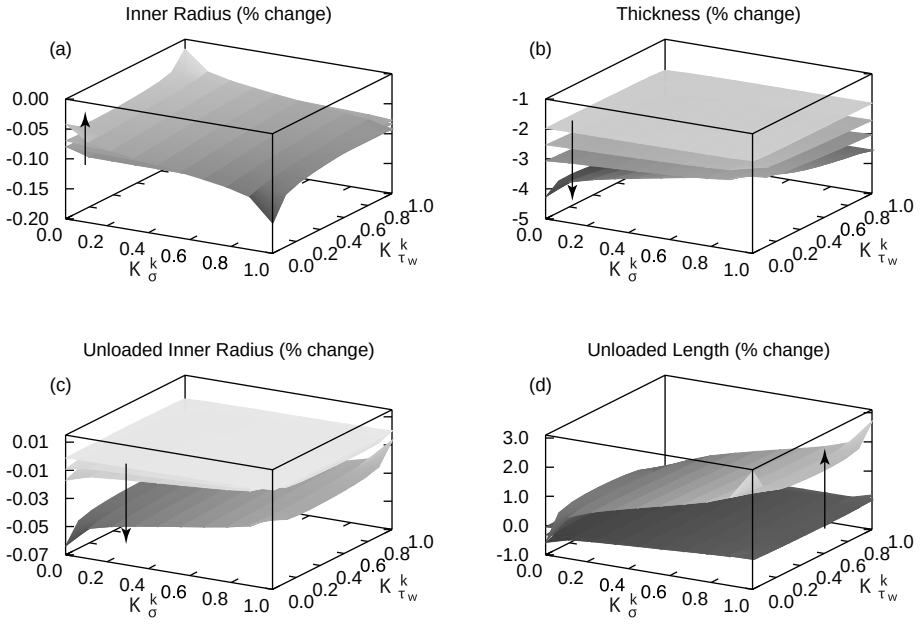

Fig. 42. Percent changes in inner radius (panel a), thickness (panel b), unloaded inner radius (panel c), and unloaded length (panel d) for a sustained 2% increase in axial length; results shown at days 1, 7, 14, and 100 of G&R with the arrows denoting advancing time. As in the case of increasing pressure, the inner radius remains nearly constant, given the constant flow. Unloaded length increases, as expected, due to increasing deposition of axial collagen at its preferred value.

allow researchers to generate, test, and refine hypotheses and theoretical concepts with much greater efficiency in terms of both time and expense. This refinement, in turn, permits the design of more rational and fruitful experiments, as called for (albeit differently) by Truesdell and Noll. The emergence of the need for multiscale models to integrate mechanobiological information and increase understanding from the genome to medical or surgical treatment at tissue and organ levels only highlights further the need for iterative observational, theoretical, experimental, and computational studies. Of these, our focus herein was limited to the role of parameter sensitivity studies within numerical simulation.

Predicted vasoactive behaviors were consistent with observed trends [89] based on the prescribed material behavior of equation (5.6) and associated parameters listed in table V. In particular, active behavior was sensitive to both the initial level of the constrictor to dilator ratio C_B and the shear stress scaling factor C_S. Coupled length dependent active behaviors and constrictor dose responses greatly affected vasoactive efficiency. For low values of C_S, smooth muscle developed peak stresses for relatively low increases in C. That is, the artery was not able to compensate well for large decreases in flow without shear stress mediated regulation, consistent with experimental observations [131, 132]. Along with appropriate passive behavior, this coupling was crucial to obtaining realistic vasoactive behavior for the artery of interest. The associated muscle activity parameters C_S, C_B, λ_M, and λ_0 can be tailored to describe a particular artery by stipulating that peak active stresses are generated at appropriate ratios of constrictors to dilators, thereby yielding realistic relationships between wall shear stress and the active response [3].

Vasoactive behavior influences long term G&R by controlling the state in which turnover occurs, thereby affecting changes in wall thickness and unloaded length, which in turn affect intramural stresses [cf. 13, 33]. The competing effects of intramu-

ral stress- and wall shear stress-regulated turnover resulted in complex G&R based on our model. This was most evident in cases of decreased flow or increased axial length; decreased (increased) wall shear stress and decreased (increased) intramural stresses provide opposite inputs to mass production. Even for the case of increased transmural pressure, where all mechanical stimuli tend to accelerate turnover, there was a competition between K_{σ}^{k} and $K_{\tau_w}^{k}$ in the evolution of unloaded axial length. This finding further emphasizes the complex interactions possible even with linear production rates.

Simulations revealed that progression of G&R for some perturbations involved the dominance of one mechanical stimulus during one phase but the emergence of another dominant stimulus during a subsequent phase. For example, reductions in flow and increases in axial extension elicit such responses. Increased MMP activity can precede mass production [62], thus resulting in initial atrophy followed by eventual compensatory hypertrophy and maintenance. These predicted time courses suggest provocative possibilities for designing intervention, as, for example, timed drug delivery. Similarly, such time courses could aid in the decision process when choosing time intervals at which to collect samples and/or use appropriate immunohistological stains or other markers, for example. Finally, predictive models promise to aid in the refinement of tissue engineering strategies to build in desirable properties via appropriately timed stimuli.

The model predicted differing modes of G&R and degrees of sensitivity to parameter values depending upon the type of perturbation, despite the similarly involved mechanisms. Most notably, the model was most sensitive to increases in axial stretch beyond the homeostatic. This extreme sensitivity is similar to the observations reported by Jackson *et al.* [45], wherein they noted "unprecedented" rates of change *in vivo* when arterial length was increased. Our numerical implementation predicted

upper and lower bounds (saturation points) in shear-induced active stress generation and values for K_i^k beyond which the system was no longer sensitive to a particular stimulus. For example, the model predicted little sensitivity beyond $K_\sigma^k = 2$ with respect to evolving thickness for cases of reduced flow for this drove mass density productions to zero.

Predicted geometric consequences of G&R, like evolving passive and active behaviors, can be compared to experimentally observed behaviors. Such comparisons will assist in formulating improved constitutive relations and determining best-fit values of the associated parameters. Nevertheless, mixture models require mechanical response parameters for each individual constituent, which increases the overall number of parameters and thereby raises concerns by some that there are too many parameters. We suggest, however, that one advantage of structurally motivated models is that many of the parameter values can be prescribed independently and in many cases prescribed directly, based on experimental data. In this way, one reduces the need to perform nonlinear regressions based on large numbers of unknown parameters, which would otherwise raise issues of non-uniqueness. Moreover, once good estimates are determined for the parameters, one can perform nonlinear regressions based on restricted (physically meaningful) parameter search spaces. We did not study the sensitivity of the constrained mixture model to ranges of observed parameters or certain bounded parameters because they are experimentally available. Indeed, noting that functional forms appear to be preserved across species, whereas parameter values vary with species and to some degree individuals, Stålhand and Klarbring [133] and Masson *et al.* [134] showed that parameter values can be estimated in individual patients in part because of known bounds on many of the parameters and prior experience in modeling [2]. There is, however, a need for better experimental data where possible to refine further the values of many of the parameters.

Constituent turnover (production and removal) as a function of mechanical stimuli remains the least well-understood aspect of arterial growth and remodeling. That is, there remains a pressing need for a better understanding of cellular responses to mechanical stimuli and how these responses manifest at the tissue and organ levels. To that end, we hope that continuum based constrained mixture models will motivate experimentalists and theorists alike to elucidate these intricately linked behaviors. Although we anticipate the need for a more rigorous analysis, hypothesis testing [64] and parameter sensitivity studies represent an important first step toward verification [85]. While no framework or numerical model can ever be strictly correct, the ultimate measure of a model's utility is to what extent it can describe and predict what is physically reasonable. Rational theories founded upon realistic fundamental cellular behavior and continuum mechanics promise to help us develop intuition, understand complex biomechanical systems, and design better experiments and ultimately clinical interventions.

CHAPTER VI

RELATION AMONG AGING, ELASTIN DEGRADATION, AND HYPERTENSION: A COMPUTATIONAL STUDY

A. Overview

Arterial responses to varied pathologies and insults likely occur via similar mechanisms. In particular, diverse studies suggest that similar mechanisms may be involved in hypertension and the natural aging of arteries. There are several parallels between hypertension, induced loss of elastin, and aging. Our goal is to show how matrix remodeling, through changing levels of elastin and collagen, ultimately impacts evolving arterial geometry and mechanical behavior. Employing a continuum theory of constrained mixtures, we show that hypertension is effectively equivalent to accelerated aging, consistent with diverse findings reported in the literature. Finally, we review briefly the potential roles of compromised elastin in arterial aging, hypertension, atherosclerosis, aneurysms, and Marfan syndrome.

B. Introduction

Elastin is an important rubber-like constituent in the mammalian vasculature [17, 135]. Unlike other structurally-significant vascular constituents, elastin undergoes no notable turnover in normal, healthy arteries. The extent to which elastin contributes to arterial behavior cannot be overstated. It is believed that elastin is primarily deposited and arranged within the extracellular matrix during the perinatal period [136–138], and as a result, it is likely responsible for the presence of residual stresses and resulting opening angles [139–142]. It is believed that these residual stresses serve to endow arteries with nearly constant circumferential stress distributions through

their thicknesses under physiological loads [143, 144].

The biomechanical properties of arteries play vital roles in vascular physiology and pathophysiology [2, 145, 146]. These properties result from the complex structure of the arterial wall, which consists primarily of collagen, elastin, proteoglycans, and three primary cell types. Specifically, the wall contains multiple types of collagen (e.g., I, III, IV, V, VI, and VIII), with the fibrillar types I and III dominating overall load bearing capability ($\sim$ 80 to 90%; [147]). When we refer to elastin, we often actually mean the elastic fibers that tend to be organized as lamellae and consist primarily of elastin ($\sim$ 90%; [148]) but also microfibrils such as fibrillin-1,-2, fibulin-1,-2,-5, microfibril-associated glycoprotein-1,-2 (MAG-1,-2), and Emilin-1. For a comprehensive list of the diverse molecules found within elastic fibers, and their individual functions, see Kelleher *et al.* [78], Kielty *et al.* [149] and Mithieux and Weiss [135]. Although these microfibrils do not appear to confer much stiffness directly [150], they likely organize and help stabilize the elastin. All of these structural constituents are embedded in a ground substance matrix consisting of abundant water and multiple proteoglycans, including versican, biglycan, decorin, and lumican [78]. The overall stiffness of the arterial wall thus depends on the mass fractions, orientations, and cross-linking of the individual constituents as well as their many interactions. Although we eventually seek to understand wall biomechanics in terms of the individual constituents, Karnik *et al.* [151] notes that "The myriad associations and interaction between the many structural proteins, proteoglycans and growth factors of the vascular matrix makes it difficult to distinguish the effects of each element from another." Hence, it continues to be advantageous to focus on but the three primary classes of structural constituents elastin, collagen, and smooth muscle in conceptual and mathematical models of the arterial wall [cf. 9]. We focus herein, however, on 'elastin-dominated' contributions to the structural integrity of the wall

for elastin endows arteries with extensibility, elastic recoil, and resilience. Indeed, damage to or loss of elastin can result in severe vascular consequences, including the formation of aneurysms, age-related stiffening, aortic dissections in Marfan syndrome, and so forth [2, 152–156].

1. Biomechanical Background

Based on *in vivo* observations, it was realized in the 1960s that many arteries experience little to no axial deformation during the cardiac cycle [e.g., 157, 158]. Soon thereafter it was suggested that this constancy of length was hemo-dynamically favorable [159]. *In vivo* observations revealed further that arteries retract significantly when resected, thus suggesting the existence of an axial prestretch that defines the preferred *in vivo* length of an artery. Dobrin *et al.* [160] showed that this axial prestretch (or "longitudinal traction") increases nearly linearly with age during postnatal development and thereby suggested that it can be "attributed to stretching of the vessels by growth and to changes in connective tissue composition." Subsequent studies by Dobrin *et al.* [161], using elastase and collagenase to selectively remove different structural components within the wall, revealed that nearly all of the axial prestretch in healthy arteries is due to the presence of intramural elastin, not collagen. Indeed, Davis [162] noted further that "the elastic laminae stretch as the vessel grows in diameter" during development.

Comparing *in vivo* measurements with results from *in vitro* biaxial mechanical tests, Van Loon *et al.* [163] showed that *in vitro* force-length data estimate well the *in vivo* axial prestretch (indicated by a "cross-over point" in force-length plots at different constant pressures). For example, the directly measured *in vivo* prestretch for canine carotids was 1.52 ± 0.10 whereas that inferred from *in vitro* mechanical data was 1.54 ± 0.11 for paired measurements ($n = 11$). This ability of *in vitro*

testing to estimate well the *in vivo* axial stretch was confirmed by Weizsäcker *et al.* [164] and Brossollet and Vito [165], which suggested further the existence of a unique property of the wall rather than merely an effect of perivascular tethering. In particular, Weizsäcker and colleagues reported directly measured and mechanically inferred values of *in vivo* prestretch for rat carotid arteries to be 1.69 ± 0.11 and 1.70 ± 0.11 ($n = 6$), respectively. It is noted, of course, that measurements must be performed carefully, for changes in body position can alter the apparent *in vivo* prestretch in arteries such as carotids [159]. It is interesting to note that Van Loon *et al.* [163] suggested that the unique *in vitro* mechanical behavior at the *in vivo* value of axial prestretch "demonstrates not only how well arteries are adapted to their function, but also that *in vitro* studies can have physiological significance." Indeed, Brossollet and Vito [165] showed via a formal stability analysis that the "*in vivo* property" of constancy of axial stretch and force during pressurization shows that "blood vessels are optimized against longitudinal buckling and body motion."

Much more recently, it has been discovered that vascular cells endothelial, smooth muscle, and fibroblasts are sensitive to changes in their mechanical environment and they seek to maintain a 'homeostatic mechanical state' that manifests on a macroscopic scale as changes in geometry, structure, and properties [3, 74]. For example, Jackson *et al.* [45] showed that surgically increasing the length of the carotid artery in a mature rabbit beyond its preferred value causes the vessel to grow axially via a rapid turnover of cells and extracellular matrix so as to restore the axial prestretch toward its original value (1.62 ± 0.02). This observation has been confirmed by a number of groups, including Gleason *et al.* [46] who studied mouse carotid arteries *ex vivo* (with an axial prestretch ~ 1.84). There is a need, however, for more data on the effects of altered axial extensions on smooth muscle contractility [cf. 166, 167] and possible phenotypic modulation. Nevertheless, it appears that arterial adaptations to

altered blood flows, pressures, and axial extensions occur via common mechanisms of growth and remodeling [6, 7, 35, 36, 168], often resulting from complementary roles of altered vasoactivity and cell-matrix turnover [3].

Elastase and collagenase have also been used to delineate separate contributions of elastin and collagen to overall biaxial wall mechanics. For example, Dobrin and Canfield [169] found an $\sim$ 50% reduction in circumferential and axial stresses, at comparable diameters, following elastase treatment. Related work by Dobrin *et al.* [170] and Fonck *et al.* [171] provide data on the effects of elastase treatment on basic pressure-diameter behaviors. For example, consistent with early reports by Roach and Burton [172], degradation of elastin causes arteries to distend more in response to pressurization, particularly at lower pressures (e.g., 165% distension relative to control at 25 mmHg and 131% at 100 mmHg; [170]. It is interesting to note that Fonck *et al.* [171] reported further that elastase decreased the residual stress related opening angle [cf. 139] and caused an $\sim$10% increase in the axial length of rabbit carotid arteries. We shall return to these observations below.

2. Elastogenesis

Just as mechanical stimuli contribute to the control of vascular adaptations during maturity, so too they play an important role, with genetics, in determining wall geometry, structure, and properties during development [173, 174]. Consider, for example, the results from two particularly clever *in vivo* experiments. Leung *et al.* [175] compared the accumulation of elastin and collagen in the rabbit ascending aorta and pulmonary trunk during postnatal development because these two vessels remain similar in length and caliber despite developing very different wall thicknesses and compositions due to the increase in blood pressure in the aorta following birth and the corresponding decrease in pressure in the pulmonary trunk. By two months of age,

nearly 3 times more elastin and 2 times more collagen accumulated in the higher pressure ascending aorta, consistent with its higher mean circumferential stress. Langille *et al.* [176] compared perinatal development regionally in the aorta of lambs because of the marked increase in blood flow in the thoracic aorta and marked decrease in blood flow in the abdominal aorta following birth, with blood pressures increasing similarly in both segments. They found that increases and decreases in blood flow resulted in marked increases and decreases in caliber, respectively, while corresponding changes in wall thickness tended to maintain mean circumferential wall stress nearly constant in both segments ([cf. 177] who found similar wall tensions in aortas from different species despite the very different calibers). They concluded that there is an important interplay between responses to altered blood flows (wall shear stress) and pressures (intramural stress), which is consistent with current mechanobiological findings [74]. Finally, note that regional differences exist in collagen-to-elastin ratios along the aorta as do differences in local pulse pressures [178, 179]. It is interesting that elastin is absent in arteries within invertebrates or primitive vertebrates having low pressures and pulse pressures, presumably because elastic fibers enable large arteries to "damp out the pulsatile flow and blood pressure" [150] and they confer arteries with the "properties of elastic recoil and resilience" [135].

Of particular note here, elastin and collagen both accumulate in the arterial wall during development, but the rate of synthesis of elastin is particularly high during the late fetal and early postnatal periods and essentially nonexistent thereafter [135, 180, 181]. Moreover, in contrast with collagen, which has a normal half-life on the order of 70 days [20], elastin is exceptionally stable biologically with a normal half-life of years to decades depending on the species [135, 153, 162, 181]. This remarkable stability appears to result from the alternating hydrophobic and lysine-based cross linking domains of tropoelastin (i.e., the elastin monomer), with nearly 90% of the

possible cross-linking domains typically cross-linked via the action of lysyl oxidases [182].

Kao *et al.* [183] reported that the secretion of soluble tropoelastin follows first order kinetics with a half-time of 60 min and similarly that the incorporation of tropoelastin into insoluble elastic fibers follows first order kinetics with a half-time of 85 minutes. They suggested that, for purposes of overall modeling, secretion and incorporation can be "described by a single first order process." More recent studies [e.g., 80] confirm synthesis times on the order of 30 minutes. Advances in molecular biology and imaging have also provided further insight into the many constituents that comprise elastic fibers [149] and the associated mechanisms of assembly [182, 184]. For example, it appears that tropoelastin is secreted and maintained temporarily at the cell surface as partially cross-linked aggregates that associate with previously secreted microfibrils (e.g., fibulin-5); these aggregates then appear to transfer to a pre-existing microfibrillar scaffold (including fibrillin-1,-2 and probably MAGPs) within the extracellular space where they may be cross-linked further. That is, there is a need for both temporal and spatial coordination, perhaps with the sequence of synthesis moving from fibronectin to fibrillin-1, MAGP-1, fibulin-5, and then elastin [182]. Whereas some microfibrils may serve primarily as scaffolds (e.g., fibrillin-2) that facilitate the early alignment and cross-linking of the polymeric elastin by lysyl oxidases, others (e.g., fibrillin-1) may serve to increase the long-term durability of the composite elastic fiber.

One of the most provocative discoveries, however, is that "cells are actively involved in the organization and alignment of elastin aggregates into linear structures and the deposition of elastin aggregates onto preexisting fibers" [182]. In particular, Czirok *et al.* [185] and Kozel *et al.* [80] show that elastic fiber assembly involves coordinated actions (e.g., motions) between cells as they align, stretch, and release elastin;

the degree of fiber stretch was as large as 50% in some cases. Subsequent deposition of elastin onto established fibers did not appear to affect the underlying length, but rather to thicken the fibers by accretion. Moreover, it appears that "motile cells help build elastic fibers by moving and connecting progressively larger segments" [80]. Although the means by which the cells "hold onto" the elastin are not yet known, candidates include elastin binding proteins, integrins, and glycosaminoglycans. Regardless, it appears that cells can control the deposition of elastic fibers, including the alignment, thickness, and possibly prestretch of the fibers based on mechano-control.

C. Methods

1. General Framework

a. Continuum Formulation

The total Cauchy stress in the arterial wall, accounting for contributions from passive constituents and active smooth muscle, is

$$\boldsymbol{\sigma} = \frac{1}{\det \mathbf{F}} \mathbf{F} \frac{\partial W}{\partial \mathbf{F}^T} + \sigma^{act}([\mathrm{Ca}^{2+}], \lambda^{m(act)})\, \mathbf{e}_\theta \otimes \mathbf{e}_\theta, \tag{6.1}$$

where $\mathbf{F}$ is the deformation gradient tensor, W is the homogenized strain energy function for the mixture, and σ^{act} is the active muscle contribution, acting in the circumferential direction, which is a function of intracellular calcium ion concentration $[\mathrm{Ca}^{2+}]$ and muscle fiber stretch $\lambda^{m(act)}$. Evolving constituent mass densities M^k are computed as [cf. 16]

$$M^k(s) = M^k(0)\, Q^k(s) + \int_0^s m^k(\tau)\, q^k(s,\tau)\, d\tau, \tag{6.2}$$

where $Q^k(s) \in [0,1]$ are survival fractions for constituents deposited before time $s = 0$,

$m^k(\tau)$ are variable mass density production rates, and $q^k(s,\tau) \in [0,1]$ are survival fractions for constituents deposited at time $\tau \in [0,s]$ that survive to current G&R time s. By the rule of mixtures approach, one can relate evolving mass fractions to total strain energy. By tracking evolving mass densities using equation (6.2), the corresponding strain energy functions are [cf. 16]

$$W^k(s) = \frac{M^k(0)}{\rho(s)}\, Q^k(s)\, \widehat{W}^k\left(\mathbf{F}^k_{n(0)}(s)\right) + \int_0^s \frac{m^k(\tau)}{\rho(s)}\, q^k(s,\tau)\, \widehat{W}^k\left(\mathbf{F}^k_{n(\tau)}(s)\right)\, d\tau, \tag{6.3}$$

where $\rho(s) \equiv \rho(0)$ is the (constant) mass density of the mixture [12, 83], and $\mathbf{F}^k_{n(\tau)}(s) = \partial \mathbf{x}^k(s)/\partial \mathbf{X}^k(\tau)$, where $\mathbf{x}^k(s) = \mathbf{x}(s)$ constrains all k structurally significant constituents to deform together, but $\mathbf{X}^k(\tau)$ allows individual evolving natural configurations for each constituent k produced at time τ [16, 22, 63].

b. Deposition Stretches

Kozel *et al.* [80] noted that "elastin-producing cells move into and become associated with networks of pre-existing elastic fibers. During this period, the elastic fiber network would assume the motion of the cell, suggesting that components of the fiber were binding to the cell. An interaction with the cell was also evident from the stretching and pulling motions of the fiber seen as the cell moved away." Further, Czirok *et al.* [185] suggested, "One may speculate that the divergent motion of two cells, both attached to the same ECM aggregate, would generate mechanical stress within the cell-ECM composite material. This mechanical stress could be sensed by appropriate receptors, and the resulting biochemical signaling would alter the cells direction of motion."

In other words, there is evidence that synthetic cells have facilities to manipulate

newly secreted fibers and incorporate new fibers within the matrix under a mechanical load. The concepts of target homeostatic mechanical states for cells and matrix and associated constant deposition stretches are fundamentally coupled to constrained mixture models of G&R [64, 74]. This idea is incorporated through the series of multiplicative deformations[16]

$$\mathbf{F}^k_{n(\tau)}(s) = \mathbf{F}(s)\,\mathbf{F}^{-1}(\tau)\,\mathbf{G}^k(\tau), \tag{6.4}$$

with $\mathbf{F}(\tau)$ and $\mathbf{F}(s)$ representing deformation gradients corresponding to motions from a common configuration of the mixture to configurations at deposition time τ and G&R time s, respectively, and $\mathbf{G}^k(\tau)$ is a deformation gradient corresponding to a motion from the k^{th} constituent's stress-free state to the mixture's loaded configuration at deposition time τ. Consistent with the idea of constant target states and deposition stretches, $\mathbf{G}^k(\tau) = \mathbf{G}^k(0)\,\forall\,\tau$.

2. Membrane Approach

For thin walled cylindrical arteries (e.g., $a \geq 10\,h$), it is convenient to employ a membrane formulation, where two equilibrium equations can be written in terms of the mean circumferential and axial stresses, namely

$$\sigma_\theta(s) = \frac{P(s)\,a(s)}{h(s)}, \tag{6.5}$$

$$\sigma_z(s) = \frac{f(s)}{\pi\,h(s)\,(2\,a(s) + h(s))}, \tag{6.6}$$

where P is the transmural pressure, a is the deformed inner radius, h is the deformed wall thickness, and f is the applied axial force, each defined at G&R time s. equations (6.5) and (6.6) can be combined with Cauchy stress resultants $T_i = \sigma_i\,h$, where $i = z, \theta$ and, by the rule of mixtures, the stored energy function for the artery

(equation (6.3)) at any G&R time s to yield [2, 66]

$$P(s)\,a(s) = T_\theta(s) = \frac{1}{\lambda_z(s)} \sum \frac{\partial W^k(s)}{\partial \lambda_\theta(s)} + \sigma_\theta^{act}(s)\,h(s), \tag{6.7}$$

$$\frac{f(s)}{\pi\,(2\,a(s) + h(s))} = T_z(s) = \frac{1}{\lambda_\theta(s)} \sum \frac{\partial W^k(s)}{\partial \lambda_z(s)}. \tag{6.8}$$

equation (6.4) can be specialized to the case of a total stretch experienced at G&R time s by a fiber deposited at time τ is [16]

$$\lambda^k_{n(\tau)}(s) = G^k_h \frac{\lambda(s)}{\lambda(\tau)}, \tag{6.9}$$

where G^k_h is the homeostatic deposition stretch for the k^{th} constituent and $\lambda(s)$ and $\lambda(\tau)$ are stretches experienced by the mixture at times s and τ, respectively.

a. Passive Mechanical Response

As in previous constrained mixture implementations [22, 63], we modeled the passive mechanical response of elastin using a neo-Hookean strain energy function [17, 18]

$$\widehat{W}^e(s) = c\left(\lambda^e_\theta(s)^2 + \lambda^e_z(s)^2 + \frac{1}{\lambda^e_\theta(s)^2\,\lambda^e_z(s)^2} - 3\right), \tag{6.10}$$

where $\lambda^e_\theta(s) = \tilde{G}^e_h\,\lambda_\theta(s)$ and $\lambda^e_z(s) = \tilde{G}^e_h\,\lambda_z(s)$ are the stretches experienced by elastin, which can be determined from arterial stretches $(\lambda_\theta(s), \lambda_z(s))$ and "growth-induced" prestretches $\tilde{G}^e_h$ [68]. Note that the total stretches experienced by elastin do not depend on deposition time τ. In contrast, functional elastin is produced and cross-linked exclusively during the perinatal period, and subsequently stretched elastically throughout normal development and maturation [65]. Finally, we employed Fung exponential strain energy functions for both collagen [18, 69]

$$\widehat{W}^c(s) = c^c_1(s)\left(e^{c^c_2\left(\lambda^c_{n(\tau)}(s)^2 - 1\right)^2} - 1\right), \tag{6.11}$$

and passive smooth muscle [6]

$$\widehat{W}^m(s) = c_1^m \left(e^{c_2^m \left(\lambda^m_{n(\tau)}(s)^2 - 1\right)^2} - 1 \right). \tag{6.12}$$

The stretch $\lambda^k_{n(\tau)}(s)$ experienced by each of these constituents depends on its deposition stretch, and the stretch experienced by the arterial wall from deposition time τ to current G&R time s, as described by equation (6.9). We allow four fiber families of collagen, oriented axially, circumferentially, and helically [18, 22, 63]. Table VI lists values of the associated material parameters. Also note that collagen, while under compression ($\lambda^m_{n(\tau)}(s) < 1.0$), has Fung parameters equal to that of smooth muscle. The resulting difference in behavior as collagen shifts from a state of compressive to tensile loading manifests in some predicted behaviors, below.

b. Active Mechanical Response

The stress actively generated by smooth muscle, which is prescribed as a function of vasoactive molecule concentration C and muscle fiber stretch [22, 63, 64, 67], namely

$$\begin{aligned} \sigma^{act}_\theta(s) = T_{max}(s)\, \phi^m(s) \, &\left(1 - e^{-C(s)^2}\right) \\ &\times \lambda^{m(act)}_\theta(s) \left[1 - \left(\frac{\lambda_M - \lambda^{m(act)}_\theta(s)}{\lambda_M - \lambda_0} \right)^2 \right], \end{aligned} \tag{6.13}$$

where $T_{max}(s)$ is a scaling parameter with units kPa, ϕ^m is the evolving mass fraction of active smooth muscle, C is a net ratio of constrictors to dilators, λ_M is the stretch at which the active force generating capability is maximum, λ_0 is the stretch at which muscle cannot generate any force, and $\lambda^{m(act)}_\theta(s)$ is the current active muscle fiber stretch. The ratio of constrictors to dilators $C(s)$ is ultimately a function of wall

Table VI. Important parameter values used to model a representative mature basilar artery, before any loss of elastin.

Geometry/loads
$a_h = 1.42$ mm, $h_h = 0.176$ mm
$P = 93$ mmHg, $Q = 3.075$ ml/s, $\tau_w^h = 5.06$ Pa
$\sigma_\theta^h = \sigma_z^h = 100$ kPa
Mass kinetics
$\phi_0^c = 0.22, \phi_0^e = 0.02, \phi_0^m = 0.76$
$K_{qh}^m = 1/80$ day^{-1}, $K_{qh}^c = 1/80$ day^{-1}, $K^e = 1/10$ day^{-1}
Vasoactivity
$T_{max}(0) = 150$ kPa
$\lambda_M = 1.1$, $\lambda_0 = 0.4$
$C_B = 0.68, C_S = 20\, C_B$
Passive elasticity
$c = 588.3$ kPa
$c_1^m = 36.5$ kPa, $c_2^m = 3.5$
$c_1^c(0) = 560.4$ kPa, $c_2^c = 22\ \forall\, \lambda_{n(\tau)}^k(s) \geq 1.0$
$c_1^c(0) = c_1^m$, $c_2^c = c_2^m\ \forall\, \lambda_{n(\tau)}^k(s) < 1.0$
$\tilde{G}_h^e = 1.4, G_h^c = 1.08, G_h^m = 1.2$

shear stress

$$C(s) = C_B - C_S \left(\frac{\tau_w(s) - \tau_w^h}{\tau_w^h} \right), \tag{6.14}$$

where C_B is the basal ratio, C_S is a scaling factor for shear stress induced changes, and τ_w^h is the homeostatic (target) wall shear stress. Assuming fully developed laminar flow of a Newtonian fluid through a cylindrical tube, $\tau_w(s) = 4\,\mu\,Q(s)/\pi\,a^3(s)$ where μ is the viscosity of blood ($\sim$3.5 centiPoise), and $Q(s)$ is the volumetric flowrate at G&R time s [63].

c. Mass Kinetics

We consider linear functions for rates of mass density production [cf. 22, 63, 64]

$$m^k(s) = m_0^k(1 + K_\sigma^k\,\Delta\sigma - K_{\tau_w}^k\,\Delta\tau_w), \tag{6.15}$$

where k denotes individual families of fibrillar collagen or contractile smooth muscle, σ is a scalar measure of intramural stress, and $K_j^k = 1.0$ are rate parameters that govern the stress-mediated production rates. $\Delta\sigma$ and $\Delta\tau$ denote normalized differences in intramural stress and wall shear stress from homeostatic (target) values. Degradation of structural proteins and cell apoptosis appear to be well described by first order type kinetics, with appropriate half-lives [72, 96]. Hence, let the survival functions be [cf. 22, 63]

$$q^k(s,\tau) = e^{-\int_\tau^s K^k(\widetilde{\tau})d\widetilde{\tau}}, \tag{6.16}$$

where $K^k(\widetilde{\tau})$ are rate-type parameters for mass removal having units of days^{-1}. These rate parameters, in turn, are prescribed as $K^k(\widetilde{\tau}) = K_{qh}^k + K_{qh}^k\,|\Delta\zeta(\widetilde{\tau})|$, where K_{qh}^k is a homeostatic value, $\Delta\zeta(\widetilde{\tau})$ is the difference in fiber tension from its homeostatic value, and $\zeta^{k(\tau)}$ is the level of tension on fiber family k that was produced at time τ.

3. Solution Procedure

Prescribing *in vivo* axial length l, transmural pressure P, and luminal flow Q at all G&R times s permits one to solve for the inner radius via equation (6.7). At each computational time step δ, we can solve for a_δ such that

$$F\left(a_\delta\right) = \frac{1}{\lambda_z} \sum \frac{\partial W^k}{\partial \lambda_\theta \left(a_\delta\right)} + \sigma_\theta^{act}\left(a_\delta\right)\, h\left(a_\delta\right) - P\, a_\delta = 0, \tag{6.17}$$

via the Newton-Raphson method. The resulting intramural stresses and stretches and wall shear stresses control mass production (equation (6.15)), mass removal (equation (6.16)), and vasoactivity (equations (6.13) and (6.14)). Membrane thickness is then $h(s) = \sum M^k(s)/(\rho\, \lambda_z(s)\, \lambda_\theta(s))$. Finally, consistent with Valentín *et al.* [63], illustrative values of the material parameters represent a normal basilar artery (table VI).

4. Specific Cases Considered

a. Elastin Degradation

Elastin is a highly elastic and normally biologically stable arterial protein. Mature healthy arteries do not experience elastin turnover ($M^e(s) \equiv M^e(0)$). Faury [150] noted that "elastin fibre keeps its elastic properties up to extensions of about 140%, with an elastic modulus in the range of 0.4 MPa". This is due, in part, to myriad cross-links, including desmosine and isodesmosine [135], which are promoted primarily by lysyl oxidase but also transglutaminases. Nevertheless, elastin is susceptible to both proteolytic degradation by matrix metalloproteinases (especially MMP-2, -9, -13) and fatigue-type degeneration [149, 153, 186, 187]. Indeed, associated losses of elasticity likely cause or are caused by many arterial diseases and injuries [153–155]. To approximate age-related elastin loss, elastin was numerically removed from the

wall gradually. Maintaining constant transmural pressure and flowrate, the survival fraction of elastin was prescribed by

$$Q^e(s) = (1.0 - M^e_\infty)\exp(-K^e\, s) + M^e_\infty, \tag{6.18}$$

where $K^e = 1/10$ day^{-1} and M^e_∞ is the remaining fraction of elastin as $s \to \infty$. Figure 43 shows the time courses of elastin mass as prescribed by equation (6.18). Although the degradation rates prescribed herein are much higher than occur in the normal aging process, the current implementation will allow us to predict important trends. Recall that elastin is assumed to be produced exclusively during the perinatal period, thus $m^e(s) \equiv 0\ \forall s \in [0, \infty)$.

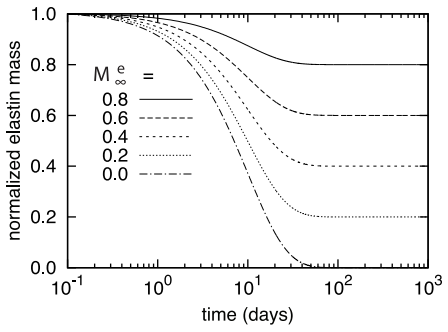

Fig. 43. Time courses of evolving elastin mass for indicated values of M^e_∞ (cf. equation (6.18)) normalized with respect to $M_e(0)$.

b. Elastin Mediated Vasoactivity

In addition to possessing important passive mechanical properties, elastin is also a potent biological regulator of smooth muscle cell activity. For example, intact "elastin induces actin stress fiber organization [and a quiescent contractile phenotype], inhibits proliferation, regulates migration and signals via a non-integrin, heterodimeric G-protein-coupled pathway" [151]. Scaling $T_{max}(s)$ (equation (6.13))

proportionally to $M^e(s)$ (equation (6.18)) allows us to approximate the deleterious vasoactive consequences of elastin degradation. In particular, we prescribe

$$T_{max}(s) = T_{max}(0)\, Q_e(s), \tag{6.19}$$

which effectively simulates increasingly compromised vasoactive function with decreasing elastin content.

c. Collagen Stiffening

Pedrigi *et al.* [188] reported significant stiffening of collagenous tissues after culture in a hyperglycemic (e.g., diabetic) environment. In particular, the authors observed an approximate doubling of c_1^c within 14 weeks in culture. Increased collagen cross-linking and stiffening, resulting primarily from pathological glycation, is an important contributing factor to age-related cardiovascular failure [189]. To investigate possible effects of pathological conditions associated with aging, we considered seperately cases in which Fung constant $c_1^c(s)$ gradually doubled by prescribing

$$c_1^c(s) = c_1^c(0)\,(1.0 - \exp\,(-K^e\, s)) + c_1^c(0). \tag{6.20}$$

Although glycation likely involves other important mechanisms (e.g., increased resistance to enzymatic degradation), we restrict our attention to a simple increase in mechanical stiffness.

D. Illustrative Results

1. Elastin Loss

Although induced elastin degradation resulted in modest changes in inner radius and thickness regardless of the degree of elastin degradation (figure 44, panels a and

c) and similarly modest changes in mass production rates total masses (figure 45, panels a, c), the collagen to elastin ratio (figure 45, panel e) changed far more appreciably. Passive distention and artery wall thinning (due to isochoric motion) both provided positive inputs to mass production; shear stress induced constrictor concentrations and constituent stresses were elevated, resulting in elevated collagen and muscle mass density production. These increases in production rates as the artery remodels to compensate for the loss of elastin result in an eventual accumulation of smooth muscle and collagen. Predicted evolving changes in artery wall composition, coupled with full vasoactive function resulted in almost negligible changes in loaded geometry. However, predicted unloaded lengths (figure 46, light curves) changed dramatically, following changes in collagen to elastin ratio. Passive pressure-radius behavior (figure 47, light curves) becomes progressively (though modestly) stiffer with increasing degrees of elastin degradation.

These results illustrate the importance of elastin content to the vessels passive behavior. However, they also suggest that the compressive behavior of collagen may be just as important. A central assumption within this model is that fibrillar collagen behaves differently in compression than in tension (i.e., collagen fibers can resist compressive loads together with smooth muscle and ground substance). Figure 46 shows that for high degrees of elastin degradation, the evolving unloaded length curves exhibits a pronounced "kink." This behavior is the result of collagen shifting from its compressive regime to its tensile regime as the remaining elastin is less able to compress collagen in the vessels unloaded configuration. For the basilar artery simulated herein, this shift occurs when $\sim$80% of the original elastin is removed. In other words, the relatively large changes in unloaded length are more strongly dependant on the extant elastins ability to compress collagen than on the gross quantity of elastin. This explains in part why this simulated basilar artery, normally consisting of a mere 2%

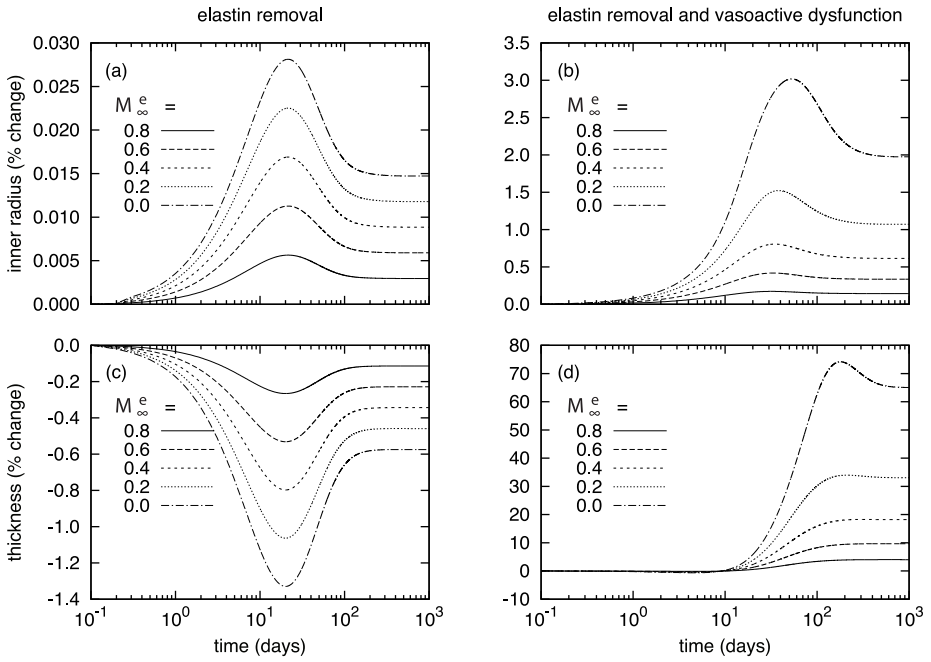

Fig. 44. Time courses of evolving inner radii (panels a and b) and thicknesses (panels c and d) for indicated degrees of elastin degradation M^e_∞ (panels a and c) and coupled elastin degradation and vasoactive dynsfunction (panels b and d). See equations (6.18) and (6.19) for the specific forms of the prescribed functions for elastin degradation and vasoactive dysfunction. All values are normalized with respect to their original values at G&R time $s = 0$ before any degradation.

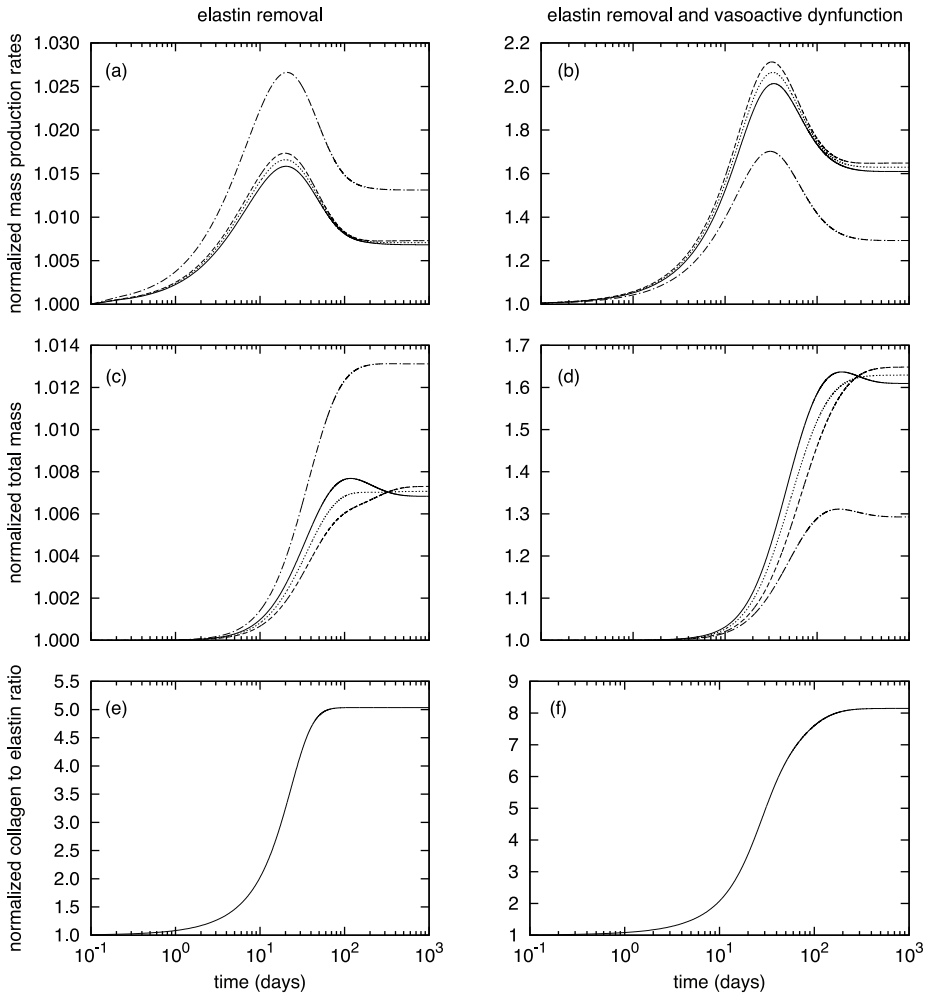

Fig. 45. Time courses of evolving mass production rates (panels a and b), total masses (panels c and d), and collagen to elastin ratio (panels e and f) for cases of elastin degradation only (panels a, c, and e) and coupled elastin degradation and vasoactive dysfunction (panels b, d, and f) where $M^e_\infty = 0.2$. In panels a-d, solid, dashed, dotted and dash-dotted curves denote quantities for axially-, circumferentially-, and helically-aligned collagen, and smooth muscle, respectively. All values are normalized with respect to their original values at G&R time $s = 0$ before any changes from homeostatic.

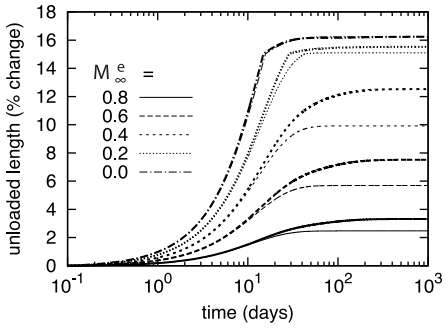

Fig. 46. Time courses of evolving unloaded axial lengths for indicated degrees of elastin degradation (light curves) and coupled elastin degradation and vasoactive dysfunction (bold curves). Note the pronounced "kink" occuring for high degrees of elastin degradation resulting from collagen shifting from its compressive regime to its tensile regime.

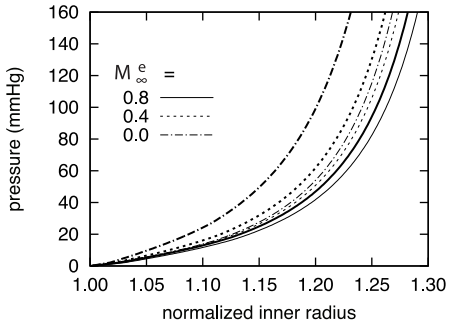

Fig. 47. Passive pressure-radius behavior at day 1000 for indicated degrees of elastin degradation (light curves) and coupled elastin degradation and vasoactive dysfunction (bold curves). The abscissa 'normalized inner radius' is expressed as the ratio of the current deformed inner radius to the current unloaded inner radius ($a(s)/A(s)$) while held at the *in vivo* length.

elastin, is predicted to increase its unloaded length by nearly 16% when 80% of its elastin is removed. This result is consistent with results of Zeller and Skalak [140]. Using elastase and collagenase to selectively remove structural proteins within unloaded segments of rat saphenous arteries, they found that "the extracellular matrix components contain residual stresses within the arterial wall itself in this average zero-stress state" and suggested that collagen may be under a residual compression and elastin under a residual tension.

2. Coupled Vasoactive Dysfunction

Coupling vasoactivity to elastin degradation via equation (6.19) resulted in marked departures from normal geometry. Figure 44 (panel a) shows larger changes in inner radius as compared to the case of elastin degradation alone, although still within 3% of $a(0)$. This dilation is due to the loss of highly prestretched elastin coupled with a diminished ability to actively maintain inner radius. Thickness increases dramatically. This hypertrophy is due to the large and sustained increases in collagen and smooth muscle production (figure 45, panels b and d);. Correspondingly, the predicted collagen to elastin ratio increases by over 7 times its original value (figure 45, panel f). Interestingly, predicted unloaded axial lengths are comparable to those of the case of elastin degradation alone (compares light and bold families of curves in figure 46). This result suggests that the degree of axial recoil is governed primarily by elastin content rather than by axial and helical collagen content.

In contrast, passive behavior becomes progressively far stiffer with increasing degree of coupled elastin degradation and vasoactive dysfunction (figure 47, bold curves) as compared to cases of elastin degradation alone. Clearly, the large amounts of newly deposited smooth muscle and circumferential and helical collagen are much more important to passive circumferential behavior. Collagen, with its relatively low

deposition stretch of 1.08, cannot serve as a substitute for elastin, herein assumed to have a prestretch $\tilde{G}_h^e = 1.4$. The behaviors predicted by simulating coupled elastin loss and vasoactive dysfunction (e.g., substantial increased circumferential passive stiffening and reduced unloaded lengths) are qualitatively similar to observed behaviors.

3. Collagen Stiffening

Prescribing a time-dependent function for collagen Fung parameter $c_1^c(s)$ via equation (6.20), we investigated numerically the cumulative effects of elastin degradation, vasoactive dynfunction, and increased glycation cross-linking of arterial collagen. Figure 48 (panel a) shows that for the case of collagen stiffening alone (i.e., $M_\infty^e = 1.0$, bold curve), inner radius remained unchanged. With the help of full vasoactive function, the simulated artery maintained its optimal inner radius. Thickness, however, increases by nearly 10% on day 100 before returning to near its original value (figure 48, panel b). Collagen production rates for this case (not shown) increase with Fung parameter $c_1^c(s)$; as collagen becomes stiffer, the stresses borne by extant fibers increases, thus driving production rates to increase.

Prescribing some degree of elastin degradation and vasoactive dysfunction results in more complex evolution. Low degrees of coupled degradation and dysfunction result in initial decreases in inner radius with eventual asymptotic stabilization. Collagen production rates increase with Fung parameter $c_1^c(s)$, and the new (stiffer) collagen tends to narrow the artery. Higher degrees of coupled degradation and dysfunction (e.g., $M_\infty^e \leq 0.8$) result in initially increased caliber as the artery distends due to loss of elastin and vasoactivity. However, collagen mass production rates continue to increase, resulting in a narrowing trend after day 20 (figure 49). Note that for any degree of coupled elastin degradation and vasoactive dynsfunction, wall thick-

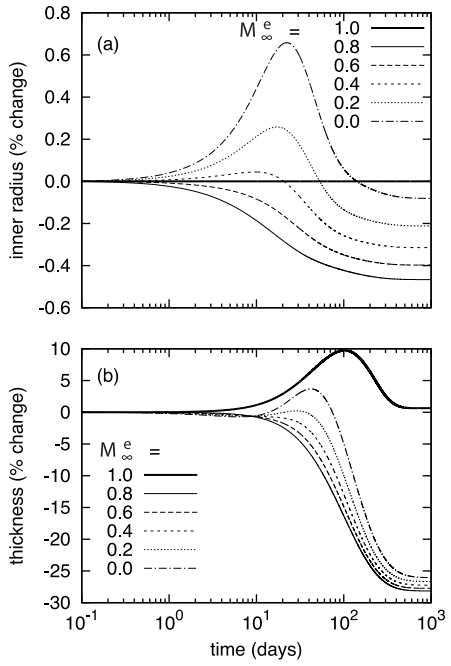

Fig. 48. Time courses of evolving inner radii (panel a) and thicknesses (panel b) for indicated degrees of coupled elastin degradation M^e_∞ and vasoactive dysnfunction where collagen stiffness parameter c^c_1 doubles gradually (as per equation (6.20)). All values are normalized with respect to their original values at G&R time $s = 0$ before any changes from homeostatic. Time courses for the cases of only elastin removal without prescribed vasoactive dysfunction (not shown) closely follow that of $M^e_\infty = 0.8$ shown here, regardless of the degree of elastin removal.

nesses decrease by nearly 30%. Collagen replaces smooth muscle as it atrophies, but the new and extant collagen's increased stiffness allows the artery to maintain static equilibrium with less total mass (figure 49, panel b).

Figure 50 shows that even for the case of no degradation or dysfunction (bold curve), increasing $c_1^c(s)$ results in increasing unloaded lengths. This occurs since , effectively shifting collagen's deposition stretch such that it bears an increased axial load. Although this stiffer collagen changes the artery's unloaded length by over 6%, the fact that the maximum increase in unloaded length is approximately 16% suggests that elastin still dominates axial recoil behavior (i.e., the upper limit of 16% is attributable to elastin's high prestretch). Figure 51 shows that, as in the case of coupled elastin degradation and vasoactive dynsfunction (figure 47, bold curves), the deposition of stiffer collagen corresponding to increasingly diminished vasoactive function results in progressively stiffer passive circumferential behavior. Note, however, that this occurs despite a nearly 30% reduction in wall thickness.

E. Discussion

Induced elastin degradation results in an immediate increase in vascular caliber and decrease in passive wall stiffness [171]. It also results in markedly increased collagen production rates and subsequent stiffening. Passive stiffening is also a characteristic of aging arteries [155, 190, 191]. The degradation and loss of elastin have been proposed as defining characteristics of aged arteries [154, 156]. Hypertension results in increased medial collagen and arterial stiffness [41, 42], and is also associated with changed unloaded geometry [43, 45]. Unloaded lengths decrease as collagen to elastin ratios increase [161, 171]. This also occurs as arteries age [192]. The manifold deleterious consequences of increased arterial stiffness are varied and are described

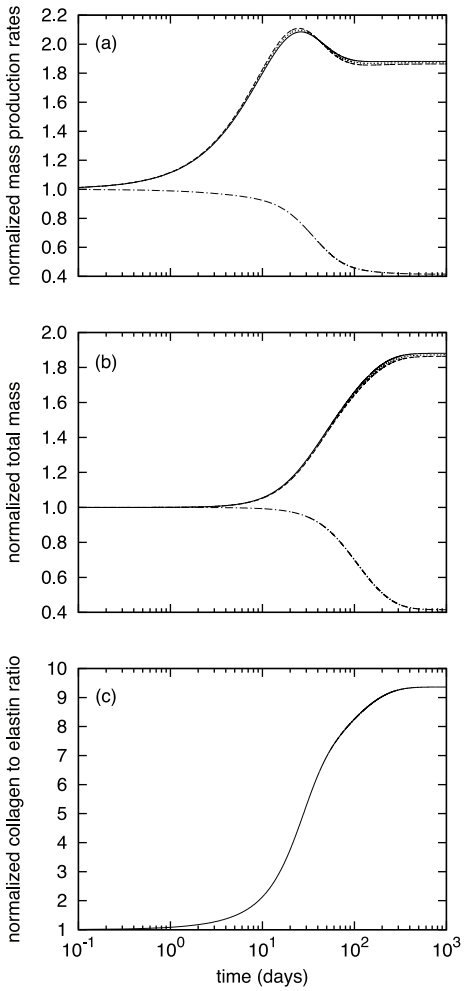

Fig. 49. Time courses of evolving mass production rates (panel a), total masses (panel b), and collagen to elastin ratio (panel c) for the case of coupled elastin degradation and vasoactive dysfunction (panels b, d, and f) where $M^e_\infty = 0.2$ and collagen stiffness parameter c^c_1 doubles gradually. In panels a and b, solid, dashed, dotted and dash-dotted curves denote quantities for axially-, circumferentially-, and helically-aligned collagen, and smooth muscle, respectively. All values are normalized with respect to their original values at G&R time $s = 0$ before any changes from homeostatic.

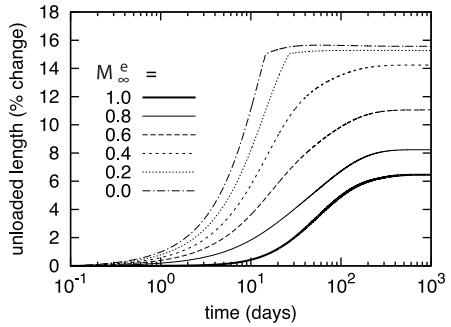

Fig. 50. Time courses of evolving unloaded axial lengths for indicated degrees of coupled elastin degradation and vasoactive dysfunction with collagen stiffness parameter c_1^c doubling gradually. Note the increasing unloaded lengths even for the case of no elastin degradation and full vasoactive function (solid bold curve).

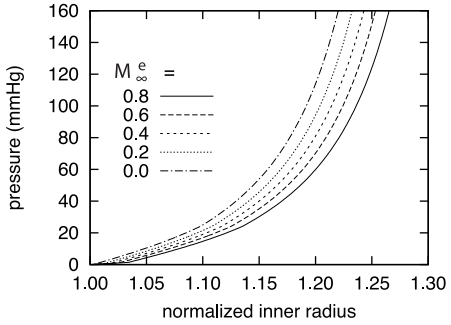

Fig. 51. Passive pressure-radius behavior at day 1000 for indicated degrees of coupled elastin degradation and vasoactive dysfunction with collagen stiffness parameter c_1^c doubling gradually. The abscissa 'normalized inner radius' is expressed as the ratio of the current deformed inner radius to the current unloaded inner radius ($a(s)/A(s)$) while held at the *in vivo* length.

elsewhere [154].

Recalling that Dobrin *et al.* [161] showed that most of the axial prestretch is due to the presence of elastin, which is now understandable in light of recent data on elastogenesis and the biological stability of elastin, it is interesting to consider these results. As can be seen, increasing collagen to elastin ratios correlate well with increasing unloaded lengths, as would be predicted based on prior findings. Recalling that aortic elastin is produced primarily during the perinatal period [cf. 136, 180], note that Bendeck *et al.* [138] reported changes in arterial lengths during this period in lambs. For example they reported a 48% increase in length from 120 days gestation to 21 days postpartum (with full term at $\sim$ 147 days). This implies that at least some of the elastin within the wall could be prestretched by 48% simply due to development, consistent with the suggestion of Dobrin *et al.* [160].

1. Aging

Changes in arterial elastin, and associated changes in arterial wall biology and mechanics, play a major role in aging related diseases of the cardiovascular system [193]. Indeed, Greenwald [154] puts it this way: "As the conduit arteries age, changes in their composition and structure lead inexorably to an increase in the stiffness of their walls, resulting ... in raised systolic and pulse pressure and greater mechanical load on the left ventricle, the systemic circulation as a whole and a consequent increase in the risk of stroke, myocardial infarction, renal failure and other sequelae of essential hypertension."

Conspicuous arterial changes due to aging include an increased wall stiffness (due in part to an increased collagen-to-elastin ratio) that causes an increase in systolic and pulse pressure (due in part to an increased pulse wave velocity and corresponding pressure augmentation due to earlier wave reflections) as well as neointimal thickening,

an increased caliber, a lengthening of loosely tethered arteries such as the abdominal aorta, and so-called endothelial dysfunction [148, 154, 155]. Notwithstanding the utility of the collagen-to-elastin ratio in many correlative studies, note that with aging the diminished, remaining elastin often shows signs of disorganization, fragmentation, or calcification whereas the collagen tends to have increased cross-linking (i.e., glycation-based cross-links in addition to normal enzymatic-based cross-links [188, 189]); together, these effects on hemodynamics and wall mechanobiology exacerbate those due to the increased collagen-to-elastin ratio. Amongst the many biochemomechanical changes in aging arteries, it appears that there is a decrease in flow-induced NO production and corresponding increase in ET-1, ACE, ANG-II, and AT1 receptors [194], which together promote increased MMP-2 production and VSMC proliferation, migration (into the intima), and synthesis of collagen via increased TGF-β [23, 56].

2. Hypertension

As in the case of simulated hypertension [63], increasing collagen to elastin content resulted in increased unloaded lengths (figure 46) and stiffening passive response (figure 47). As elastin is degraded, the vessels ability to retract becomes progressively reduced. That is, its unloaded length increases. This occurs since elastins much higher prestretch normally compresses axial and helical collagen, which has a much lower prestretch. The evolving passive behavior stiffens irreversibly. These trends are similar to those of a hypertensive vessel [41, 42] and suggest that similar mechanisms (namely, increasing collagen to elastin ratios) contribute to both aging and hypertension.

It has been suggested that essential hypertension can lead to "elastic fibre fatigue and accelerated degradation, leading to loss of arterial wall resilience" [153].

Indeed, this hypothesis finds support via *in vitro* mechanical studies by Lillie and Gosline [187], who show that long-term cyclic loading can cause elastic fibers to fail at extensions well less than normal; they propose that this fatigue-type damage may initiate due to a failure of or separation from microfibrils, not elastin per se. It is possible that elastin fragmentation occurs as a result of fatigue [154, 187]

3. Marfan Syndrome

Marfan patients have dramatically reduced levels of the elastin-associated microfibril fibrillin-1 [195] and frequently present with fragmented elastic laminae. It has also been observed in mouse models of Marfan syndrome that "Subsequent breach of the internal or external elastic laminae in fibrillin-1-deficient mice allows infiltration of inflammatory cells into the media, resulting in intense elastolysis that contributes to the structural collapse of the aortic wall" [152]. Finally, note that Marfan syndrome patients tend to suffer from dissections of the ascending aorta. One key question is, Why this particular site? It is interesting to note that the collagen-to-elastin ratio is remarkably low in the ascending aorta (0.49 based on values of 19.6% collagen and 41.1% elastin in the canine [196], which are consistent with values from Leung *et al.* [175] of 0.23 based on 11% collagen and 48% collagen in the rabbit). Note, too, that the ascending aorta is unique in that it experiences considerable axial and torsional deformations during the cardiac cycle.

4. Conclusions

Gleason *et al.* [6] and Gleason and Humphrey [7] showed via computationally modeling, for example, that allowing elastin to turnover may allow optimal arterial adaptations to increased blood flow and blood pressure but disallowing elastin to turnover may cause "sub-optimal" adaptations. Despite the ability of vascular cells

to produce new elastin in the mature arterial wall in response to disease or injury, potential reparative processes are generally not effective [153, 197], perhaps due to the inability to recapitulate all of the necessary temporal and spatial processes that occur in development [148, 182]. Indeed, elastin fragments can stimulate smooth muscle proliferation, migration, and synthesis of collagen, perhaps by interacting with elastin-laminin receptors, opening calcium channels, and activating tyrosine kinase signaling pathways [153].

The present work highlights the importance of the complementary effects of elastin content, vasoactivity, and collagen stiffness in normal (healthy) vascular function. As previous computational studies suggest [63, 64], these complementary roles serve to endow arteries with a number of unique properties that optimize structure and function. In particular, elastin production and cross-linking during development furnish arteries with a highly elastic material that 'locks in', by way of its biological stability, a preferred mode of behavior. Active smooth muscle plays a similar role in 'locking in' a preferred inner radius. The passive mechanical behaviors of collagen and smooth muscle also seem to be tuned to . This remarkable system gives rise to a high degree of optimization via a some constant cellular behaviors; synthetic and force generating cells follow the same general guidelines throughout the vascular tree, but diverse conditions during development result in amazingly diverse vascular function.

CHAPTER VII

SUMMARY AND RECOMMENDATIONS

The past four decades have yielded tremendous advances in arterial mechanics and thus our comprehension of the underlying mechanobiology and pathophysiology. Most prior analyses have focused on material properties and stress-strain analyses at single instants, however, not how these quantities change over time as an artery grows and remodels. Recently, the dearth of appropriate theoretical models has motivated a drive to develop new theoretical frameworks and the experiments upon which they must be built. The constrained mixture approach has shown itself to be a powerful means by which to test basic concepts and to build intuition.

The described theoretical framework and illustrative constitutive relations yield predictions consistent with many reported observations. It is shown that vasoactive changes influence the rapid change in caliber that is needed to maintain wall shear stress near its homeostatic level and the longer term changes in wall thickness that are needed to maintain circumferential wall stress near its homeostatic target. Furthermore, it is shown that competing effects of intramural and wall shear stress regulated rates of turnover can develop complex coupled responses. Also, the implemented constrained mixture model appears to capture conspicuous features of arterial G&R in response to increased axial extension, and coupled elastin degradation, smooth muscle dysfunction, and collagen stiffening.

Additionally, this work involved the classification of different varieties of parameters and constitutive relations. Particular attention was directed toward complementary roles of smooth muscle vasoactivity and matrix remodeling, with an emphasis on mechanosensitive changes in the rates of turnover of intramural collagen and smooth muscle. Finally, results demonstrate that the sensitivity to parameter values depends

upon the type of perturbation from normalcy, with the model basilar artery being most sensitive to changes in axial stretch. The results presented in this dissertation should motivate experiments to determine actual morphological changes, thus narrowing the range of values for unknown parameters.

Each chapter of this dissertation highlights our limited understanding of constituent turnover rates. Although there exists an extensive literature on the turnover of cells and extracellular matrix that underlies all of arterial growth and remodeling, we lack the requisite detailed information on the time-courses of constituent production and removal. Literally hundreds of papers report time dependent, mechano-stimulated changes in cell or matrix turnover as part of the ubiquitous growth and remodeling that occurs in arteries during development as well as during adaptations to sustained changes in hemodynamic loading, disease progression, and in response to injury or clinical intervention. Unfortunately, data are usually reported at only a few time points, often only as "before" and "after" the perturbation of interest. Lacking detailed production/removal rate time-course information, we will continue to focus on the here and now and not be able to predict dynamic changes.

It bears mentioning that, regardless of the production rate of interest, it is ultimately gene expression and thus basic cellular activity that is of primary interest. With continuing advances in molecular biomechanics and systems biology, it is hoped that one day the complexities of transcriptional, translational, and post-translational kinetics can be modeled. Continuum based constrained mixture models may motivate experimentalists and theorists alike to elucidate these intricately linked behaviors. Until then, however, and indeed even after that time, there will continue to be a need for simpler models that can be integrated within continuum biomechanical and multiscale analyses.

Present limitations notwithstanding, given the burgeoning understanding of mod-

eling arterial mechanobiology and the associated growth and remodeling mechanics, there is a need to advance toward more unidealized scenarios wherein actual hemodynamics and wall mechanics can be solved simultaneously. Owing to complexities from molecular to organ levels, the necessity for integrative multiscale computational models possessing both illustrative and predictive capabilities remains urgent.

REFERENCES

[1] Rodbard, S., 1975, "Vascular caliber," Cardiology, **60**, pp. 4–49.

[2] Humphrey, J. D., 2002, "Cardiovascular Solid Mechanics: Cells, Tissues, and Organs," Springer-Verlag, New York.

[3] Dajnowiec, D. and Langille, B. L., 2007, "Arterial adaptations to chronic changes in haemodynamic function: Coupling vasomotor tone to structural remodelling," Clin Sci (Lond), **113**, pp. 15–23.

[4] Taber, L. A., 1998, "A model for aortic growth based on fluid shear and fiber stresses," J Biomech Eng, **120**, pp. 348–54.

[5] Rachev, A., Manoach, E., Berry, J., and Moore, J. E. J., 2000, "A model of stress-induced geometrical remodeling of vessel segments adjacent to stents and artery/graft anastomoses," J Theor Biol, **206**, pp. 429–43.

[6] Gleason, R. L., Taber, L. A., and Humphrey, J. D., 2004, "A 2-D model of flow-induced alterations in the geometry, structure, and properties of carotid arteries," J Biomech Eng, **126**, pp. 371–81.

[7] Gleason, R. L. and Humphrey, J. D., 2004, "A mixture model of arterial growth and remodeling in hypertension: Altered muscle tone and tissue turnover," J Vasc Res, **41**, pp. 352–63.

[8] Humphrey, J. D. and Na, S., 2002, "Elastodynamics and arterial wall stress," Ann Biomed Eng, **30**, pp. 509–23.

[9] Humphrey, J. D. and Taylor, C. A., 2008, "Intracranial and abdominal aortic aneurysms: Similarities, differences, and need for a new class of computational models," Annu Rev Biomed Eng, **10**, pp. 221–46.

[10] Humphrey, J. D. and Delange, S. L., 2004, "An Introduction to Biomechanics: Solids and Fluids, Analysis and Design," Springer-Verlag, New York.

[11] Humphrey, J. D. and Wilson, E., 2003, "A potential role of smooth muscle tone in early hypertension: A theoretical study," J Biomech, **36**, pp. 1595–601.

[12] Humphrey, J. D. and Rajagopal, K. R., 2002, "A constrained mixture model for growth and remodeling of soft tissues," Math Models Methods Appl Sci, **12**, pp. 407–30.

[13] Lehman, R. M., Owens, G. K., Kassell, N. F., and Hongo, K., 1991, "Mechanism of enlargement of major cerebral collateral arteries in rabbits," Stroke, **22**, pp. 499–504.

[14] Zamir, M., 1977, "Shear forces and blood vessel radii in the cardiovascular system," J Gen Physiol, **69**, pp. 449–61.

[15] Murray, C. D., 1926, "The physiological principle of minimum work: I. the vascular system and the cost of blood volume," Proc Natl Acad Sci USA, **12**, pp. 207–14.

[16] Baek, S., Rajagopal, K. R., and Humphrey, J. D., 2006, "A theoretical model of enlarging intracranial fusiform aneurysms," J Biomech Eng, **128**, pp. 142–9.

[17] Dorrington, K. and McCrum, N., 1977, "Elastin as a rubber," Biopolymers, **16**, pp. 1201–1222.

[18] Holzapfel, G. A., Gasser, T. C., and Ogden, R. W., 2000, "A new constitutive framework for arterial wall mechanics and a comparative study of material models," J Elasticity, **61**, pp. 1–48.

[19] Stenmark, K. R. and Mecham, R. P., 1997, "Cellular and molecular mechanisms of pulmonary vascular remodeling," Annu Rev Physiol, **59**, pp. 89–144.

[20] Langille, B. L., 1996, "Arterial remodeling: Relation to hemodynamics," Can J Physiol Pharmacol, **74**, pp. 834–41.

[21] Rachev, A. and Hayashi, K., 1999, "Theoretical study of the effects of vascular smooth muscle contraction on strain and stress distributions in arteries," Ann Biomed Eng, **27**, pp. 459–468.

[22] Baek, S., Valentín, A., and Humphrey, J. D., 2007, "Biochemomechanics of cerebral vasospasm and its resolution: II. Constitutive relations and model simulations," Ann Biomed Eng, **35**, pp. 1498–1509.

[23] Rizvi, M. A. D. and Myers, P. R., 1997, "Nitric oxide modulates basal and endothelin-induced coronary artery vascular smooth muscle cell proliferation and collagen levels," J Mol Cell Cardiol, **29**, pp. 1779–1789.

[24] Rizvi, M. A. D., Katwa, L., Spadone, D. P., and Myers, P. R., 1996, "The effects of endothelin-1 on collagen type I and type III synthesis in cultured porcine coronary artery vascular smooth muscle cells," J Mol Cell Cardiol, **28**, pp. 243–252.

[25] Uematsu, M., Ohara, Y., Navas, J. P., Nishida, K., Murphy, T. J., Alexander, R. W., Nerem, R. M., and Harrison, D. G., 1995, "Regulation of endothelial cell

nitric oxide synthase mRNA expression by shear stress," Am J Physiol, **269**, pp. C1371–8.

[26] Malek, A. and Izumo, S., 1992, "Physiological fluid shear stress causes down-regulation of endothelin-1 mRNA in bovine aortic endothelium," Am J Physiol, **263**, pp. C389–96.

[27] Wicker, B. K., Hutchens, H. P., Wu, Q., Yeh, A. T., and Humphrey, J. D., 2008, "Normal basilar artery structure and biaxial mechanical behaviour," Comput Meth Biomech Biomed Eng, **11**, pp. 539–551.

[28] Kamiya, A. and Togawa, T., 1980, "Adaptive regulation of wall shear stress to flow change in the canine carotid artery," Am J Physiol, **239**, pp. H14–21.

[29] Langille, B. L. and O'Donnell, F., 1986, "Reductions in arterial diameter produced by chronic decreases in blood flow are endothelium-dependent," Science, **231**, pp. 405–407.

[30] Langille, B. L., Bendeck, M. P., and Keeley, F. W., 1989, "Adaptations of carotid arteries of young and mature rabbits to reduced carotid blood flow," Am J Physiol, **256**, pp. H931–9.

[31] Brownlee, R. D. and Langille, B. L., 1991, "Arterial adaptations to altered blood flow," Can J Physiol Pharmacol, **69**, pp. 978–983.

[32] Rudic, R. D., Shesely, E. G., Maeda, N., Smithies, O., Segal, S. S., and Sessa, W. C., 1998, "Direct evidence for the importance of endothelium-derived nitric oxide in vascular remodeling," J Clin Invest, **101**, pp. 731–736.

[33] Zarins, C. K., Zatina, M. A., Giddens, D. P., Ku, D. N., and Glagov, S., 1987,

"Shear stress regulation of artery lumen diameter in experimental atherogenesis," J Vasc Surg, **5**, pp. 413–420.

[34] Faraci, F. M., 1990, "Role of nitric oxide in regulation of basilar artery tone *in vivo*," Am J Physiol, **259**, pp. H1216–21.

[35] Gleason, R. L. and Humphrey, J. D., 2005, "A 2D constrained mixture model for arterial adaptations to large changes in flow, pressure and axial stretch," Math Med Biol, **22**, pp. 347–369.

[36] Gleason, R. L. and Humphrey, J. D., 2005, "Effects of a sustained extension on arterial growth and remodeling: A theoretical study," J Biomech, **38**, pp. 1255–61.

[37] Xu, C., Zarins, C. K., Bassiouny, H. S., Briggs, W. H., Reardon, C., and Glagov, S., 2000, "Differential transmural distribution of gene expression for collagen types I and III proximal to aortic coarctation in the rabbit," J Vasc Res, **37**, pp. 170–82.

[38] Wolinsky, H., 1970, "Response of the rat aortic media to hypertension. Morphological and chemical studies," Circ Res, **26**, pp. 507–522.

[39] Matsumoto, T. and Hayashi, K., 1996, "Stress and strain distribution in hypertensive and normotensive rat aorta considering residual strain," J Biomech Eng, **118**, pp. 62–73.

[40] Fridez, P., Makino, A., Kakoi, D., Miyazaki, H., Meister, J. J., Hayashi, K., and Stergiopulos, N., 2002, "Adaptation of conduit artery vascular smooth muscle tone to induced hypertension," Ann Biomed Eng, **30**, pp. 905–916.

[41] Hu, J.-J., Fossum, T. W., Miller, M. W., Xu, H., Liu, J.-C., and Humphrey, J. D., 2007, "Biomechanics of the porcine basilar artery in hypertension," Ann Biomed Eng, **35**, pp. 19–29.

[42] Hu, J.-J., Baek, S., and Humphrey, J. D., 2007, "Stress-strain behavior of the passive basilar artery in normotension and hypertension," J Biomech, **40**, pp. 2559–2563.

[43] Vaishnav, R. N., Vossoughi, J., Patel, D. J., Cothran, L. N., Coleman, B. R., and Ison-Franklin, E. L., 1990, "Effect of hypertension on elasticity and geometry of aortic tissue from dogs," J Biomech Eng, **112**, pp. 70–74.

[44] Fung, Y. C., 1993, "Biomechanics: Mechanical Properties of Living Tissues," Springer-Verlag, New York.

[45] Jackson, Z. S., Gotlieb, A. I., and Langille, B. L., 2002, "Wall tissue remodeling regulates longitudinal tension in arteries," Circ Res, **90**, pp. 918–25.

[46] Gleason, R. L., Wilson, E., and Humphrey, J. D., 2007, "Biaxial biomechanical adaptations of mouse carotid arteries cultured at altered axial extension," J Biomech, **40**, pp. 766–776.

[47] Humphrey, J. D., 2008, "Mechanisms of Arterial Remodeling in Hypertension. Coupled Roles of Wall Shear and Intramural Stress," Hypertension, **52**, pp. 195–200.

[48] Tsamis, A. and Stergiopulos, N., 2007, "Arterial remodeling in response to hypertension using a constituent-based model," Am J Physiol Heart Circ Physiol, **293**, pp. H3130–9.

[49] Masuda, H., Zhuang, Y. J., Singh, T. M., Kawamura, K., Murakami, M., Zarins, C. K., and Glagov, S., 1999, "Adaptive remodeling of internal elastic lamina and endothelial lining during flow-induced arterial enlargement," Arterioscler Thromb Vasc Biol, **19**, pp. 2298–2307.

[50] Fridez, P., Zulliger, M., Bobard, F., Montorzi, G., Miyazaki, H., Hayashi, K., and Stergiopulos, N., 2003, "Geometrical, functional, and histomorphometric adaptation of rat carotid artery in induced hypertension," J Biomech, **36**, pp. 671–680.

[51] Matsumoto, T. and Hayashi, K., 1994, "Mechanical and dimensional adaptation of rat aorta to hypertension," J Biomech Eng, **116**, pp. 278–283.

[52] Mondy, J. S., Lindner, V., Miyashiro, J. K., Berk, B. C., Dean, R. H., and Geary, R. L., 1997, "Platelet-derived growth factor ligand and receptor expression in response to altered blood flow *in vivo*," Circ Res, **81**, pp. 320–7.

[53] Singh, T. M., Abe, K. Y., Sasaki, T., Zhuang, Y. J., Masuda, H., and Zarins, C. K., 1998, "Basic fibroblast growth factor expression precedes flow-induced arterial enlargement," J Surg Res, **77**, pp. 165–73.

[54] Xu, C., Lee, S., Singh, T. M., Sho, E., Li, X., Sho, M., Masuda, H., and Zarins, C. K., 2001, "Molecular mechanisms of aortic wall remodeling in response to hypertension," J Vasc Surg, **33**, pp. 570–8.

[55] Sluijter, J. P. G., Smeets, M. B., Velema, E., Pasterkamp, G., and de Kleijn, D. P. V., 2004, "Increase in collagen turnover but not in collagen fiber content is associated with flow-induced arterial remodeling," J Vasc Res, **41**, pp. 546–55.

[56] Dooley, A., Gao, B., Shi-Wen, X., Abraham, D. J., Black, C. M., Jacobs, M.,

and Bruckdorfer, K. R., 2007, "Effect of nitric oxide and peroxynitrite on type I collagen synthesis in normal and scleroderma dermal fibroblasts," Free Radic Biol Med, **43**, pp. 253–264.

[57] Rodriguez-Vita, J., Ruiz-Ortega, M., Ruperez, M., Esteban, V., Sanchez-Lopez, E., Plaza, J. J., and Egido, J., 2005, "Endothelin-1, via ETA receptor and independently of transforming growth factor-β, increases the connective tissue growth factor in vascular smooth muscle cells," Circ Res, **97**, pp. 125–134.

[58] Slattery, J. C., 1981, "Momentum, Energy, and Mass Transfer in Continua," Krieger, New York.

[59] Fry, D. L., 1968, "Acute vascular endothelial changes associated with increased blood velocity gradients," Circ Res, **22**, pp. 165–197.

[60] Miyashiro, J. K., Poppa, V., and Berk, B. C., 1997, "Flow-induced vascular remodeling in the rat carotid artery diminishes with age," Circ Res, **81**, pp. 311–319.

[61] Humphrey, J. D., Eberth, J. F., Dye, W. W., and Gleason, R. L., 2009, "Fundamental role of axial stress in compensatory adaptations by arteries," J Biomech, **42**, pp. 1–8.

[62] Strauss, B. H., Robinson, R., Batchelor, W. B., Chisholm, R. J., Ravi, G., Natarajan, M. K., Logan, R. A., Mehta, S. R., Levy, D. E., Ezrin, A. M., and Keeley, F. W., 1996, "*In vivo* collagen turnover following experimental balloon angioplasty injury and the role of matrix metalloproteinases," Circ Res, **79**, pp. 541–50.

[63] Valentín, A., Cardamone, L., Baek, S., and Humphrey, J. D., 2009, "Complementary vasoactivity and matrix remodelling in arterial adaptations to altered flow and pressure," J R Soc Interface, **6**, pp. 293–306.

[64] Valentín, A. and Humphrey, J. D., 2009, "Evaluation of fundamental hypotheses underlying constrained mixture models of arterial growth and remodeling," Phil Trans R Soc Lond A, (in press).

[65] Cardamone, L., Valentín, A., Eberth, J., and Humphrey, J., 2009, "Origin of axial prestretch and residual stress in arteries," Biomech Model Mechanobiol, (in press).

[66] Pipkin, A. C., 1968, "Integration of an equation in membrane theory," Z Angew Math Phys, **19**, pp. 818–819.

[67] Valentín, A. and Humphrey, J. D., 2009, "Parameter sensitivity study of a constrained mixture model of arterial growth and remodeling," J Biomech Eng, (in press).

[68] Figueroa, C. A., Baek, S., Taylor, C. A., and Humphrey, J. D., 2009, "A computational framework for fluid-solid-growth modeling in cardiovascular simulations," Comput Meth Appl Mech Eng, (in press).

[69] Lanir, Y., 1983, "Constitutive equations for fibrous connective tissues," J Biomech, **16**, pp. 1–12.

[70] Lehoux, S., Castier, Y., and Tedgui, A., 2006, "Molecular mechanisms of the vascular responses to haemodynamic forces," J Intern Med, **259**, pp. 381–392.

[71] Li, Y.-S. J., Haga, J. H., and Chien, S., 2005, "Molecular basis of the effects of shear stress on vascular endothelial cells," J Biomech, **38**, pp. 1949–1971.

[72] Niedermüller, H., Skalicky, M., Hofecker, G., and Kment, A., 1977, "Investigations on the kinetics of collagen-metabolism in young and old rats," Exp Gerontol, **12**, pp. 159–68.

[73] Willett, T. L., Labow, R. S., Avery, N. C., and Lee, J. M., 2007, "Increased proteolysis of collagen in an *in vitro* tensile overload tendon model," Ann Biomed Eng, **35**, pp. 1961–1972.

[74] Humphrey, J. D., 2008, "Vascular adaptation and mechanical homeostasis at tissue, cellular, and sub-cellular levels," Cell Biochem Biophys, **50**, pp. 53–78.

[75] Reneman, R. and Hoeks, A., 2008, "Wall shear stress as measured *in vivo*: Consequences for the design of the arterial system," Med Biol Eng Comput, **46**, pp. 499–507.

[76] Rigamonti, D., Saleh, J., Liu, A. M., Hsu, F. P., Mergner, W. J., and Humphrey, J. D., 1994, "Dolichoectatic aneurysm of common carotid artery: An animal model with histological correlation," Pathobiology, **62**, pp. 8–13.

[77] Krams, R., Breeuwer, M., and van de Vosse, F., 2008, "Personalised imaging and biomechanical modelling of large vessels," Med Biol Eng Comput, **46**, pp. 1057–1058.

[78] Kelleher, C. M., McLean, S. E., and Mecham, R. P., 2004, "Vascular extracellular matrix and aortic development," Curr Top Dev Biol, **62**, pp. 153–88.

[79] Meshel, A. S., Wei, Q., Adelstein, R. S., and Sheetz, M. P., 2005, "Basic mechanism of three-dimensional collagen fibre transport by fibroblasts," Nat Cell Biol, **7**, pp. 157–164.

[80] Kozel, B. A., Rongish, B. J., Czirok, A., Zach, J., Little, C. D., Davis, E. C., Knutsen, R. H., Wagenseil, J. E., Levy, M. A., and Mecham, R. P., 2006, "Elastic fiber formation: A dynamic view of extracellular matrix assembly using timer reporters," J Cell Physiol, **207**, pp. 87–96.

[81] Langille, B. L., 1993, "Remodeling of developing and mature arteries: Endothelium, smooth muscle, and matrix," J Cardiovasc Pharmacol, **21**, pp. S11–7.

[82] Skalak, R., 1981, "Growth as a finite displacement field," In: Proceedings of the IUTAM Symposium on Finite Elasticity (Carlson, D. E. and Shield, R. T. eds.) pp. 347–355. Martinus Nijhoff, The Hague.

[83] Rodriguez, E. K., Hoger, A., and McCulloch, A. D., 1994, "Stress-dependent finite growth in soft elastic tissues," J Biomech, **27**, pp. 455–67.

[84] Rachev, A., Stergiopulos, N., and Meister, J. J., 1998, "A model for geometric and mechanical adaptation of arteries to sustained hypertension," J Biomech Eng, **120**, pp. 9–17.

[85] Anderson, A. E., Ellis, B. J., and Weiss, J. A., 2007, "Verification, validation and sensitivity studies in computational biomechanics," Comput Methods Biomech Biomed Engin, **10**, pp. 171–184.

[86] Na, S., Trache, A., Trzeciakowski, J., Sun, Z., Meininger, G. A., and Humphrey, J. D., 2008, "Time-dependent changes in smooth muscle cell stiffness and focal adhesion area in response to cyclic equibiaxial stretch," Ann Biomed Eng, **36**, pp. 369–380.

[87] Ruch, T. C. and Patton, H. D., 1966, "Physiology and Biophysics," W. B. Saunders Company, Philadelphia.

[88] Guyton, A. C. and Hall, J. E., 1997, "Human Physiology and Mechanisms of Disease," Sanders, Philadelphia.

[89] Price, J. M., Davis, D. L., and Knauss, E. B., 1981, "Length-dependent sensitivity in vascular smooth muscle," Am J Physiol, **241**, pp. H557–63.

[90] Nissen, R., Cardinale, G. J., and Udenfriend, S., 1978, "Increased turnover of arterial collagen in hypertensive rats," Proc Natl Acad Sci USA, **75**, pp. 451–453.

[91] Fung, Y. C., 1991, "What are the residual stresses doing in our blood vessels?," Ann Biomed Eng, **19**, pp. 237–249.

[92] Leung, D. Y., Glagov, S., and Mathews, M. B., 1976, "Cyclic stretching stimulates synthesis of matrix components by arterial smooth muscle cells *in vitro*," Science, **191**, pp. 475–477.

[93] Wilson, E., Mai, Q., Sudhir, K., Weiss, R. H., and Ives, H. E., 1993, "Mechanical strain induces growth of vascular smooth muscle cells via autocrine action of PDGF," J Cell Biol, **123**, pp. 741–7.

[94] Li, Q., Muragaki, Y., Hatamura, I., Ueno, H., and Ooshima, A., 1998, "Stretch-induced collagen synthesis in cultured smooth muscle cells from rabbit aortic media and a possible involvement of angiotensin II and transforming growth factor-β," J Vasc Res, **35**, pp. 93–103.

[95] Rachev, A., 2000, "A model of arterial adaptation to alterations in blood flow," J Elasticity, **61**, pp. 83–111.

[96] Cho, A., Courtman, D. W., and Langille, B. L., 1995, "Apoptosis (programmed cell death) in arteries of the neonatal lamb," Circ Res, **76**, pp. 168–75.

[97] Alford, P. W., Humphrey, J. D., and Taber, L. A., 2008, "Growth and remodeling in a thick-walled artery model: Effects of spatial variations in wall constituents," Biomech Model Mechanobiol, **7**, pp. 245–262.

[98] Menzel, A., 2007, "A fibre reorientation model for orthotropic multiplicative growth," Biomech Model Mechanobiol, **6**, pp. 303–320.

[99] Fridez, P., Rachev, A., Meister, J. J., Hayashi, K., and Stergiopulos, N., 2001, "Model of geometrical and smooth muscle tone adaptation of carotid artery subject to step change in pressure," Am J Physiol Heart Circ Physiol, **280**, pp. H2752–60.

[100] Hariton, I., de Botton, G., Gasser, T. C., and Holzapfel, G. A., 2007, "Stress-driven collagen fiber remodeling in arterial walls," Biomech Model Mechanobiol, **6**, pp. 163–175.

[101] Kuhl, E., Maas, R., Himpel, G., and Menzel, A., 2007, "Computational modeling of arterial wall growth," Biomech Model Mechanobiol, **6**, pp. 321–331.

[102] Driessen, N. J. B., Wilson, W., Bouten, C. V. C., and Baaijens, F. P. T., 2004, "A computational model for collagen fibre remodelling in the arterial wall," J Theor Biol, **226**, pp. 53–64.

[103] Davies, P. F., 1995, "Flow-mediated endothelial mechanotransduction," Physiol Rev, **75**, pp. 519–560.

[104] Zulliger, M. A., Rachev, A., and Stergiopulos, N., 2004, "A constitutive formulation of arterial mechanics including vascular smooth muscle tone," Am J Physiol Heart Circ Physiol, **287**, pp. H1335–43.

[105] Stålhand, J., Klarbring, A., and Holzapfel, G. A., 2008, "Smooth muscle contraction: Mechanochemical formulation for homogeneous finite strains," Prog Biophys Mol Biol, **96**, pp. 465–481.

[106] Alberts, B., Johnson, A., Lewis, J., Raff, M., Roberts, K., and Walter, P., 2002, "The Molecular Biology of the Cell," Garland Science, London.

[107] Eastwood, M., McGrouther, D. A., and Brown, R. A., 1998, "Fibroblast responses to mechanical forces," Proc Inst Mech Eng [H], **212**, pp. 85–92.

[108] O'Callaghan, C. J. and Williams, B., 2000, "Mechanical strain-induced extracellular matrix production by human vascular smooth muscle cells: Role of TGF-β_1," Hypertension, **36**, pp. 319–24.

[109] Swartz, M. A., Tschumperlin, D. J., Kamm, R. D., and Drazen, J. M., 2001, "Mechanical stress is communicated between different cell types to elicit matrix remodeling," Proc Natl Acad Sci USA, **98**, pp. 6180–5.

[110] Baek, S., Rajagopal, K. R., and Humphrey, J. D., 2005, "Competition between radial expansion and thickening in the enlargement of an intracranial saccular aneurysm," J Elasticity, **80**, pp. 13–31.

[111] Lodi, C. A. and Ursino, M., 1999, "Hemodynamic effect of cerebral vasospasm in humans: A modeling study," Ann Biomed Eng, **27**, pp. 257–73.

[112] Fischer, G. M. and Llaurado, J. G., 1966, "Collagen and elastin content in canine arteries selected from functionally different vascular beds," Circ Res, **19**, pp. 394–399.

[113] Walmsley, J. G., Campling, M. R., and Chertkow, H. M., 1983, "Interrela-

tionships among wall structure, smooth muscle orientation, and contraction in human major cerebral arteries," Stroke, **14**, pp. 781–790.

[114] Nevo, E. and Lanir, Y., 1989, "Structural finite deformation model of the left ventricle during diastole and systole," J Biomech, **111**, pp. 342–349.

[115] Cho, A., Mitchell, L., Koopmans, D., and Langille, B. L., 1997, "Effects of changes in blood flow rate on cell death and cell proliferation in carotid arteries of immature rabbits," Circ Res, **81**, pp. 328–37.

[116] Jamal, A., Bendeck, M., and Langille, B. L., 1992, "Structural changes and recovery of function after arterial injury," Arterioscler Thromb, **12**, pp. 307–17.

[117] Sluijter, J. P. G., Smeets, M. B., Velema, E., Pasterkamp, G., and de Kleijn, D. P. V., 2004, "Increased collagen turnover is only partly associated with collagen fiber deposition in the arterial response to injury," Cardiovasc Res, **61**, pp. 186–95.

[118] Strauss, B. H., Chisholm, R. J., Keeley, F. W., Gotlieb, A. I., Logan, R. A., and Armstrong, P. W., 1994, "Extracellular matrix remodeling after balloon angioplasty injury in a rabbit model of restenosis," Circ Res, **75**, pp. 650–8.

[119] Karim, M. A., Miller, D. D., Farrar, M. A., Eleftheriades, E., Reddy, B. H., Breland, C. M., and Samarel, A. M., 1995, "Histomorphometric and biochemical correlates of arterial procollagen gene expression during vascular repair after experimental angioplasty," Circ, **91**, pp. 2049–57.

[120] Bendeck, M. P., Irvin, C., Reidy, M., Smith, L., Mulholland, D., Horton, M., and Giachelli, C. M., 2000, "Smooth muscle cell matrix metalloproteinase pro-

duction is stimulated via $\alpha_v\beta_3$ integrin," Arterioscler Thromb Vasc Biol, **20**, pp. 1467–72.

[121] Weiser-Evans, M. C., Quinn, B. E., Burkard, M. R., and Stenmark, K. R., 2000, "Transient reexpression of an embryonic autonomous growth phenotype by adult carotid artery smooth muscle cells after vascular injury," J Cell Physiol, **182**, pp. 12–23.

[122] Shi, Y., Pieniek, M., Fard, A., O'Brien, J., Mannion, J. D., and Zalewski, A., 1996, "Adventitial remodeling after coronary arterial injury," Circ, **93**, pp. 340–8.

[123] Thakker-Varia, S., Tozzi, C. A., Poiani, G. J., Babiarz, J. P., Tatem, L., Wilson, F. J., and Riley, D. J., 1998, "Expression of matrix-degrading enzymes in pulmonary vascular remodeling in the rat," Am J Physiol, **275**, pp. L398–406.

[124] Gelman, R. A., Williams, B. R., and Piez, K. A., 1979, "Collagen fibril formation. Evidence for a multistep process," J Biol Chem, **254**, pp. 180–6.

[125] Gelman, R. A., Poppke, D. C., and Piez, K. A., 1979, "Collagen fibril formation *in vitro*. The role of the nonhelical terminal regions," J Biol Chem, **254**, pp. 11741–5.

[126] Kao, W. W., Berg, R. A., and Prockop, D. J., 1977, "Kinetics for the secretion of procollagen by freshly isolated tendon cells," J Biol Chem, **252**, pp. 8391–7.

[127] Jackson, Z. S., Dajnowiec, D., Gotlieb, A. I., and Langille, B. L., 2005, "Partial off-loading of longitudinal tension induces arterial tortuosity," Arterioscler Thromb Vasc Biol, **25**, pp. 957–962.

[128] Ellsmere, J. C., Khanna, R. A., and Lee, J. M., 1999, "Mechanical loading of bovine pericardium accelerates enzymatic degradation," Biomaterials, **20**, pp. 1143–1150.

[129] Ruberti, J. W. and Hallab, N. J., 2005, "Strain-controlled enzymatic cleavage of collagen in loaded matrix," Biochem Biophys Res Commun, **336**, pp. 483–489.

[130] Truesdell, C. A. and Noll, W., 1965, "The Non-Linear Field Theories of Mechanics," Springer, Berlin.

[131] Furchgott, R. F. and Zawadzki, J. V., 11 1980, "The obligatory role of endothelial cells in the relaxation of arterial smooth muscle by acetylcholine," Nature, **288**, pp. 373–376.

[132] Pohl, U., Holtz, J., Busse, R., and Bassenge, E., 1986, "Crucial role of endothelium in the vasodilator response to increased flow *in vivo*," Hypertension, **8**, pp. 37–44.

[133] Stålhand, J. and Klarbring, A., 2005, "Aorta *in vivo* parameter identification using an axial force constraint," Biomech Model Mechanobiol, **3**, pp. 191–199.

[134] Masson, I., Boutouyrie, P., Laurent, S., Humphrey, J. D., and Zidi, M., 2008, "Characterization of arterial wall mechanical behavior and stresses from human clinical data," J Biomech, **41**, pp. 2618–2627.

[135] Mithieux, S. M. and Weiss, A. S., 2005, "Elastin," Adv Protein Chem, **70**, pp. 437–61.

[136] Davidson, J. M., Hill, K. E., and Alford, J. L., 1986, "Developmental changes in collagen and elastin biosynthesis in the porcine aorta," Dev Biol, **118**, pp. 103–11.

[137] Bendeck, M. P. and Langille, B. L., 1991, "Rapid accumulation of elastin and collagen in the aortas of sheep in the immediate perinatal period," Circ Res, **69**, pp. 1165–9.

[138] Bendeck, M. P., Keeley, F. W., and Langille, B. L., 1994, "Perinatal accumulation of arterial wall constituents: Relation to hemodynamic changes at birth," Am J Physiol, **267**, pp. H2268–79.

[139] Greenwald, S. E., J. E. Moore, J., Rachev, A., Kane, T. P. C., and Meister, J.-J., 1997, "Experimental Investigation of the Distribution of Residual Strains in the Artery Wall," J Biomech Eng, **119**, pp. 438–444.

[140] Zeller, P. J. and Skalak, T. C., 1998, "Contribution of individual structural components in determining the zero-stress state in small arteries," J Vasc Res, **35**, pp. 8–17.

[141] Stergiopulos, N., Vulliemoz, S., Rachev, A., Meister, J. J., and Greenwald, S. E., 2001, "Assessing the homogeneity of the elastic properties and composition of the pig aortic media," J Vasc Res, **38**, pp. 237–246.

[142] Gleason, R. L., Hu, J.-J., and Humphrey, J. D., 2004, "Building a functional artery: Issues from the perspective of mechanics," Front Biosci, **9**, pp. 2045–2055.

[143] Chuong, C. J. and Fung, Y. C., 1986, "On residual stresses in arteries," J Biomech Eng, **108**, pp. 189–92.

[144] Liu, S. Q. and Fung, Y. C., 1988, "Zero-stress states of arteries," J Biomech Eng, **110**, pp. 82–4.

[145] Nichols, W. and O'Rourke, M., 1990, "McDonald's Blood Flow in Arteries," Edward Arnold, London.

[146] Levy, B. I. and Tedgui, A., 1999, "Biology of the Arterial Wall," Kluwer Academic, Dordrecht.

[147] Kucharz, E., 1992, "The Collagens, Biochemistry and Pathophysiology," Springer-Verlag, Berlin.

[148] Jacob, M. P., 2003, "Extracellular matrix remodeling and matrix metalloproteinases in the vascular wall during aging and in pathological conditions," Biomed Pharmacother, **57**, pp. 195–202.

[149] Kielty, C. M., Wess, T. J., Haston, L., Ashworth, J. L., Sherratt, M. J., and Shuttleworth, C. A., 2002, "Fibrillin-rich microfibrils: Elastic biopolymers of the extracellular matrix," J Muscle Res Cell Motil, **23**, pp. 581–96.

[150] Faury, G., 2001, "Function-structure relationship of elastic arteries in evolution: From microfibrils to elastin and elastic fibres," Pathol Biol (Paris), **49**, pp. 310–325.

[151] Karnik, S. K., Brooke, B. S., Bayes-Genis, A., Sorensen, L., Wythe, J. D., Schwartz, R. S., Keating, M. T., and Li, D. Y., 2003, "A critical role for elastin signaling in vascular morphogenesis and disease," Development, **130**, pp. 411–23.

[152] Dietz, H. C. and Mecham, R. P., 2000, "Mouse models of genetic diseases resulting from mutations in elastic fiber proteins," Matrix Biology, **19**, pp. 481–488.

[153] Arribas, S. M., Hinek, A., and Gonzalez, M. C., 2006, "Elastic fibres and vascular structure in hypertension," Pharmacol Ther, **111**, pp. 771–791.

[154] Greenwald, S. E., 2007, "Ageing of the conduit arteries," J Pathol, **211**, pp. 157–172.

[155] O'Rourke, M. F. and Hashimoto, J., 2007, "Mechanical factors in arterial aging: A clinical perspective," J Am Coll Cardiol, **50**, pp. 1–13.

[156] O'Rourke, M. F., 2007, "Arterial aging: Pathophysiological principles," Vasc Med, **12**, pp. 329–341.

[157] Patel, D. J. and Fry, D. L., 1966, "Longitudinal tethering of arteries in dogs," Circ Res, **19**, pp. 1011–1021.

[158] Tickner, E. G. and Sacks, A. H., 1967, "A theory for the static elastic behavior of blood vessels," Biorheology, **4**, pp. 151–168.

[159] Cox, R. H., 1975, "Anisotropic properties of the canine carotid artery *in vitro*," J Biomech, **8**, pp. 293–300.

[160] Dobrin, P., Canfield, T., and Sinha, S., 1975, "Development of longitudinal retraction of carotid arteries in neonatal dogs," Experientia, **31**, pp. 1295–1296.

[161] Dobrin, P. B., Schwarcz, T. H., and Mrkvicka, R., 1990, "Longitudinal retractive force in pressurized dog and human arteries," J Surg Res, **48**, pp. 116–20.

[162] Davis, E. C., 1995, "Elastic lamina growth in the developing mouse aorta," J Histochem Cytochem, **43**, pp. 1115–23.

[163] Van Loon, P., Klip, W., and Bradley, E. L., 1977, "Length-force and volume-pressure relationships of arteries," Biorheology, **14**, pp. 181–201.

[164] Weizsäcker, H. W., Lambert, H., and Pascale, K., 1983, "Analysis of the passive mechanical properties of rat carotid arteries," J Biomech, **16**, pp. 703–715.

[165] Brossollet, L. J. and Vito, R. P., 1995, "An alternate formulation of blood vessel mechanics and the meaning of the *in vivo* property," J Biomech, **28**, pp. 679–687.

[166] Takamizawa, K., Hayashi, K., and Matsuda, T., 1992, "Isometric biaxial tension of smooth muscle in isolated cylindrical segments of rabbit arteries," Am J Physiol Heart Circ Physiol, **263**, pp. H30–34.

[167] Zulliger, M. A., Kwak, N. T. M. R., Tsapikouni, T., and Stergiopulos, N., 12 2002, "Effects of longitudinal stretch on VSM tone and distensibility of muscular conduit arteries," Am J Physiol Heart Circ Physiol, **283**, pp. H2599–2605.

[168] Valentín, A. and Humphrey, J. D., 2009, "Modeling Effects of Axial Extension on Arterial Growth and Remodeling," Med Biol Eng Comput, (accepted).

[169] Dobrin, P. B. and Canfield, T. R., 1984, "Elastase, collagenase, and the biaxial elastic properties of dog carotid artery," Am J Physiol Heart Circ Physiol, **247**, pp. H124–131.

[170] Dobrin, P. B., Baker, W. H., and Gley, W. C., 1984, "Elastolytic and collagenolytic studies of arteries. Implications for the mechanical properties of aneurysms," Arch Surg, **119**, pp. 405–409.

[171] Fonck, E., Prod'hom, G., Roy, S., Augsburger, L., Rüfenacht, D. A., and Stergiopulos, N., 2007, "Effect of elastin degradation on carotid wall mechanics as assessed by a constituent-based biomechanical model," Am J Physiol Heart Circ Physiol, **292**, pp. H2754–63.

[172] Roach, M. R. and Burton, A. C., 1957, "The reason for the shape of the distensibility curves of arteries," Can. J. Biochem. Physiol., **35**, pp. 181–190.

[173] Taber, L., 1995, "Biomechanics of growth, remodeling, and morphogenesis," App. Mech. Rev., **58**, pp. 487–545.

[174] Hungerford, J. E. and Little, C. D., 1999, "Developmental biology of the vascular smooth muscle cell: Building a multilayered vessel wall," J Vasc Res, **36**, pp. 2–27.

[175] Leung, D. Y., Glagov, S., and Mathews, M. B., 1977, "Elastin and collagen accumulation in rabbit ascending aorta and pulmonary trunk during postnatal growth. Correlation of cellular synthetic response with medial tension," Circ Res, **41**, pp. 316–23.

[176] Langille, B. L., Brownlee, R. D., and Adamson, S. L., 1990, "Perinatal aortic growth in lambs: Relation to blood flow changes at birth," Am J Physiol, **259**, pp. H1247–53.

[177] Wolinsky, H. and Glagov, S., 1967, "A lamellar unit of aortic medial structure and function in mammals," Circ Res, **20**, pp. 99–111.

[178] McCloskey, D. I. and Cleary, E. G., 1974, "Chemical composition of the rabbit aorta during development," Circ Res, **34**, pp. 828–835.

[179] Davidson, J. M., Hill, K. E., Mason, M. L., and Giro, M. G., 1985, "Longitudinal gradients of collagen and elastin gene expression in the porcine aorta," J Biol Chem, **260**, pp. 1901–8.

[180] Gerrity, R. G. and Cliff, W. J., 1975, "The aortic tunica media of the developing

rat. I. Quantitative stereologic and biochemical analysis," Lab Invest, **32**, pp. 585–600.

[181] Johnson, D. J., LaBourene, J., Rabinovitch, M., and Keeley, F. W., 1993, "Relative efficiency of incorporation of newly synthesized elastin and collagen into aorta, pulmonary artery and pulmonary vein of growing pigs," Connect Tissue Res, **29**, pp. 213–21.

[182] Wagenseil, J. E. and Mecham, R. P., 2007, "New insights into elastic fiber assembly," Birth Defects Res C Embryo Today, **81**, pp. 229–240.

[183] Kao, W. W., Bressan, G. M., and Prockop, D. J., 1982, "Kinetics of the incorporation of tropoelastin into elastic fibers in embryonic chick aorta," Connect Tissue Res, **10**, pp. 263–274.

[184] Kielty, C. M., Baldock, C., Lee, D., Rock, M. J., Ashworth, J. L., and Shuttleworth, C. A., 2002, "Fibrillin: From microfibril assembly to biomechanical function," Phil Trans R Soc Lond B, **357**, pp. 207–17.

[185] Czirok, A., Zamir, E. A., Filla, M. B., Little, C. D., Rongish, B. J., and Schatten, G. P., 2006, "Extracellular Matrix Macroassembly Dynamics in Early Vertebrate Embryos," In: Current Topics in Developmental Biology, Academic Press, New York.

[186] Rabinovitch, M., 1999, "Pulmonary hypertension: Pathophysiology as a basis for clinical decision making," J Heart Lung Transplant, **18**, pp. 1041–1053.

[187] Lillie, M. A. and Gosline, J. M., 2007, "Limits to the durability of arterial elastic tissue," Biomaterials, **28**, pp. 2021–2031.

[188] Pedrigi, R. M., Staff, E., David, G., Glenn, S., and Humphrey, J. D., 2007, "Altered multiaxial mechanical properties of the porcine anterior lens capsule cultured in high glucose," J Biomech Eng, **129**, pp. 121–125.

[189] Bailey, A. J., Paul, R. G., and Knott, L., 1998, "Mechanisms of maturation and ageing of collagen," Mech Ageing Dev, **106**, pp. 1–56.

[190] Hayashi, K., Handa, H., Nagasawa, S., Okumura, A., and Moritake, K., 1980, "Stiffness and elastic behavior of human intracranial and extracranial arteries," J Biomech, **13**, pp. 175–184.

[191] Briones, A. M., Gonzalez, J. M., Somoza, B., Giraldo, J., Daly, C. J., Vila, E., Gonzalez, M. C., McGrath, J. C., and Arribas, S. M., 2003, "Role of elastin in spontaneously hypertensive rat small mesenteric artery remodelling," J Physiol, **552**, pp. 185–195.

[192] Okamoto, R. J., Xu, H., Kouchoukos, N. T., Moon, M. R., and Sundt III, T. M., 2003, "The influence of mechanical properties on wall stress and distensibility of the dilated ascending aorta," J Thorac Cardiovasc Surg, **126**, pp. 842–50.

[193] Pezet, M., Jacob, M.-P., Escoubet, B., Gheduzzi, D., Tillet, E., Perret, P., Huber, P., Quaglino, D., Vranckx, R., Li, D. Y., Starcher, B., Boyle, W. A., Mecham, R. P., and Faury, G., 2008, "Elastin haploinsufficiency induces alternative aging processes in the aorta," Rejuvenation Res, **11**, pp. 97–112.

[194] Wang, M., Zhang, J., Spinetti, G., Jiang, L.-Q., Monticone, R., Zhao, D., Cheng, L., Krawczyk, M., Talan, M., Pintus, G., and Lakatta, E. G., 2005, "Angiotensin II Activates Matrix Metalloproteinase Type II and Mimics Age-Associated Carotid Arterial Remodeling in Young Rats," Am J Pathol, **167**, pp. 1429–1442.

[195] Ramirez, F. and Pereira, L., 1999, "Mutations of extracellular matrix components in vascular disease," Ann Thorac Surg, **67**, pp. 1857–8.

[196] Dobrin, P. "Physiology and pathophysiology of blood vessels." In: The Basic Science of Vascular Disease, pp. 69–105. Futura, New York, 1997.

[197] Krettek, A., Sukhova, G. K., and Libby, P., 2003, "Elastogenesis in human arterial disease: A role for macrophages in disordered elastin synthesis," Arterioscler Thromb Vasc Biol, **23**, pp. 582–587.

APPENDIX A

FRAMEWORK DETAILS

Rather than writing mass balance for constituent k in terms of a net mass density production (which can be positive, negative, or zero), it proves convenient to use the true mass density production (always non-negative) and an associated survival function. To appreciate this choice better, consider the special case wherein the true mass density production rate is constant up time $s = 0$, at which time an altered G&R stimulus changes the production rate to a different constant value. Hence, let

$$\int_{-\infty}^{s} \frac{\partial M^k}{\partial \tau}\, d\tau = \int_{-\infty}^{0} m^k(\tau)\, q^k(s,\tau)\, d\tau + \int_{0}^{s} m^k(\tau)\, q^k(s,\tau)\, d\tau \tag{A.1}$$

$$= m^k(s_0) \int_{-\infty}^{0} q^k(s,\tau)\, d\tau + m^k(s_n) \int_{0}^{s} q^k(s,\tau)\, d\tau. \tag{A.2}$$

Moreover, consider the *special case* wherein the survival function is given as a constant exponential decay, namely $q^k(s,\tau) = e^{-K^k(s-\tau)}$, whereby our result becomes

$$\begin{aligned} M^k(s) &= m^k(s_0)\, e^{-K^k s} \int_{-\infty}^{0} e^{K^k \tau}\, d\tau \\ &\quad + m^k(s_n)\, e^{-K^k s} \int_{0}^{s} e^{K^k \tau}\, d\tau \\ &= \frac{m^k(s_0)}{K^k}\, e^{-K^k s} + \frac{m^k(s_n)}{K^k} \left(1 - e^{-K^k s}\right). \end{aligned} \tag{A.3}$$

Evaluating this result at $s = 0$ requires that $M^k(0) = m^k(s_0)/K^k$, thus placing a restriction on initial/homeostatic rates of production and decay. Notice, too, that if

the two production rates are the same (say m_0^k as expected when there is no change in stimulus at $s = 0$, as in tissue maintenance), then $M^k(s) = m_0^k/K^k$. Based on these results, it proves convenient to consider the more general form

$$M^k(s) = M^k(0)\, Q^k(s) + \int_0^s m^k(\tau)\, q^k(s,\tau)\, d\tau, \tag{A.4}$$

whereby $Q^k(0) = 1$.

Next, consider the strain energy needed to model the elastic stress response. At $s = 0$, equation (2.6) becomes

$$\begin{aligned} W^k(0) &= \frac{M^k(0)\, Q^k(s)}{\rho}\, \widehat{W}^k\left(\mathbf{C}^k_{n(0)}\right) \\ &\equiv \phi^k(0)\, \widehat{W}^k\left(\mathbf{C}^k_{n(0)}\right), \end{aligned} \tag{A.5}$$

or $\phi^k\, \widehat{W}^k$, which yields the classical rule of mixtures relation for the stresses. Alternatively, if the turnover occurs in an unchanging mechanical state (i.e., the natural configurations remain fixed and thus $n(\tau) = n(0)$), then

$$\begin{aligned} W^k(s) = \widehat{W}^k &\left(\mathbf{C}^k_{n(0)}\right) \\ &\times \left(\frac{M^k(0)\, Q^k(s)}{\rho} + \int_0^s \frac{m^k(\tau)}{\rho}\, q^k(s,\tau)\, d\tau \right), \end{aligned} \tag{A.6}$$

which from the relation for mass density can be written as,

$$\begin{aligned} W^k(s) &= \widehat{W}^k\left(\mathbf{C}^k_{n(0)}\right) \left(\frac{M^k(s)}{\rho(s)}\right) \\ &\equiv \phi^k(s)\, W^k\left(\mathbf{C}^k_{n(0)}\right). \end{aligned} \tag{A.7}$$

This, too, recovers a classical rule of mixtures relation for the stored energy as it should. Hence, we see that the proposed constitutive framework recovers basic special cases as it should.

VITA

Name:

Arturo Valentín III

Address:

Department of Biomedical Engineering, 337 Zachry Engineering Center, 3120 TAMU, Texas A&M University, College Station, TX 77843-3120

Email address:

avalentin@tamu.edu

Education:

B.S., Mechanical Engineering, University of South Carolina, 2002

M.S., Mechanical Engineering, University of South Carolina, 2004

Ph.D., Biomedical Engineering, Texas A&M University, 2009